UNIVERSITAT POLITÈCNICA DE CATALUNYA BARCELONATECH

DEPARTMENT OF ELECTRICAL ENGINEERING

PH.D. THESIS

# Corona discharges from grounded rods and 337/777 nm emissions of laboratory long sparks

Marcelo Augusto Sousa Arcanjo

Barcelona, January 2022

UNIVERSITAT POLITÈCNICA DE CATALUNYA BARCELONATECH

# Corona discharges from grounded rods and 337/777 nm emissions of laboratory long sparks

Thesis by compendium of publications to qualify for the degree of

PhD in Electrical Engineering


Presented by:

Marcelo Augusto Sousa Arcanjo

Thesis advisor:

Joan Montanyà Puig

Polytechnical University of Catalonia

Electrical Engineering Department


---

Barcelona, January 2022

**Abstract**

This thesis presents an investigation on the signatures of corona discharges from grounded rods under thunderstorms and in the laboratory, with optical detections in the 337/777 nm wavelengths for high voltage sparks. This PhD project is contextualized in the European program: Science and Innovation with thunderstorms (SAINT), funded by the Horizon 2020 / Marie Skłodowska Curie Action (Grant agreement ID: 722337).

Under conditions of electrification, charged clouds produce an enhancement of the electric field at the ground level. That, in turn, can lead to corona discharges that produce a space charge layer in the vicinity of grounded structures. The study of this phenomenon is useful for the understanding of lightning-related processes and attachment. In addition to the electrical current obtained from the discharges, another important variable is the optical signature generated by the plasma channels. Emissions in many spectra lines associated with reactions of streamers and leaders with the main components of the atmosphere are relevant for visual observations.

This work presents a chapter for current literature review of the processes associated with lightning and the main concepts applied. Then, a detailed description of the instrumentation available for the tests carried out in the laboratory and in the field is provided.

The first article of this compendium presents data obtained with experiments of a grounded rod under high background electric field in the laboratory and the field. A limited number of works in the literature have presented such data. An analysis correlating pulse frequency, electric field level and average wind speed is the main novelty of the article. A congress paper annexed in the thesis complements the findings comparing the discharges observed at two other experimental sites.

The second article describes a compilation of results obtained in the laboratory for investigating optical signatures in two specific lines of the spectra (337 nm and 777 nm), the ones with stronger emissions in lightning-like events. There is special relevance of such experiments for supporting satellite-based observations of lightning by the Atmosphere-Space Interactions Monitor (ASIM) that perform optical measurements in the same wavelength ranges and the operational lightning imagers such as Geostationary Lightning Mapper (GLM) and the future Meteosat Third Generation Lightning Imager (MTG-LI).

The conclusions are presented, together with the prospects for future work following the original results achieved with this PhD. This thesis ends with a detailed description of the dissemination activities (presentation at seminars and

conferences, co-authored publications in journals and at conferences) and training activities received throughout this project.

Finally, the appendix present additional developments and applications of the sensor developed during this doctorate, comprising experiments performed during a two-month internship at the Eindhoven University of Technology (TU/e), and one section with results for the use of photometers to determine the initiation of an upward leader. Such experiments are particularly interesting for understanding space charge production and in the validation of lightning rods. The concepts applied to the development of a corona discharge current sensor were patented together with Dena Desarrollos, the company where the investigations were carried out during this doctorate.

**Resumen**

Esta tesis presenta una investigación sobre las huellas de descargas de corona en estructuras conectadas a la tierra durante tormentas eléctricas y en el laboratorio, con detecciones ópticas en las longitudes de onda de 337/777 nm para descargas de alto voltaje. Este proyecto de doctorado se contextualiza en el programa europeo: *Science and Innovation with thunderstorm*s (SAINT), financiado por la Acción *Horizon 2020 / Marie Skłodowska Curie* (Acuerdo de subvención ID: 722337).

En condiciones de electrificación, las nubes cargadas producen un aumento del campo eléctrico a nivel del suelo. Eso, a su vez, puede ocasionar descargas de corona que producen una capa de carga espacial en las proximidades de las estructuras conectadas a tierra. El estudio de este fenómeno es útil para comprender los procesos y la conexión de los canales de los rayos. Además de la corriente eléctrica obtenida de las descargas, otra variable importante es la huella óptica (las señales ópticas a lo largo del tiempo) generada por los canales de plasma. Las emisiones en muchas líneas espectrales asociadas con reacciones de *streamers* y líderes con los componentes principales de la atmósfera son relevantes para las observaciones visuales.

Este trabajo presenta un capítulo de revisión de la literatura actual sobre los procesos asociados a las descargas atmosféricas y los principales conceptos aplicados. A continuación, se realiza una descripción detallada de la instrumentación disponible para las pruebas realizadas en laboratorio y en campo.

El primer artículo de este compendio presenta datos obtenidos con experimentos de una varilla puesta a tierra sujeta a un campo eléctrico de fondo elevado en laboratorio y en campo. Un número limitado de trabajos en la literatura han presentado dichos datos. Un análisis que correlaciona la frecuencia del pulso, el nivel del campo eléctrico y la velocidad media del viento es la principal novedad del artículo. Un artículo presentado en congreso adjunto a la tesis complementa los resultados y realiza una comparación de las descargas observadas en otros dos sitios experimentales.

El segundo artículo presenta una recopilación de resultados obtenidos en el laboratorio para la investigación de la huella óptica en dos líneas específicas de los espectros (337 nm y 777 nm), las que tienen emisiones más intensas en los rayos. Existe una relevancia especial de dichos experimentos para respaldar las observaciones de rayos basadas en satélites por el Monitor de Interacciones Atmosfera-Espacio (ASIM) que realiza mediciones ópticas en los mismos rangos de longitud de onda y los generadores de imágenes de rayos operacionales como *Geostationary Lightning Mapper* (GLM) y el futuro *Meteosat Third Generation Lightning Imager* (MTG-LI).

Se presentan las conclusiones, junto con las perspectivas de trabajo futuro siguiendo los resultados originales alcanzados con este doctorado. Esta tesis finaliza con una descripción detallada de las actividades de difusión (presentación en seminarios y congresos, publicaciones en coautoría en revistas y congresos) y actividades formativas recibidas a lo largo de este proyecto.

Finalmente, el apéndice presenta desarrollos y aplicaciones adicionales del sensor desarrollado durante este doctorado, que comprende experimentos realizados durante período de prácticas de dos meses en la Universidad Tecnológica de Eindhoven (TU/e), y un apartado con resultados para el uso de fotómetros para determinar la iniciación de un líder ascendente. Estos experimentos son particularmente interesantes para comprender la producción de cargas espaciales y en la validación de pararrayos. Los conceptos aplicados al desarrollo del sensor de corriente de descarga corona fueron patentados junto con Dena Desarrollos, empresa donde se llevaron a cabo las investigaciones durante este doctorado.

**Acknowledgements**

First, I thank God! There is still a long way to go, but without Him, I would never have achieved everything I have already achieved. His company strengthens me, gives me peace, health, and wisdom.

To my parents Geraldo and Angela and to my brother Lucas. For their unconditional support since my first days. No words can describe my gratitude.

To my professor Joan Montanyà, for his valuable contribution in coordinating this work and for his enthusiasm and commitment to carry out the research. To my supervisor at Dena Desarrollos S.L., Victor Lorenzo, for all help and discussions provided during the development of this work.

To Angel Illa and Silvia Alés for all support given through Dena Desarrollos in everything needed for the execution of this investigation.

To my current and former colleagues at work, who helped me along this journey: Irene, Josep, Eva, Laura, Patricia, Sandra, Guillem, Joan and Aleix from Dena and Pol, David, José Andrés, Jesús, Oscar and Nicolau at the Lightning Research Group of the UPC. In particular, I would like to thank Enric Pons, Michele Urbani and Miguel Guimarães for all the encouragement, support, and collaboration along with the development of this work.

To the SAINT network for the good times sharing research and the experiences we had along this journey, especially to the seniors Christoph Köhn and Sander Nijdam, for all support and collaboration for the secondments. And the colleagues I met there, in particular Matthias, Ny, Shahriar and Adam.

To my friends around the world with whom I shared all my expectations, joys and frustrations. Thank you for the contribution in my personal development. This work is dedicated to Rhaissa, that from thousands of kilometers was so present in my daily life. To Aline, Pamela, Jaime, Raimefer, Josiane, Camila, Thelma, Fabrício, Pedro, Caio, Gyan, Anthony, Lucie, Sebastian, Barbara and the 'Choque⚡'. To all the ones that were not mentioned, but are part of my life, my sincere thanks.

This work has received funding from the European Union Horizon 2020 Framework Programme under the Marie Skłodowska-Curie Grant Agreement SAINT 722337.

## List of Abbreviations

| | |
|---|---|
| **ASIM** | Atmosphere-Space Interactions Monitor |
| **BNC** | Bayonet Nut Coupling |
| **CG** | Cloud-to-Ground |
| **CWL** | Center wavelength |
| **DC** | Direct Current |
| **DNL** | Downward Negative Leader |
| **DPL** | Downward Positive Leader |
| **EF** | Electric Field |
| **EMC** | Electromagnetic Compatibility |
| **ESR** | Early Stage Researcher |
| **FEDER** | Fondo Europeo de Desarrollo Regional / European Regional Development Fund |
| **FM** | Field Mill |
| **FWHM** | Full Width Half Maximum |
| **GLM** | Geostationary Lightning Mapper |
| **IC** | Intra-Cloud |
| **ICLP** | International Conference on Lightning Protection |
| **ISS-LIS** | International Space Station – Lightning Imaging Sensor |
| **ITN** | Innovative Training Network |
| **LI** | Lightning Impulse |
| **LINET** | Lightning detection Network (nowcast GmbH) |
| **MINECO** | Ministerio de Economía y Empresa de España / Ministry of Economy and Business of Spain |
| **MSCA** | Marie Skłodowska Curie Action |
| **MTG-LI** | Meteosat Third Generation Lightning Imager |
| **PMT** | Photomultiplier Tube |
| **PR** | Punta de Referencia / Reference rod |
| **RREA** | Relativistic Runaway Electron Avalanche |
| **SAINT** | Science and Innovation with Thunderstorms |
| **SI** | Switching Impulse |
| **SIPDA** | Symposium on Lightning Protection |

| | |
|---|---|
| **SMC** | Servei Meteorològic de Catalunya / Meteorological Service of Catalonia |
| **TGE** | Thunderstorm Ground Enhancements |
| **TGF** | Terrestrial Gamma-ray Flash |
| **UCL** | Upward Connecting Leader |
| **UV** | Ultraviolet |
| **VHF** | Very High Frequency |
| **YSA** | Young Scientist Award |

# Contents

## List of Figures

# 1 Introduction

## 1.1 Relevance and motivation

Lightning involves a complex phenomenon that influences the dynamics of the planet's atmospheric processes and whose occurrence has a relevant impact on society as a source of accidents, damage, and death (Rakov and Uman, 2003). Processes associated with weather conditions cause the movement of suspended water particles that result in the formation of charged clouds. Since the atmosphere is a good insulator, a great number of charges are build-up, which establishes an electric field within the thundercloud and from cloud to ground, that in its turn can produce favorable conditions for lightning.

As a result of the charges on the Earth's surface and its conductivity in fair weather, a background electric field of around 100-120 V/m persists in the continental regions (Harrison, 2011). The fair-weather electric field has diurnal and seasonal variations. The typical diurnal time variation of the electric field was first identified by measurements taken by the Carnegie ship in the 1920s (Harrison, 2013). Although there is a variation pattern with the universal time, the time when the electric field is at its maximum presents small differences, indicating changes in the longitude of maximum storm activity.

The enhancement of the electric field caused by the presence of charged clouds in the atmosphere affects the distribution of charges on the earth's surface. Notably, the first observed effect is the appearance of a layer of space charges of opposite polarity to the cloud's dominant charge, the corona layer. Storm clouds commonly produce an electric field of opposite polarity to the good-weather electric field, with significantly greater magnitudes. Grounded structures with sharp edges or corners also experience significant local electric field increase caused by the concentration of charges at their ends. Corona discharges are a phenomenon of the ionization of local spots on the surroundings of these structures, transferring electrical charges to the air (Chauzy and Raizonville, 1982). Figure 1.1 shows a scheme of the space charges that establish the background electric field in fair weather ($E_{FW}$) and stormy weather ($E_{SW}$).

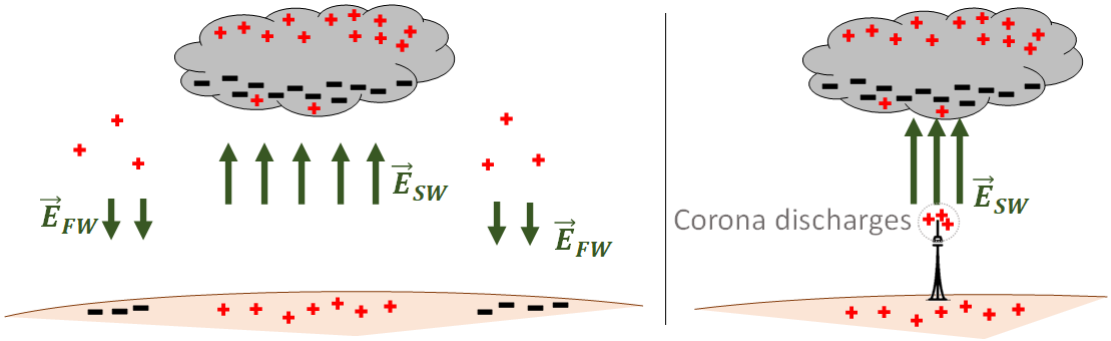


Figure 1.1 - Scheme of typical Electric field distribution and enhancement of local electric field caused by elevated structures.

The fast movement of charges through the plasma channels (leaders) that forges the discharges can affect the spatial electric field over long distances momentarily. During lightning strikes, the leader potential is nullified through a charge transfer process (return stroke) that significantly modifies the background electric field. In this context, the emergence of corona discharges and possible upward leaders from grounded structures produces signatures in the corresponding electrical current and the optical spectra (Gallimberti et al., 1974; Moore et al., 2003; Arcanjo et al., 2019; Schumann et al., 2019).

Continuous direct and indirect effects of lightning arise several issues related to the electrical protection of structures and equipment. The lightning rods are conductive elements electrically connected to the ground that bring the null potential to the top of buildings and structures to be protected. They aim to provide a safe path for the dissipation of energy associated with the lightning. Despite the considerable volume of investigations in this field, there are still important knowledge gaps in the topic, notably involving the processes that occur in the instants before and after the beginning of the return stroke, and the connection of upward and downward channels (attachment). Corona and point discharges that occur under high background electric fields can shield grounded structures and also play a key role in the striking point of lightning. In a certain way, such knowledge gaps come from the lack of experimental data of natural lightning, required to support the proposition of consistent interpretations about such processes and to validate models eventually proposed for their description.

## 1.2 Objectives

This PhD project is contextualized in the European program: Science and Innovation with thunderstorms (SAINT), being part of Marie Skłodowska Curie Action Innovative Training Network (MSCA-ITN-2016) funded by the European program Horizon 2020 (Grant agreement ID: 722337). SAINT is an educational platform within a multidisciplinary scientific network of scientists developed through the CAL FP5 project leading to the European space missions of ASIM, and the US mission ISS-LIS. The SAINT Training Program supports PhD education for

15 Early-Stage Researchers (ESR) within the environment of 8 universities, 8 industrial partners, and 3 agencies and research institutes. This research was carried out within the Lightning Research Group of the UPC, and with the participation of Dena Desarrollos, in Terrassa, Spain.

In this project, several quantities associated with lightning phenomena are studied, focusing on the electrical current and the optical signature of lightning-like discharges performed in the laboratory.

The specific objectives accomplished during this PhD are:

- To study the properties of corona current and point discharges from sharp grounded tips under high background electric field in the laboratory and in natural conditions.
- To investigate the influence of space charges produced near grounded structures under high electric field conditions on lightning upward leaders.
- To study the features of streamers and leaders of laboratory discharges, mainly with regard to its electrical current and optical signature.
- To make a design of a sensor that will be a core for a new device that can integrate information of corona currents with lightning protection.

## 1.3 Thesis structure

This work proposes an investigation of the properties of streamers associated with corona discharges from grounded rods in the laboratory and in the field, as well as the optical characteristics of the lightning-like discharges produced in laboratory. This document is divided into 6 chapters, planned as a compendium of two articles.

Chapter 1 presents an introduction and the objectives of the work performed during the PhD. Chapter 2 focuses on the state of the art of the main concepts discussed in this work, the corona discharges and the lightning phenomena. Chapter 3 details the experimental investigation performed in the laboratory, presenting instrumentation and methods.

Chapter 4 summarizes the results from the publications with the corresponding post-prints of the accepted manuscripts. The first article is focused on the current signatures of corona and their correlation with the background electric field and wind speed. Unprecedented data of current measurements were performed and revealed the features of the discharges. In the second article, the optical signatures associated with streamers and leaders of laboratory discharges are studied in detail. The optical detections are particularly focused on two of the strongest emissions of lightning: the blue, mainly due to emissions of the second

positive system of the nitrogen at the wavelength of 337 nm, and the red, caused by the neutral oxygen triplet emissions at the wavelength of 777.4 nm.

Chapter 5 presents the conclusions of the thesis and shows a list of all related publications and presentations performed during the PhD. The appendix contains applications and other publications derived from this work. Detailing the development of a small current sensor for corona discharges, experiments of corona discharges performed in a controlled environment during an external internship, and the use of photometers to determine the leader initiation.

# 2 State of the art

## 2.1 Corona discharges

Corona discharges from an electrode originate from the collision of free electrons accelerated by high levels of the electric field in the surroundings and hence triggering avalanche ionization in the strong electric field area. The initial free electrons that are the seed for initiating the ionization process can be due to cosmic radiation or a radioactive background (Bartnikas, 1979). The investigation and improvement of lightning protection systems require a better understanding of corona discharges. Protection systems that employ a single conductor date back to the 18th century when Benjamin Franklin conducted kite experiments and demonstrated the connection between lightning and electricity. His research led to protecting buildings from lightning strikes with lightning rods. Research on lightning physics and lightning protection continues to improve the understanding of the phenomena and the strategies used to protect structures, aircrafts, and lives.

Many studies were conducted on the effects of the electric field enhancement below thunderclouds (Whipple and Scrase, 1936; Hutchinson, 1951; Chauzy and Raizonville, 1982; D'Alessandro, 2009). The development from the simple corona discharge through the stages of glow corona and streamer corona and finally to a hot leader is a remarkably critical part of the lightning attachment process.

Measurements of the corona current through a grounded needle under thunderstorms reported an average current of a few microamperes (Whipple and Scrase, 1936; Hutchinson, 1951). An electric field threshold is required for corona inception, and the average current increases with the increase of the background electric field. The geometry of the system, and weather conditions such as humidity and wind can significantly affect these parameters. D'Alessandro (2009) conducted a more recent study on corona discharges from a sharp point under a thunderstorm, finding an average current of a few microamperes and electric field thresholds of about 0.5 kV/m to 1.5 kV/m. His experimental data indicated that higher wind speeds may lead to an increase in the average corona current and a decrease in the electric field threshold for corona onset.

The features of corona discharges according to the tip of the electrode have been extensively investigated to discuss the effectiveness of lightning protection systems. Moore et al. (2000 and 2003) showed measurements of point discharges

from different types of lightning rods in response to lightning strikes nearby. Sharper rods presented low amplitude pulses with high frequency, whereas blunt rods presented higher amplitude pulses with lower frequency, much closer in time to the lightning impact. They suggested that blunt rods could be more efficient as a receptor for lightning strikes than sharp rods, but that has not been successfully proven in other works.

Irregularities on the surfaces of grounded structures can provide conditions for corona discharges that generates ions and form a space charge layer that attenuates the electric field at the vicinities of grounded conductors. This can affect the initiation of upward leaders and even change the point of lightning impacts (Aleksandrov et al., 2001; Becerra et al., 2007; Becerra, 2014; Bazelyan, 2015; Guo and Zhang, 2017). Investigations have indicated that the corona layer could delay the streamer inception from structures, although this would not cause severe effects (Becerra, 2013; 2014). In elevated rotating structures, such as wind turbines, observations suggested that the movement of these structures avoids the shielding effect caused by space charges, increasing the probability of lightning strikes (Montanyà et al., 2014).

### *2.1.1 Positive streamer corona*

In positive corona, negative ions and electrons present in the air are absorbed by the needle electrode, while positive ions drift away from it (Chang et al., 1991). The conical shape observed is composed of the ionization region and the drift region. The ionization region is dominated by positive ions and electrons, in the strongest electric field (Loeb, 1948; Morrow, 1997). These ions are accelerated in the electric field, drifting away from the tip, causing an “electrical wind” (Robinson, 1961; Moreau and Touchard, 2008; Moreau et al., 2018). The mechanism for sustaining the discharge is activated with energized electrons, moving towards the tip that collide with molecules in the air, generate excited molecules and new positive ions and electrons. When returning to their ground states, the molecules emit photons that trigger a photoionization process in farther locations, producing electrons that also are accelerated towards the needle. In this path, impact ionization and new excitation of atoms and molecules sustain the process (Zheng et al., 2015).

The initial stage of positive corona is a pulsating regime known as burst pulse corona (Chang et al., 1991). As the electric field increase further, the phenomenon reaches the glow corona stage, in which the accumulation of space charges leads to a steady-state uniform corona glow around the needle electrode. For an even higher electric field, intense onset streamers develop, constituting a new region called breakdown streamer. These streamers can create an unstable region that leads to the ionization across the entire gap and trigger a spark discharge (Trichel, 1939; Gallo, 1977; Chang et al., 1991).

### 2.1.2 Negative streamer corona

In negative corona, seed electrons are present in the air due to cosmic radiation and other phenomena. They are accelerated and collide with neutral molecules, creating positive ions and an electron layer closer to the tip of the electrode, forming an ionization layer. Outside this region, with the decrease of the electric field, attachment creates a cloud of negative ions, in the drift region. The current reaches a maximum value and as soon as the process of deposition of positive ions on the corona electrode starts, and subsequently, decreases, as well as the ionization and the avalanche process (Trichel, 1938; Loeb, 1948; Dordizadeh et al., 2015). The number of negative ions in the air gap increases after the pulse, and they move away from the tip, leading to another increase of the electric field near the electrode, restarting the process (Dordizadeh et al., 2015).

The pulsating regime of the initial stage of negative corona is known as Trichel Pulse corona (Trichel, 1938). The increase of the applied electric field leads to the superposition of the many pulses one into another, developing a pulseless stage. This stage can be unstable in normal temperature and pressure conditions and the discharge can rapidly evolve to a spark (Chang et al., 1991).

In reported laboratory experiments, different configurations based on the electrode geometries have been used to perform experiments, the most common being point-to-plane (e.g. Trichel, 1938 and 1939; Gallo, 1977; Dordizadeh et al., 2015). In these cases, the high voltage electrode is typically a needle, and the second electrode is a plate grounded through a shunt resistor. The so-called corona current is the current measured through the resistor. For the initial stages of corona discharge (burst corona and Trichel pulse corona), the current is observed as a regular train of pulses with a short rise time (tens of nanoseconds), and time decay in the order of few hundreds of nanoseconds and rather long inter-pulse time (a few microseconds to milliseconds, depending on the configuration of electrodes and the voltage applied) (Dordizadeh et al., 2015; Wang et al., 2018).

### 2.1.3 Laboratory discharges

Different stages of electric discharges can be achieved in the laboratory at atmospheric pressure. Three factors play a key role in the discharges: gap distance, electrode geometry, and electric field level achieved through the applied voltage. In the papers presented for the thesis compendium, the streamer and leader stages are explored more in detail.

Figure 2.1 shows a scheme of concept of laboratory discharges. Electric field enhancement can provide the stage change depending strongly also on the geometry of electrodes and gap distance. For example, in cases with a very short gap, electron avalanches can turn rapidly into streamers that can directly evolve to a spark. Streamers can also evolve directly into a leader depending on the

geometry and electric field level. Glow coronas can be achieved in a steady state when the electric field reaches a quasi-DC level that is insufficient for the streamer-to-leader transition, they can have streamer bursts at their ends.

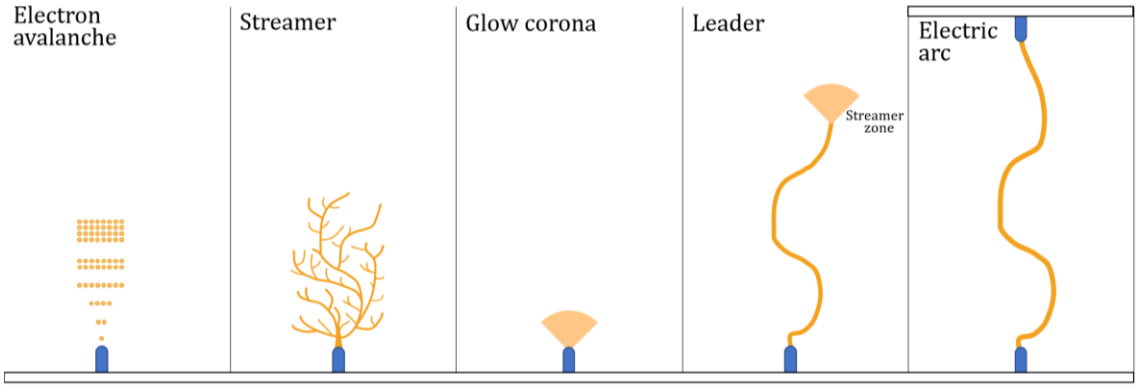


Figure 2.1 - Scheme of concept for laboratory discharges (out of scale).

### *Electron avalanches:*

Many species play a critical role in electrical discharges: atoms and molecules (excited or not), ions (positive and negative), photons, and free electrons. The discharge process is governed by free electrons because of their features, such as the drift velocity, which is about two orders of magnitude higher than ions for the same electric field level (Liu, 2017). Free electrons can be produced through many processes: impact-ionization, detachment, and photoionization. Instead, they can be lost through collision, recombination, and attachment.

The avalanche process consists of the strong acceleration of the electric field provided to the free electrons. Subsequently, they collide with other atoms in the medium, thereby ionizing them through impact ionization. A chain reaction generates additional electrons, and the process continues. If secondary electrons are produced during the avalanche, the avalanche can grow and evolve to the streamer stage, depending on the electron density of the avalanche.

### *Streamers:*

Streamers are moving ionization fronts that can have complex shapes (finger / tree-like). They are usually characterized by pulsating discharges that may have a superimposed DC current. They are part of the cold atmospheric plasma discharges that can be precursors of spark discharges. Nevertheless, they can also exist individually depending on conditions and have many industrial applications due to their chemical properties (ozone generation, medicine, and others).

Streamers are a transient phenomenon, existing for a very brief period. They can penetrate areas where the background electric field is below the ionization threshold. They present good conductivity, are internally neutral and

composed of a thin layer of space charges, that strongly enhance the electric field at their tips. Generally, the propagation of streamers follows electric field lines, though in opposite directions since electrons drift opposite to the local electric field vector. In many cases, streamers can deviate from the idealized paths, since their own charge change the electric field distribution, also causing a repelling effect between neighboring streamers (Nijdam et al., 2020).

### *Glow corona:*

Glow corona or pulseless corona is the stage of discharge in which a glowing envelope layer appears around the emitting electrode. When this stage is stationary, the glow often changes with time into the tuft form, a process associated with successive avalanches through more efficient mechanisms (Chang et al., 1991). The transition from single filament (streamer) to transient glow is characterized by the sudden decrease in the pulse repetition frequency and the abrupt increase in the current amplitude (Wu et al., 2018).

Figure 2.2 shows a picture of a typical experiment performed with the Corona Finder camera. This device is a low distortion quartz UV lens that enhance the ultraviolet component from the discharges and filters most of the visible spectra. On the left side, the rod in a plate-to-point experiment, with background lights on. On the middle, when a high DC background electric field is applied, small filamentary streamers are observed from the tip of the sharp rod. On the right side, when the applied voltage increases, the average current also increases but the shape of the discharges converts into a tiny glow spot around the tip of the grounded electrode.

Figure 2.2 - Sharp rod (left) producing streamer discharges (middle) and tiny glow corona (right)-

### *Leader:*

Leaders are highly conductive channels of ionized gas that propagate in the direction of the electric field (or otherwise) to regions charged opposed to the leader tip. Often, in laboratory and in the nature, they can split and form branches in a tree-like shape (Bazelyan and Raizer, 1998; Rakov and Uman ,2003; Biagi et al., 2009; Tianyu et al., 2020).

Figure 2.3 shows two pictures taken of the same discharge revealing the main leader features. The experiment corresponds to a plate-to-point setup with a Marx generator producing a fast-rising negative voltage. The picture on the left is taken with a Xybion camera ISG-250, for a very short-time exposure (10

microseconds), when the current through the round rod rises from 0 to 15 amperes. At the time this image is taken, one can observe an upward propagating leader with several branches and a glow-like zone ahead of it, correspondent to the zone previously ionized by streamers. On the right side, a still picture of the entire discharge. During the breakdown, all channels previously forged by the leader reilluminate due to the sudden change of potential along the entire leader and the charge transferred in the course of this stage.

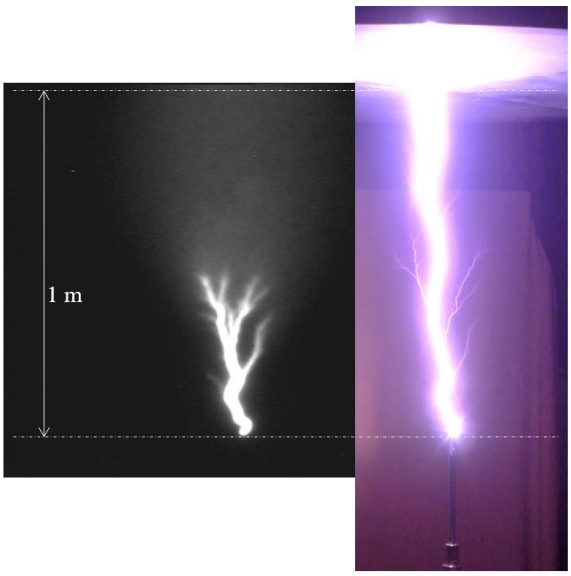


Figure 2.3 - 10 microsecond picture of an upward leader development (left) and later spark discharge (right) produced with a Marx Generator.

The streamer-to-leader transition has been investigated for many researchers and many models have been created to represent the physical process observed in laboratory discharges and lightning (e.g., da Silva and Pasko, 2013; Arevalo and Cooray, 2017). In this process, the thin ionized streamer is forced by a strong current and heats the ambient gas and increase the electrical conductivity of the channel. This transition happens not only during the leader inception but during the leader propagation, that is usually directed by a streamer zone.

The connection of an upward and downward leader, named attachment, produces a common streamer zone between the two leaders. The lightning attachment process is critical for the protection of electrical equipment and structures. In section 2.2, the propagation features of leaders and the attachment process are revised in more detail.

### *Electric arc:*

When the entire path between the anode and cathode are ionized by streamers or leaders, the electric breakdown is established. The current flow of the discharge is characterized by an impulsive waveform with rise time of a few microseconds and time duration that can vary from microseconds to milliseconds, depending on the setup.

The arc channel is a plasma conductor and a great amount of energy from the arc is spent on thermalizing the channel. At atmospheric pressure, electric arcs have much higher current and temperature than for leader channels. Kieu et al. (2020; 2021) reports temperatures in the range of 25 000 k for the electric breakdown of laboratory discharges, similarly to the estimated temperatures of the lightning channel (Zhang et al., 2020).

## 2.2 Lightning

In this section, five topics associated with lightning discharges are revised: the lightning initiation process; the bidirectional leader theory; the thunderstorm cloud models that are responsible for the enhancement of the background electric field; leader propagation and attachment in negative cloud-to-ground discharges and the features of typical lightning currents.

### *2.2.1 Lightning Initiation*

Despite the progress achieved by scientific research into lightning, the main issue still under discussion is the initiation of lightning in clouds. It is extremely difficult to carry out reliable measurements *in situ* of variables associated with the formation of discharges, and the reproduction of conditions of temperature, pressure, humidity, and particle disposition as in clouds in the laboratory is practically infeasible.

The theory based on effects of hydrometeors considers that particles can provide electric field enhancement for streamer inception from such particles. From in-cloud measurements, concentrations of different particles increase significantly during thunderstorms, making it assumable that there are clusters of hydrometeors of different sizes. Laboratory experiments have been performed trying to explore lightning initiation from suspended conductive particles or ice particles (e.g. Petersen et al., 2015; Mazur, 2015).

The second theory is associated with cosmic rays that could initiate a relativistic runaway electron avalanche breakdown (RREA) (Gurevich, 1961; Gurevich et al., 1992; Gurevich and Zybin, 2001). That would provide energy enhancement for ionization processes inside the cloud, leading to the initiation of lightning streamers/leaders.

Chilingarian et al. (2017) analyzed the so-called Thunderstorm Ground Enhancements (TGEs). The energy spectra before and after the lightning demonstrates that the high-energy part of the TGE energy spectra disappears just after lightning, suggesting that RREA in the thundercloud assist the initiation of the negative cloud-to-ground lightning. Petersen et al. (2008) and Dubinova et al. (2015) proposed hybrid mechanisms that present RREAs that provide electric field

levels sufficient for the initiation of streamers from ice particles, subsequently leading to the leader inception, combining the two theories.

The latest research on lightning initiation is heading for fast breakdown events (see chapter 12 in Mazur, 2016 book). A volumetrically distributed system of positive streamers with very high current precedes intracloud discharges (Rison et al., 2016) and it is likely to be present in the initiation of lower altitude events (such as cloud-to-ground discharges). Further, Stolzenburg et al. (2021) showed with high-speed video observations of intracloud events that the lightning initiation produce almost no visible light, supporting that they could be associated with streamer discharges. Many questions regarding this mechanism are still open (e.g. Dwyer and Uman, 2014; Lyu et al., 2019; Kostinskiy et al., 2020)

### *2.2.2 Bidirectional Leader*

The model of the bidirectional leader was initially proposed by Kasemir (1950), and consolidated in his later work (Kasemir, 1960). These investigations introduce a qualitative model that establishes the formation of the negative cloud-to-ground discharge from an initial disruption in a region of a high electric field within the thundercloud. This initial discharge configures a bipolar leader with zero total net charge.

The charge distribution in the bipolar channel is determined by the electrical potential of the environment. Under the effect of very intense electric fields in the region in front of the two ends of the bipolar leader, disruptive processes extend it in both directions. In this model, the positive and negative charges are distributed by virtue of electrostatic induction and tend to be deposited at the upper and lower ends, respectively. The leader can propagate as long as the potential difference between the leader and the cloud environment allows, and the zero net charge condition persists. In negative cloud-to-ground lightning, the weaker positive charge region is penetrated by the negative leader which then propagates toward the inductively charged ground.

As assumed in Mazur and Ruhnke (1998), the leader does not collect charges from the cloud. Positive charges (positive ions) and negative charges (electrons) are produced by disruptive processes at the ends of the bipolar channel by ionization. The charge separation process is caused by the electric field external to the channel, produced by the charge distribution of the cloud. A graphical representation of the conditions assumed in Kasemir (2012) is shown in Figure 2.4. Parts (a) and (b) correspond to a negative cloud-to-ground discharge, during the development of the bidirectional leader and after the attachment, respectively. Parts (c) corresponds to intracloud lightning at the beginning of the leader propagation.

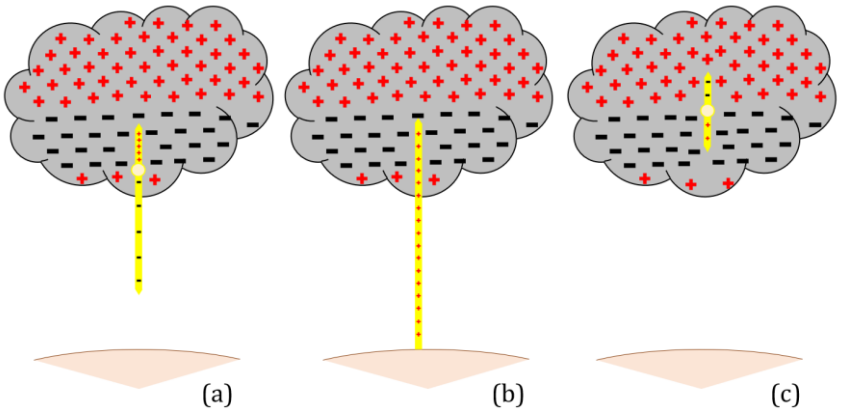


Figure 2.4 - Leader scheme for (a and b) negative cloud-to-ground lightning and (c) intracloud lightning.

Based on high-speed video camera analysis, Montanyà et al. (2015) and Warner et al. (2016) observed cases of open-air development of bidirectional leaders, close to a previously established leader. In these situations, the differences in the propagation of the positive and negative ends were clearly identified. Other recent works conducted observations that show the leader's bidirectional evolution (van der Velde and Montanyà, 2013; Tran and Rakov, 2016).

### *2.2.3 Thundercloud models and implications*

The formation of thunderclouds occurs under turbulent environments. Frequent upward currents of air (updrafts) transport water particles to high regions of the storm. In the collision between ice particles within the cloud (hail, ice, graupels, and water particles), charges are removed from the ascending particles and collected on the descending ones. Hence, ordinary thunderstorms are negatively charged at their base and positively charged at their top.

The electric potential and electric field distributions in the atmosphere are factors that determine the initiation and development of lightning leaders. They depend on the position and intensity of the cloud charges. Thundercloud models propose a charge distribution obtained from electric field measurements performed at the ground level and inside the clouds (using balloon probes). The significant variability in the measurements inside thunderclouds results from differences between individual storms, storm type, the various phases within the same storm, and the positions of the balloon (Stolzenburg and Marshall, 2009; Karunarathna et al., 2017). Such models agree with the simplified representation that uses a tripole charge structure, consisting of a negative charge on the main part of the cloud, a positive charge above it, and a smaller portion of the positive charge below it.

The electric field intensity $E$ due to a system of charges can be calculated by replacing the perfectly conducting ground with the image of charges and using the principle of superposition. In this case, the total electric field at a distance $r$ from the point charge $Q$, placed at a height $H$ is calculated as

$$|E| = \frac{|Q| * H}{2\pi\, \varepsilon_0\, (H^2 + r^2)^{\frac{3}{2}}} \qquad [V/m] \tag{2.1}$$

In which $\varepsilon_0$ is the permittivity of vacuum, equals to $8{,}85 \times 10^{-12}\ F/m$.

An elementary tripole model, developed by Rakov and Uman (2003), uses three point charges $Q_P$, $Q_N$ and $Q_{LP}$, at different heights $H_P$, $H_N$ and $H_{LP}$, corresponding to the positive, negative, and lower positive charge cores, respectively. Figure 2.5 shows the structure placed on a flat ground and the electric field at the ground level calculated for each of the charges ($E_P$, $E_N$, $E_{LP}$ and $E_{TOTAL}$) according to the potential gradient convention, in which a downward electric field is considered positive.

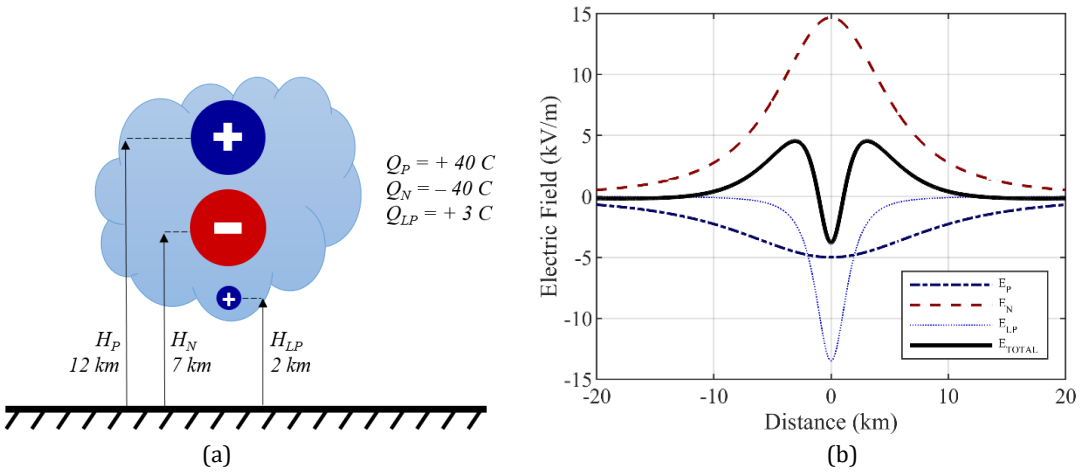


Figure 2.5 - Representation of the tripole charge model (a); electric field at ground level for tripole structure (b). Adapted from Rakov and Uman (2003).

The tripole charges produce an electric field of -3.8 kV/m at the ground level, on the axis of the structure. Moving horizontally away from the axis, the magnitude of the electric field decreases and changes polarity, indicating the greater influence of the negative charge of the tripole, farther from the axis the magnitude of the electric field decreases.

Another thundercloud model presented by Mazur and Ruhnke (1998) consists of a uniform cylindrical charge distribution. In this reference, the thundercloud electric charge model was used for explaining the development of the leaders, but it might not be realistic. Figure 2.6 shows the cylindrical structure for representing the cloud. It comprises two main regions with 10 km of diameter, 50 C (region A) and -80 C (region B). Two secondary regions represent the storm cell, with -10 C (region C) and 3 C (region D), extending 1 km horizontally. On the right side of the figure, the electric field magnitude varying with the horizontal distance is presented. Below the axis of the thundercloud, the electric field is -25.7 kV/m. This value is higher than that obtained by the tripolar model shown in Figure 2.5, although it is consistent with measurements of the electric field in

storms if we consider that space charges protect the electric field, decreasing it to about a tenth of a magnitude (Bazelyan et al., 2015).

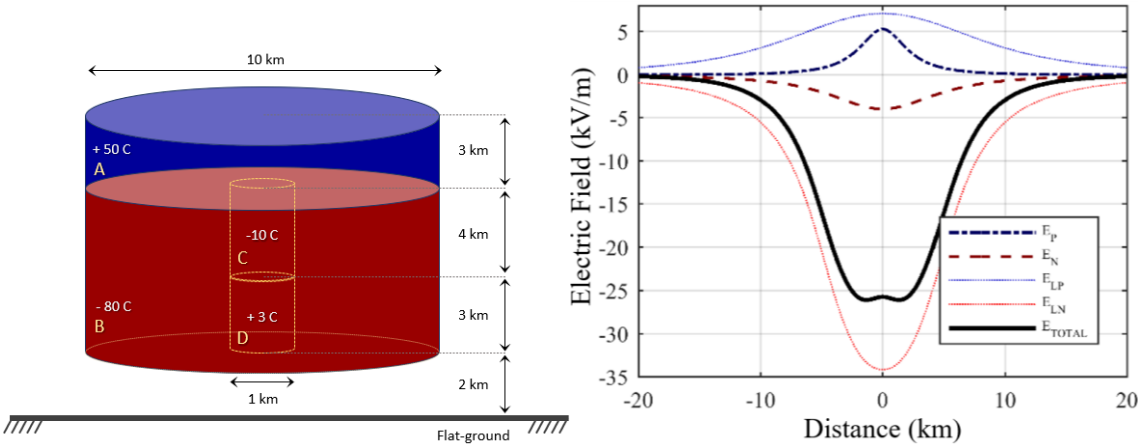


Figure 2.6 - Cylindrical structure representing the storm cloud and electric field profile for different distances from the thundercloud axis. Adapted from Mazur, 1998.

The distribution proposed by Mazur reproduces the typical profile of the distributions of electric potential and electric field in the atmosphere along the axis of the cylinder. Figure 2.7 shows the electric field and potential profile along a vertical axis when the charged structure is placed 2 km above the ground level. The maximum electric field values occur at the edges of the positive and negative regions of the thundercloud's cylindrical structure, which is correspondent to altitudes of 5 and 9 km. The first region is attributed to the region of initiation of cloud-to-ground lightning and the second, the region of intracloud lightning.

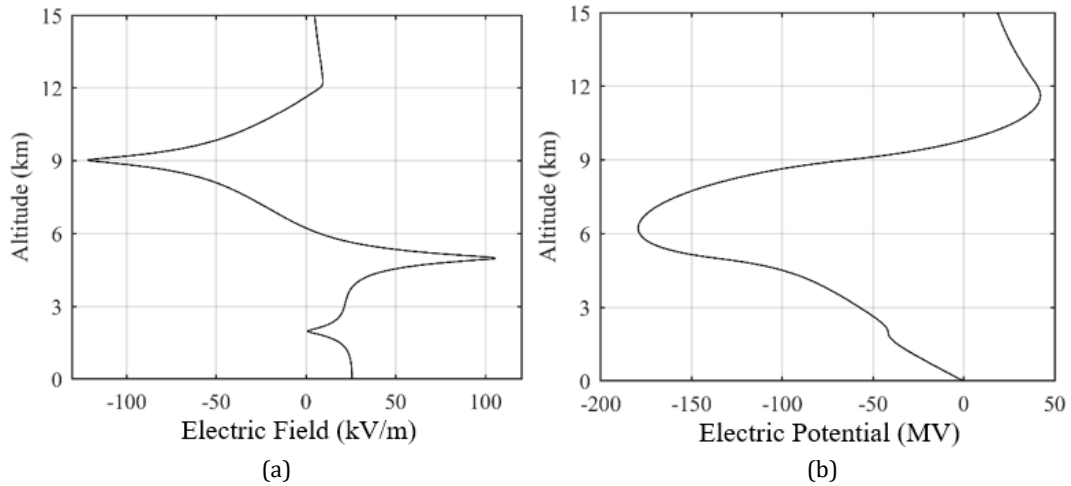


Figure 2.7 - Vertical Electric Field (a) and Electric Potential (b) on the thundercloud axis.

Costa et al. (2021) employed the charge distribution proposed by Mazur to estimate the striking distance to a flat ground as a function of the return stroke charge. Although their approach is based on several simplifying assumptions, substantial physical aspects of the leader development and the return stroke charge are considered such as the bidirectional leader model and the

characterization of the return stroke process as the addition and redistribution of charges in the leader.

Given the complexities of direct and indirect measurement of natural lightning currents, the electric field at ground level is the main parameter used in the detection of atmospheric activity, as it contains signatures of the formation and evolution processes of lightning. Electric field measurements can be implemented at the ground level, through specific equipment such as the field mill, used to monitor the absolute values of the ambient electric field, before and after the variations associated with lightning strikes, and the whip or plate antennas, capable of measuring their fast variations (Rakov and Uman, 2003). Instrumented balloons and airplanes also perform measurements of the electric field inside the thunderclouds, which is a more complex task (e.g. Marshal and Rust, 1991; Stolzenburg and Marshal, 2008). These measurements allow the estimation of the spatial charge density for other modelling strategies and studies of the role of the discharges in rearranging the ambient electric field inside thunderclouds (e.g. Riousset et al., 2007).

Using a Lightning Mapping Array for mapping very high-frequency sources of leaders, López et al. (2017; 2019) computed the duration and extension of several lightning flashes and reconstructed the temporal development of the cloud structure. Tropical thunderstorms analyzed in Colombia revealed the typical tripolar charge structure. Furthermore, the initiation of the flashes was found to be in a wide vertical range (from 6 to 14 km of altitude).

Based on several measurements, Uman (1969) developed a characteristic profile for the electric field of negative downward lightning for different observation distances at the ground level. According to this profile, there are three phases of the electric field identified prior to the lightning strike. Each of these periods is associated with a stage in the process of forming the leader.

In the representation shown in Figure 2.8, B (breakdown) corresponds to the initial disruption that occurs inside the cloud and initiates the propagation of the downward leader, I (intermediate) refers to the slow variation of the electric field observed when the leader propagates inside the cloud and L (leader) refers to the propagation of the channel outside the cloud, towards the ground.

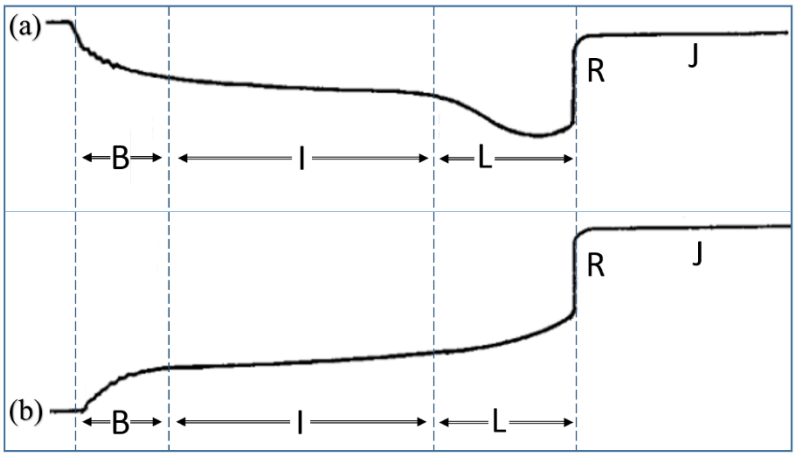


Figure 2.8 - Electric field profile illustrating the typical stages of a negative downward discharge at a representative distance of (a) 2 km and (b) 5 km. Adapted from Uman (1969).

Two other phases are considered in Figure 2.8: The R phase corresponds to the return stroke interval and the J phase represents a slow variation of the electric field value after the flow of the first (or only) return stroke.

## *2.2.4 Negative cloud-to-ground discharges*

### *Lightning leaders*

The lower portion of the floating bipolar leader corresponds to the Downward Negative Leader (DNL), which is negatively charged, determines the macroregion of the striking point and is responsible for the enhancement of the electric field at the ground level. This increase in the electric field can lead to the emergence of a positive Upward Connecting Leader (UCL), which evolves and eventually connects to the downward leader. The UCL defines the exact point of incidence of lightning.

Biagi et al. (2009) and Hill et al. (2011) verified elements that precede the development of DNL in negative discharges. The formation of floating plasma bodies (stems) was detected in front of the corona region of the negative channel. Such observations coincide with results obtained through laboratory experiments for the extension of negative channels (Bazelyan and Raizer, 2000). Based on these observations, Hill et al. (2011) presented a schematic model that represents the stages of propagation of the negative leader in lightning strikes, as seen in Figure 2.9.

The formation of floating light segments with estimated lengths between 1 and 4 m in front of the corona region of the negative channel (from 1 to 10 m away) was reported by Biagi et al. (2010). From Figure 2.9 the negative channel is developing (1). Then, a floating channel is observed (2), which is preceded by stems in front of the DNL. A corona region (3) begins to establish that precedes the effective connection between the downward leader and the floating channel (4).

After the connection, the leader step is consolidated, with the consequent propagation of a light wave from the lower end of the downward leader (5).

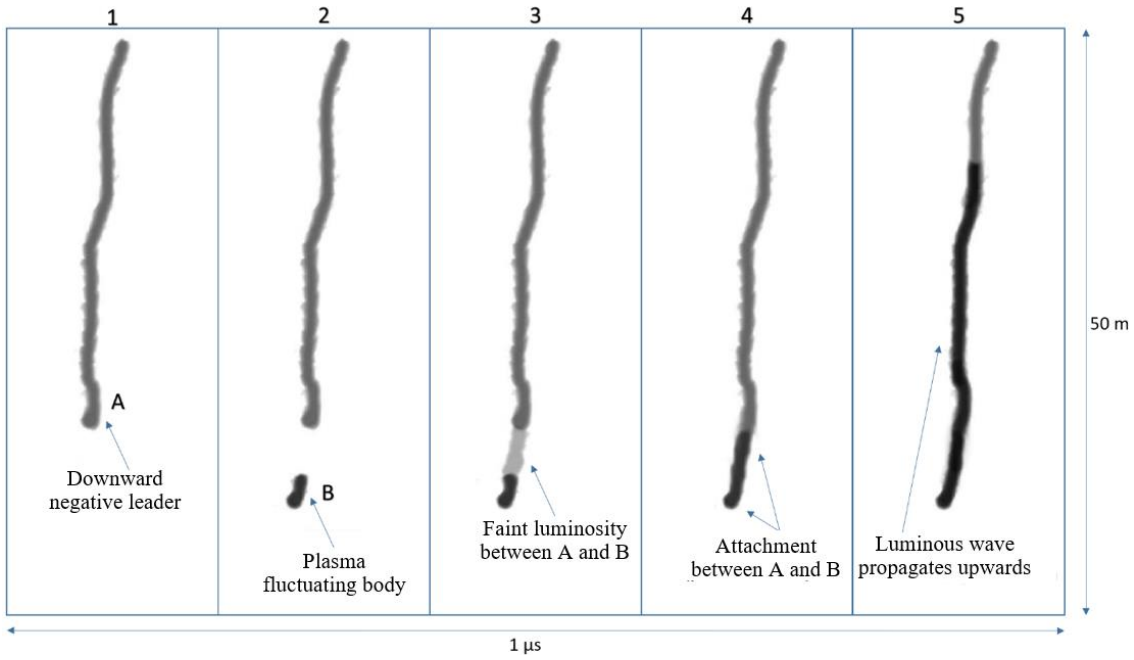


Figure 2.9 - Negative leader stepwise propagation model. Adapted from Hill et al. (2011).

Laboratory tests indicate that the common propagation mode observed for positive leaders is well defined: the development of the channel occurs from the progressive increase in temperature at its tip, caused by the confinement of the bases of several streamers in this region, which results in processes continuous extension, without abrupt variations in its geometry (Bazelyan and Raizer, 2000; Rakov and Uman, 2003; Mazur, 2016).

The observation of current profiles in the initial phase of upward lightning is evidence of the continuous propagation of positive channels. In the initial moments of the current waveform of upward discharges induced by close negative discharges, it is possible to detect the presence of unipolar current pulses, superimposed on a measured direct current. Some authors attribute these pulses to a stepwise propagation of the positive leader. However, in self-initiated upward lightning, these pulses are not detected. In such a way, the current pulses cannot be attributed to the development of positive channels but the induced effect that negative leaders have on the grounded structures.

Guimaraes (2017) considers that, if the existence of induced pulses of current in positive upward leaders that propagate continuously is assumed, the same characteristics attributed to the propagation in steps would be observed (such as space leaders/stems). It is possible to identify luminosity due to the surge current induced along the channel, which does not corroborate the development in steps of the positive channel. The detection of magnetic pulses and pulses irradiated from the electric field can originate both from the current induced in the

upward leader, as well as the current flowing in the downward leader when new steps are formed. Likewise, Saba et al. (2015) observed pulses in electric field records corresponding to the incidence of positive discharges, in the final phase that precedes the attachment. Using synchronized video records, it was possible to observe that such pulses appear from the detection of the negative upward leader starting from the grounded structure, therefore, they would be associated only with the evolution of the negative channel and could not be attributed to the approach of the downward positive leader.

Based on the records and analyzes previously reported in the literature, Guimaraes (2017) developed a schematic model for the evolution of the negative downward leader and the emergence of the positive upward leader, highlighting the behavior of the current and the electric field in this phase, as shown in Figure 2.10.

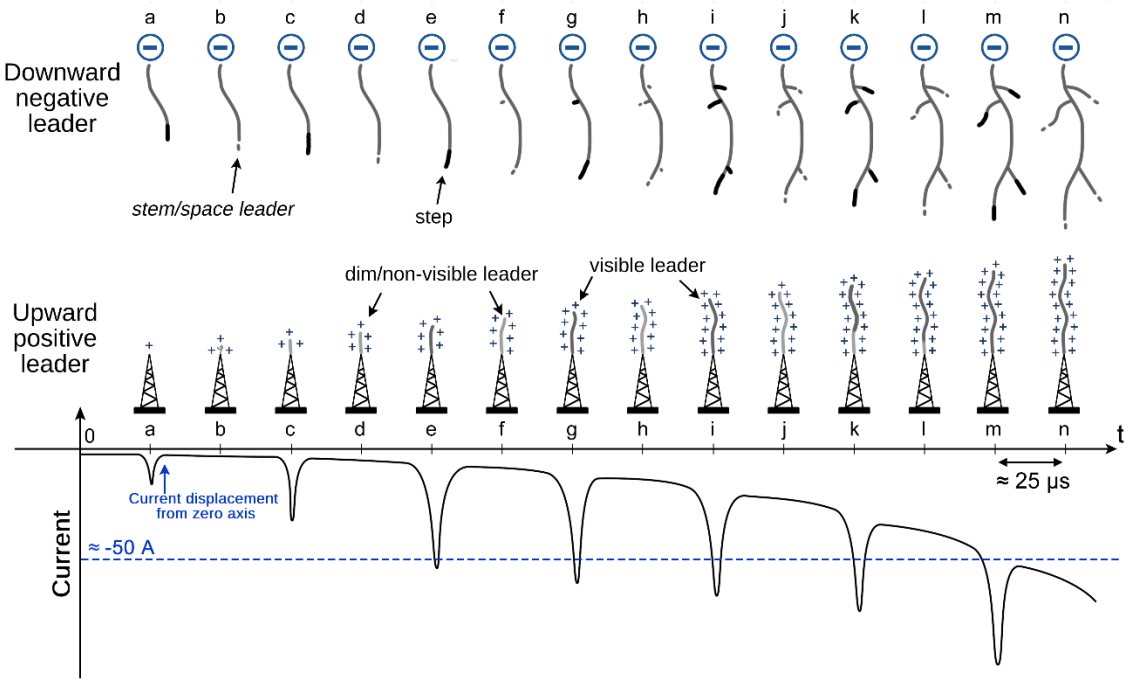


Figure 2.10 - Scheme of the pre-return stroke phase. Adapted from Guimaraes (2017).

In the initial stage of development of the downward leader, only pulses of current are induced along with the grounded structure, increasing the charged deposited at the upper end of the structure (a). When the electric field at the tip reaches a critical value, there is a low intensity electric current flow corresponding to the development of corona discharges in the structure (b). Current pulses induced when there is a continuous component of the electric current can induce the sustained formation of the upward leader (c). However, such a channel is still imperceptible (d) and becomes visible only when induced current pulses exceeding -50 A are recorded (e). The positive leader persists in developing continuously (f-j) until the intensity of the continuous current reaches a level that

makes the channel sufficiently visible regardless of the pulses induced by the descending channel.

### *Lightning attachment*

Despite outstanding advances in lightning research, another topic that remains poorly understood is the lightning attachment phase, which is the transition between the leader and the return stroke stage. Concepts associated with lightning protection such as the electrogeometrical model, rolling sphere method, and striking distance depend on a thorough knowledge of the attachment process. Saba et al. (2017) investigated events of lightning attachment to common buildings and determined typical parameters used in lightning attachment models and protection standards such as the speed of downward and upward leader and the striking distance.

Rakov and Tran (2019) present a comprehensive review of detailed observations of the breakthrough phase performed in natural lightning, rocket-and-wire triggered lightning and long sparks. The attachment process begins when the streamers zones of the connecting leaders are in contact with each other. Kostinskiy et al. (2016) presented observations of the connection of positive and negative leaders in meter-scale electric discharges generated by clouds of negatively charged water droplets. They revealed that leaders can branch inside a common streamer zone that connects the downward and upward leaders. Another important finding was that the downward leader can connect to the upward leader below its tip, such as reported by Lu et al. (2013) for natural lightning.

Figure 2.11 shows a frame with a time exposure of 80 ns taken in a point-to-point discharge performed with the Marx Generator in switching impulse mode. The picture is taken approximately 200 ns before the breakdown, when preliminary connections between the leaders are consolidating (see enhanced view on the right side). This acquisition was performed during the laboratory investigations of this work. Rakov and Tran (2019) showed pictures of negative sparks in a 5.5-m gap with the view of stem/streamers inside the common streamer zone, before it is completely bridged by the hot channels of the connecting leaders.

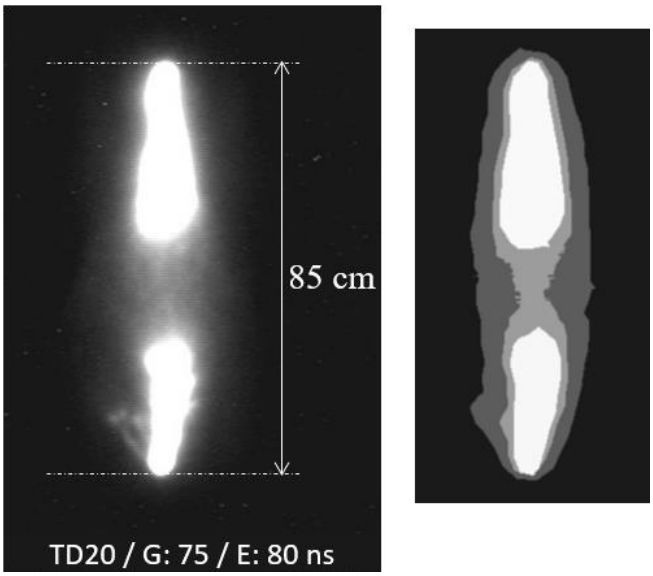


Figure 2.11 - Connecting zone in laboratory spark. Raw B&W picture (left) and enhanced view (right).

### *2.2.5 Lightning currents*

The first recordings of lightning current waveforms were obtained using tethered balloons in Russia (Stekolnikov and Valeev, 1937) and in England (Davis and Standring, 1947). Later, instrumented towers emerged as one of the preferred methods for studying natural lightning (Berger et al., 1975; Hussein et al., 1995; Diendorfer et al., 2000; Heidler et al., 2001; Guimaraes et al., 2014; Romero et al., 2012).

The most common types of transducers used in instrumented towers are the shunt devices and the Rogowski and Pearson coils. The position of current transducers may vary, however, most commonly, they are installed at the base of the tower or at the top. The number of current measurement stations installed worldwide is relatively small. The Monte San Salvatore station installed since 1958 in Lugano, Switzerland, constitutes the largest database available internationally in lightning currents.

Lightning is mainly classified into intracloud (IC) discharges and cloud-to-ground (CG) discharges. Some authors also consider a cloud-to-cloud type, but in general, since the clouds do not correspond to a solid and well-defined volume, the discharges that do not have a striking point on the ground are classified as intracloud.

Intracloud lightning accounts for about 70% of the total discharges. Since the severe effects of lightning are associated with the direct incidence of strikes, the effects of intracloud lightning are related to irradiated electromagnetic waves. The remaining 30% of discharges are cloud-to-ground, and among them, negative CG discharges and negative upward lightning are the most observable events (Rakov and Uman, 2003). Table 2.1 reviews a simple classification of lightning.

Table 2.1 – Lightning phenomena classification

| | | |
|---|---|---|
| **Intracloud discharges** | -- | -- |
| **Clout-to-Ground discharges** | Negative | CG Lightning |
| | | Upward Lightning |
| | | Unconnected Positive Leader |
| | Positive | CG Lightning |
| | | Upward Lightning |
| | | Unconnected Negative Leader |

### *Negative cloud-to-ground lightning*

Figure 2.12 shows the typical waveform of a first return-stroke current of a negative CG lightning measured in a tropical region. Arcanjo et al. (2019) discuss the features of the pre-return stroke phase, in which unipolar pulses of current are measured and attributed to induced effects of the approaching downward negative leader. The lightning strike shown in the figure lasts about 3 milliseconds, added to about 1.2 milliseconds of the pre-return stroke phase. It has a peak current of about 33 kA and a rise time of about 8 microseconds.

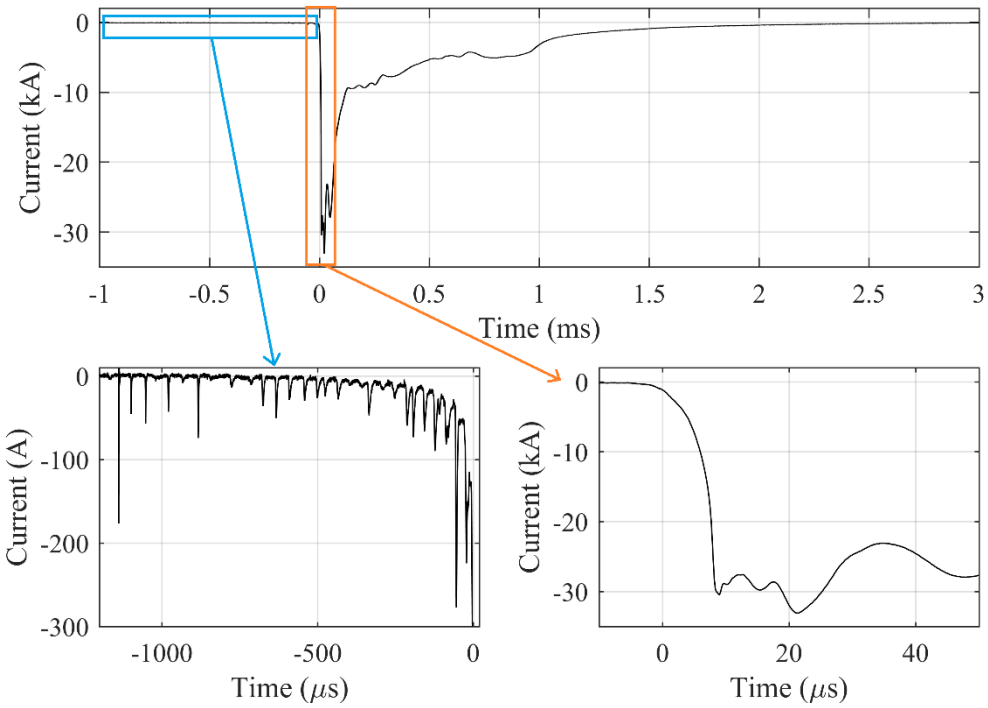


Figure 2.12 - Current of the first stroke with a zoom in the pre-return stroke phase and in the peak current. Adapted from Arcanjo et al. (2019).

After the first stroke, within typically tens or hundreds of milliseconds, other strokes can use partially or entirely the forged channel. Most of the subsequent strokes have lower peak currents and rise time. The typical

parameters of negative CG lightning, collected by Rakov and Uman (2003), are summarized in Table 2.2.

Table 2.2 – Typical parameters of negative CG lightning

| | First return strokes | Subsequent strokes |
|---|---|---|
| **Rise time** | 5 μs | 1 μs |
| **Duration** | 100 μs | 50 μs |
| **Peak current** | 30 kA | 10-15 kA |
| **Return Stroke Charge** | 5 C | 1 C |

### *Negative upward lightning*

Under some specific meteorological conditions, upward leaders can develop from tall structures and result in upward lightning (e.g. Soula et al., 2021). They are usually classified as self-initiated or triggered by nearby lightning. The initial stage of upward lightning consists of the positive upward leader development, characterized by a current flow of low intensity (hundreds of amperes) and long duration (in the range of milliseconds).

After the initial stage, the channel forged by the upward leader can be used for one or several return strokes. These return strokes are very similar to subsequent strokes found in negative CG lightning. Figure 2.13 shows the waveform of one negative upward lightning with the initial stage and several return strokes measured in the Eagle Nest Tower, in Spain.

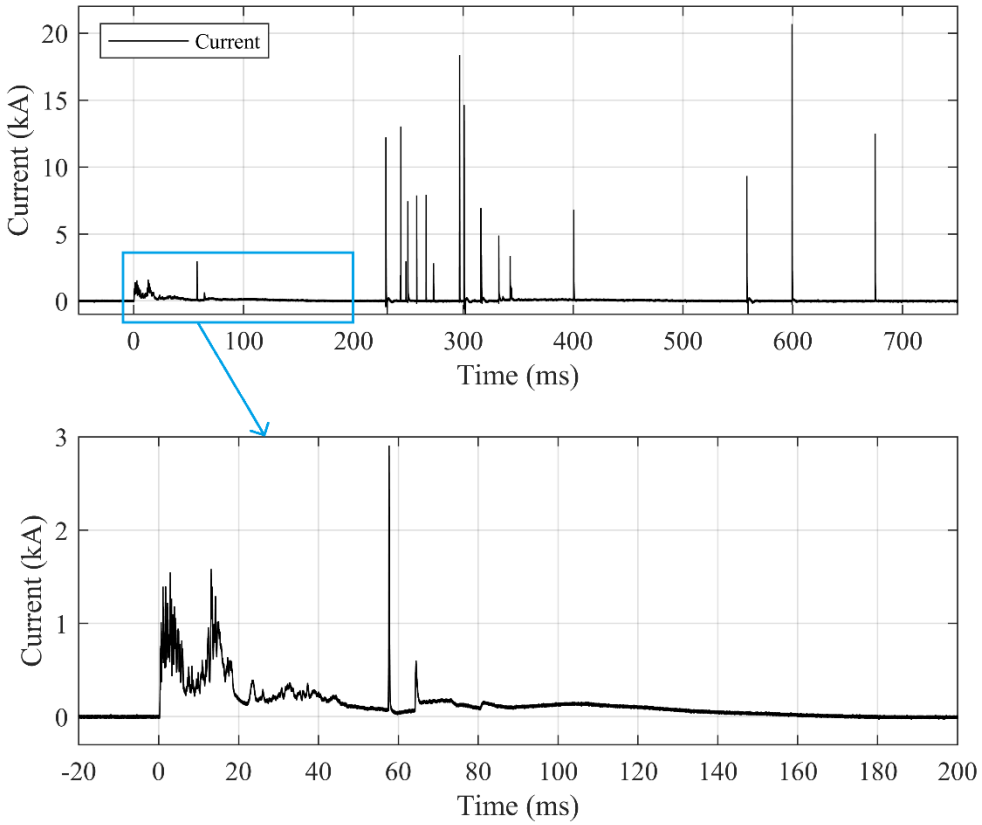


Figure 2.13 - Typical current waveform measured for negative upward lightning at the Eagle Nest Tower, Spain.

The initial stage of upward lightning is usually not detected by lightning location systems, due to the slow variation of the current. This can be damaging for structures since it involves the same charge level of -CG return strokes, with lower current peaks but that last longer. Table 2.3 summarizes parameters of the initial stage and the associated return strokes.

Table 2.3 – Typical parameters of negative upward lightning

| | Initial stage | Return strokes |
|---|---|---|
| **Rise time** | 4 ms | 1 μs |
| **Duration** | 28 ms | 20 μs |
| **Peak current** | 500 A | 7 kA |
| **Return Stroke Charge** | 3 C | 2.6 C |

### *Unconnected upward positive leader*

In negative CG lightning, during the process of the downward leader development, the enhancement of the electric field on grounded structures lead to positive upward leaders that attempt to connect to downward leader. Usually, when the discharge strikes one point, unconnected (aborted) leaders from other structures dissipate their accumulated charge. Figure 2.14 depicts the pre-return stroke stage of an unconnected upward positive leader reported by Arcanjo et al. (2019). The initial phase is similar to the common negative downward lightning,

but at the instant of the lightning strike, most of the charge stored in the channel returns to the ground and the channel is dissipated.

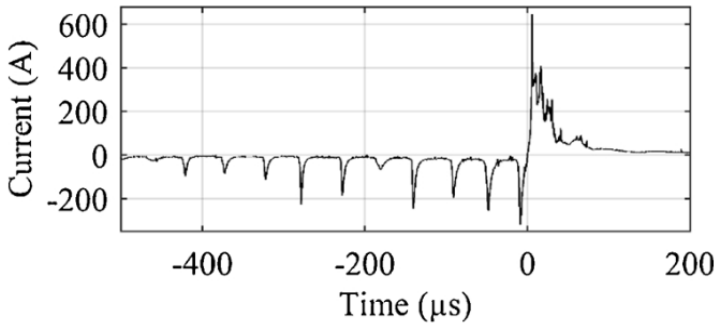


Figure 2.14 - Current waveform of unconnected upward leaders. Adapted from Arcanjo et al. (2019).

Nag et al. (2021) also analyzed in detail the currents associated with upward leaders from lightning strikes occurring within one kilometer far from the Kennedy Space Center. The mean net charge transferred by unconnected events due to the energy dissipation of the aborted leader was found in the range of millicoulombs (average of 1.7 mC). Other typical parameters for the induced pulses are summarized in Table 2.4.

Table 2.4 – Typical parameters of unconnected upward leaders

| (Induced pulses) | |
|---|---|
| **Rise time** | 2.5 μs |
| **Duration** | 5-20 μs (average of 14.1 μs) |
| **Peak current** | 10-200 A (average of 50 A) |
| **Pulse Charge** | 213 μC |
| **Interpulse Interval** | 20.9 μs |

### *Positive cloud-to-ground lightning*

Positive discharges are known to be more intense but less frequent than the negative counterpart (Nag and Rakov, 2012). They are usually observed in compact cloud cells or from cloud structures where the positive structure is not shielded by the negative one, with meteorological conditions favoring the development of the downward positive leader.

Saba et al. (2015) presented one high-speed video and electric field observation of a negative upward leader connecting to a downward positive leader. The initiation of the upward negative leader and electric field pulses occur simultaneously at approximately 1 ms before the return stroke. The pulses are attributed to the stepped fashion propagation of the leader.

The parameters of positive lightning were obtained with a compilation performed by Rakov and Uman (2003), combined with more recent observations of Romero et al. (2013). From Table 2.5, one can see that the positive CG lightning

present higher rise times and duration, as well as higher peak currents and charges, if compared to negative CG lightning.

Table 2.5 – Typical parameters of positive lightning

| Parameters | |
|---|---|
| Rise time | 20 μs |
| Duration | From tens of μs to tens of ms |
| Peak current | 35/12 kA |
| Return Stroke Charge | 80/150 C |

### *Positive upward lightning*

Positive upward lightning is a rare event reported in the literature. They consist of upward negative leaders that emerge from the ground towards the cloud. Their initial stage presents a signature of several pulses in the current waveform. Miki et al. (2014) analyses events of negative upward leaders that led to positive lightning strikes. They present current waveforms of some occurrences. First, a high density of pulses is recorded, during the development of the upward negative leader, then a superimposed current indicates that the development happens further away from the structure. Peak currents in the order of tens of kiloamperes are detected.

### *Unconnected upward negative leader*

There are not many studies and statistics for unconnected negative leaders. Qie et al. (2019) investigated the development of an event with high-speed video acquisition simultaneously to current measurements. Negative leader pulses are very similar to the ones detected in the initial stage of negative lightning, with higher current values. The branching of the upward leader doubles the pulse frequency since alternating current pulses are detected.

In general, the amplitude of pulses associated with positive lightning (upwards and unconnected negative leaders) are higher than the induced pulses observed for negative lightning. In the case of negative lightning, these pulses are induced by propagating negative leaders. On the contrary, in positive lightning, they are precisely the measurement of the current associated with the stepping process of the upward leader's propagation.

# 3 Experimental Investigation

## 3.1 General objectives

Most of the work presented in this thesis was carried out at the Dena Desarrollos facilities and at Labelec (Terrassa, Spain). In the next sections, the characteristics of the main equipment used in experiments carried out in the laboratory and the field are presented.

Considering the interest in the effects of corona and lightning-like discharges through grounded rods, the current is one of the most important parameters to detect and describe electrical activity from the rod. Other variables investigated are the applied voltages, the background electric field, the fast variations of the electric field, and the optical intensity obtained with photometers and with a spectrometer.

Later, a low-current sensor was developed with optimized bandwidth for measuring corona discharges. The sensor was tested in three different sites and the results obtained were presented in the first paper of this compendium and in a conference presentation at the 35th International Conference on Lightning Protection.

## 3.2 Laboratory Setup

The experiments in the laboratory aimed, at first, a comprehensive characterization of the corona discharges from grounded rods at atmospheric pressure. Subsequently, long air-gap discharges were performed for a study of optical and current characteristics. The available power supplies allowed DC voltages of both polarities up to 50 kV. A Marx Generator up to 1 MV was used for experiments with impulsive voltages. Figure 3.1 shows the installations of the DC high voltage power supply and the Marx generator.

Figure 3.1 - Picture of the two installations where the experiments published were performed.

High-current power supplies were used for other experiments and collaborations developed during this project. The P-Surge can produce 8/20μs waveforms with currents varying from tens of amperes to about one kiloampere. Two other power supplies allow high energy discharges with 8/20μs or 10/350μs typical waveforms and currents ranges from 10 kA to 150 kA.

### *3.2.1 Setup for minimum corona discharges*

In the laboratory, at first, two approaches were used to measure the corona current: a current transformer and a shunt resistor. Figure 3.2 shows a diagram of the connections of the two sensors to the rod in the setup. The experiments were performed using a grounded conductive rod of 80 cm, placed between two plates (with 1.4 m and 2.0 m of diameter) separated by 100 cm, leading to a gap distance of 20 cm. The high voltage power supply provides up to 30 kV DC at positive or negative polarity, and it is connected to the upper plate. The bottom plate is grounded through the resistor. This setup reproduces the conditions of sharp grounded structures that are subject to high electric fields when charged clouds are in the vicinities.

We used a 50-ohm shunt resistor for the characterization of the corona pulse, and after that, the resistor was substituted by an ultra-low-current ammeter that measures the average DC current flow through the grounding cable.

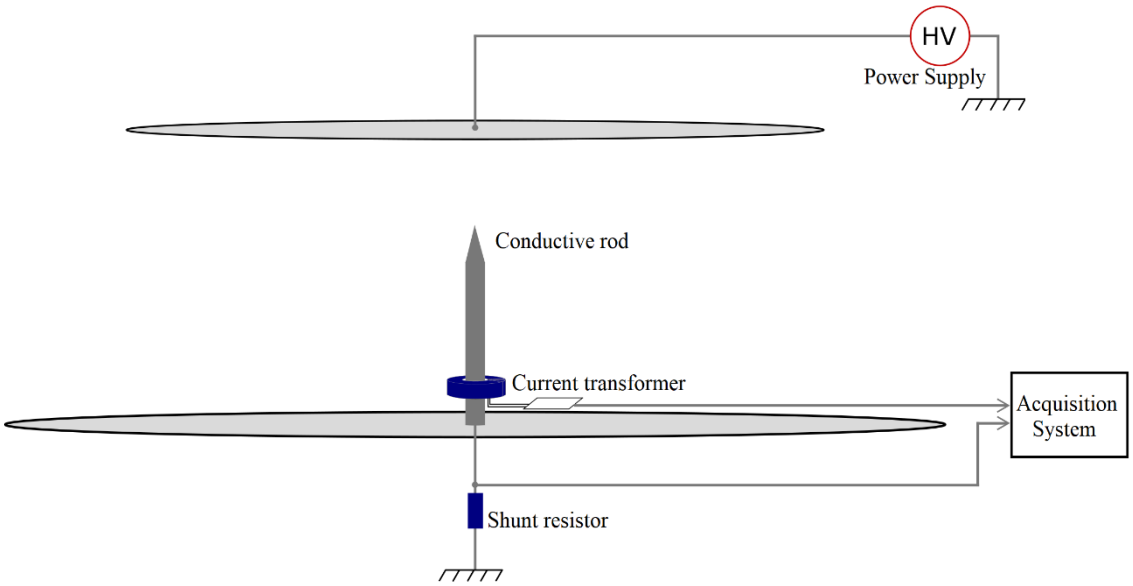


Figure 3.2 - Conductive sharp rod in the plane-to-point setup.

### *Corona discharges: current and optical characteristics*

Figure 3.3 shows the typical pulse for impulsive corona discharges at atmospheric pressure. The discharges are observed as a regular train of pulses with a short rise time (tens of nanoseconds) and time decay in the order of a few hundreds of nanoseconds. The interpulse interval varies from a few microseconds to milliseconds, depending on the configuration of electrodes and the voltage applied (e.g. Dordizadeh et al., 2015; Wang et al., 2018). The waveform of the current sensor presents a good match with the measurement of the shunt resistor. Oscillations observed during the decay of the pulse are related to their high frequency content and possible reflections in the measuring system.

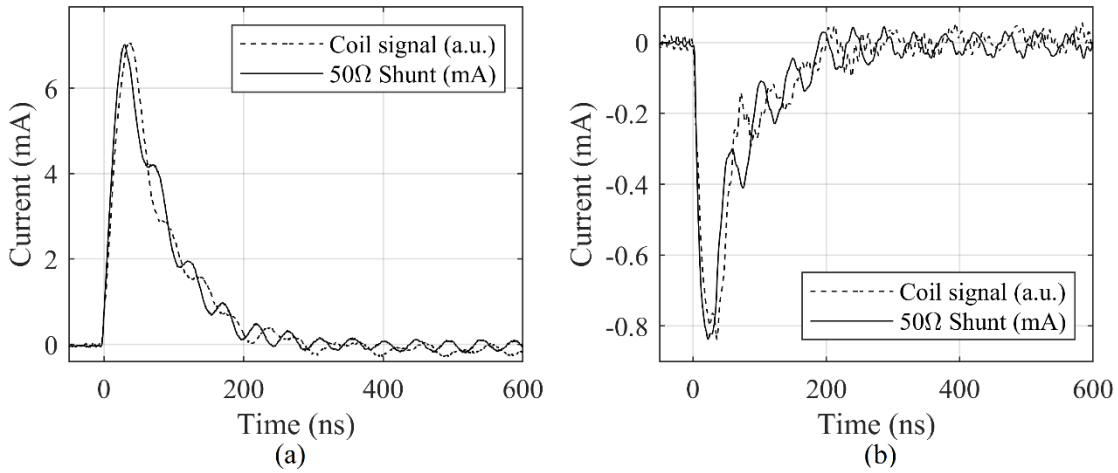


Figure 3.3 - Measurements obtained with the shunt resistor and the current transformer for (a) Positive corona and (b) Negative corona.

An optical cable connected to a spectrometer was used for observing the typical spectra of the discharges, the obtained signal is shown in Figure 3.4. The spectra are composed mainly of the radiation of nitrogen molecules, both neutral (second positive system) and ionized (first negative system), and the strongest lines are localized between the wavelengths of 300 and 400 nm. These findings are in agreement with experiments reported in literature (e.g. Gallimberti 1974; Kozyrev et al., 2012; Krzewinski et al., 2017).

Streamer corona discharges are known to be cold plasmas in which the electrons and ions are at high temperature due to excitation and ionization, but the neutral molecules are at room temperature ("cold"). This plasma is not at thermochemical equilibrium, and it is able to activate molecular species like $N_2$, $O_2$ and $H_2O$ by electron-impact collisions that have a high impact on the environmental chemistry (Nna-Mvondo et al., 2005; Soler et al., 2021).

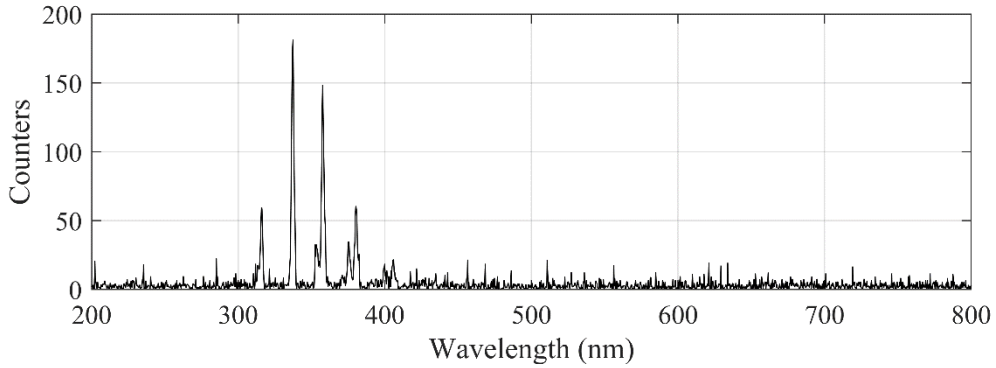


Figure 3.4 - Corona discharge spectra.

### *3.2.2 Marx-Generator setup*

In this work, a Marx generator is used to produce high-voltage pulses from a DC power supply. It can operate in switching impulse (SI) and lightning impulse (LI) modes. Standard LI discharges have a front time of 1,2 μs and a time to half-value of 50 μs (known as 1.2/50 μs). SI discharges are performed with a rise time of about 250 μs. After the peak, the voltage decreases (standard waveform is known as 250/2500 μs), and in the case of breakdown, returns to zero in about 0.5 μs. In comparison to the LI mode, the SI mode allows a significantly slower Spatio-temporal development for the streamers and leaders in the gap.

Figure 3.5 shows the two setups used for investigating positive and negative leaders in laboratory discharges. In (a), one can see the plate-to-rod arrangement (1-m gap) with the secondary sphere-to-sphere path, separated by 30 cm. The spheres are considerably far from the upper plate to avoid interferences in the main setup. In (b), the scheme of the rod-to-rod setup with an 85-cm gap is shown. In this case, there is only one path for the discharges.

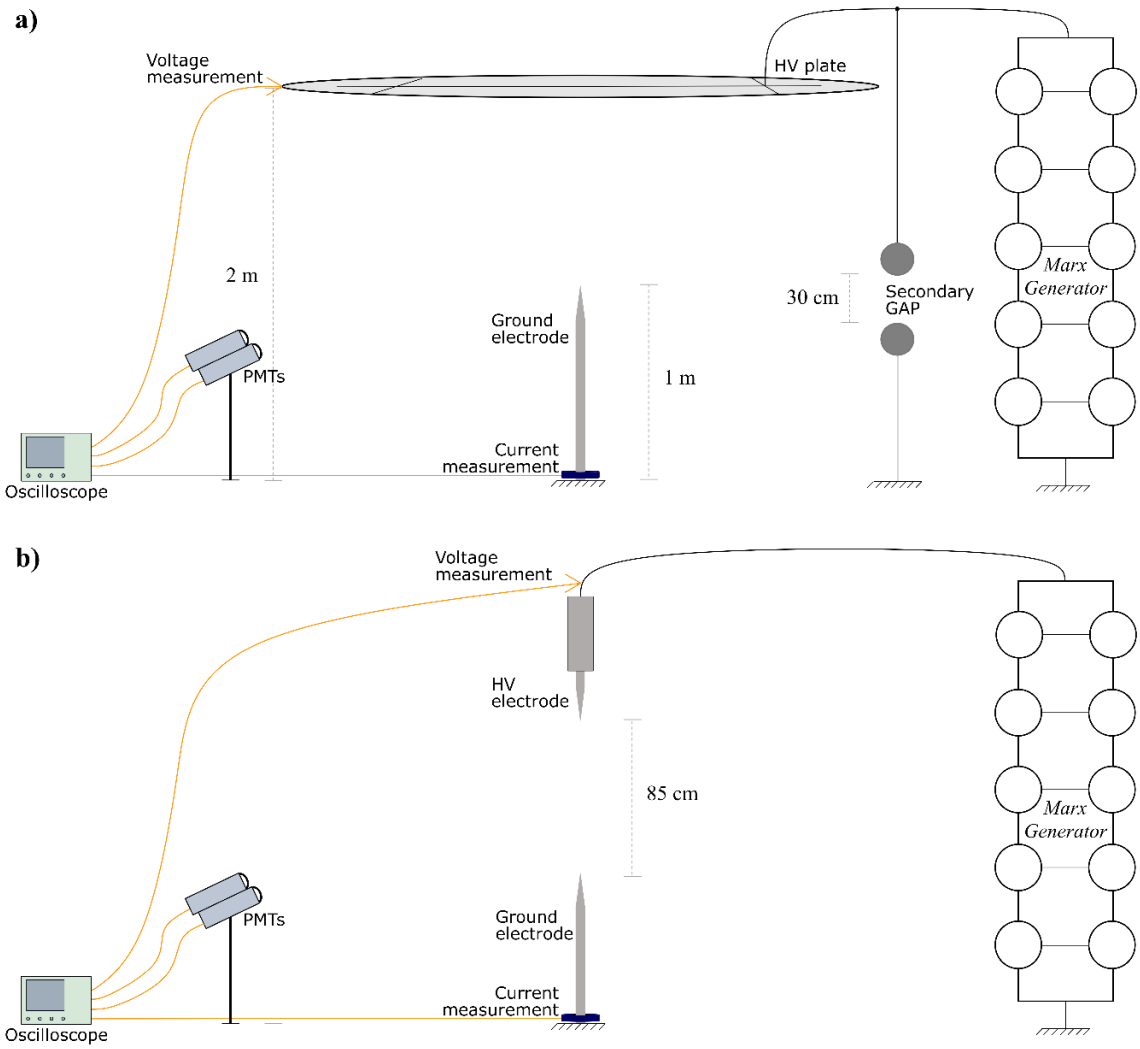


Figure 3.5 - Sketch of setups for investigating the laboratory discharges.
(a) 1-m Plate-to-rod configuration with detail of the 30-cm sphere-to-sphere parallel gap.
(b) Rod-to-rod configuration with gap distance of 85 cm.

The signals were digitized by an oscilloscope at a sampling rate of 2.5 GHz with a bandwidth of 500 MHz. The oscilloscope was kept inside one electromagnetic compatible (EMC) cabinet. The Marx generator was connected to the discharge gap and a calibrated capacitive divider was used to measure the applied voltage. The current through the grounded electrode was measured by two Pearson Coils, one with a voltage ratio of 0.1 V/A and a bandwidth from 1 Hz to 20 MHz, and another with a voltage ratio of 0.01 V/A and a bandwidth from 0.25 Hz to 4 MHz.

The photomultiplier tubes (PMTs) used in the experiments have a wide detection spectrum. The sensors were placed in a metallic box, each one with its independent power supply connected to batteries to minimize measurement noises. Shielded BNC cables connected the PMTs to the oscilloscope. The spectral responses of the PMTs near the wavelengths of interest are 56.8 mA/W at the 337 nm, and 14.5 mA/W at the 777.4 nm. The PMTs' faceplates are attached to

bandpass optical filters of 1″ of diameter. The central wavelength (CWL) of the near-UV filter is ≃ 340 nm, and a full width at half maximum (FWHM) of 10 nm. The peak transmittance at the CWL is 36.1% and the transmittance at 337 nm is equal to 26.1%. The near-IR filter has a CWL at ≃ 780 nm, and FWHM of 10 nm. The peak transmittance at the CWL is 59% and the transmittance at 337 nm is equal to 51.4%. The response of the optical filters used in the experiments are shown in Figure 3.6.

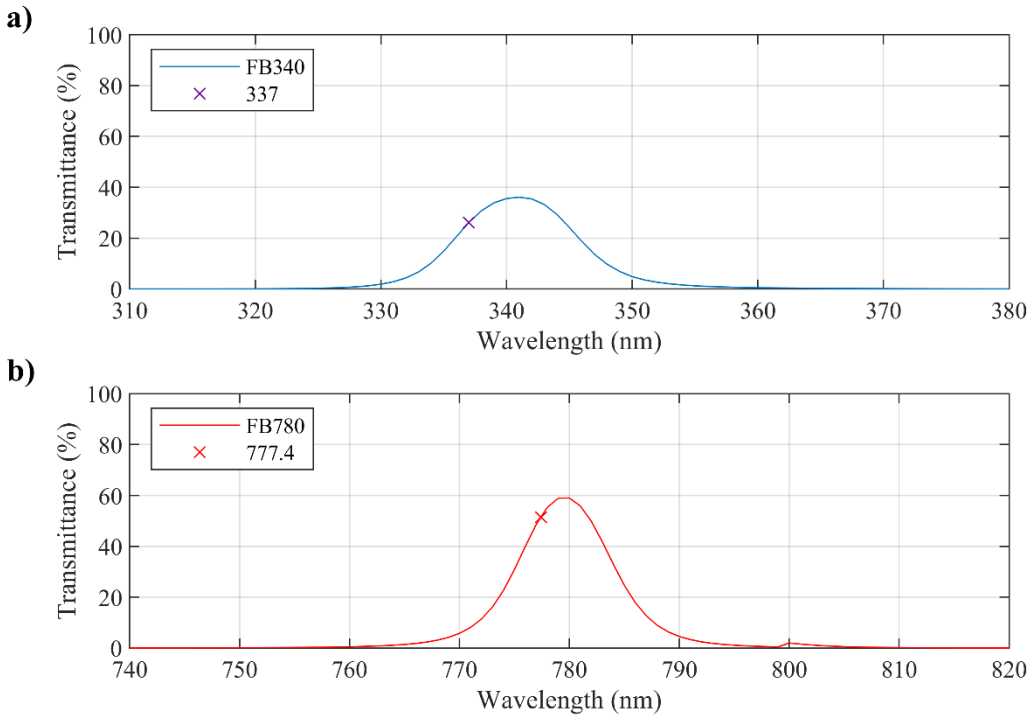


Figure 3.6 - Transmittance of optical filters used in the experiments.
(a) Near-UV optical filter with transmittance of 26.1% at the wavelength of 337 nm.
(b) Near-IR optical filter with transmittance of 51.4% at the wavelength of 777.4 nm.

From the output current provided by the PMTs, one can retrieve the optical power received by the sensor by using the spectral response, PMT gain, and filter attenuation at the wavelength of interest. This estimation procedure is approximate and considers that the power received by the sensors is concentrated at these wavelengths (337 nm and 777.4 nm).

Time-integrated images of the pre-breakdown stage are obtained using a Xybion ICCD camera, located at 3 m from the gap. The camera was placed inside an EMC cabinet, and it was triggered by an optical system connected to the oscilloscope; exposure times varied from as low as 80 ns to 20 µs. By recording the sent and received signals, it is possible to perform proper synchronization with a jitter lower than 50 ns. One Nikon camera coupled to UV lenses was used to take still images of the discharges with a total time exposure of 3 seconds.

## 3.3 Field experiments

The current sensor developed and verified in the laboratory experiments was coupled to a rod and tested in the field. Three test sites were instrumented for capturing data and waveforms in partly uncontrolled environments, each one having its own peculiarities.

Figure 3.7 shows the scheme of the installations. In some of the installations, the current was measured using both a shunt resistor and a current sensor. The resistor was placed in series with the grounding cable of the rod with low inductance and low resistance to ensure the quality of the measurements. The current sensor consisted of a ferrite core with a secondary winding and a measuring circuit and does not affect the discharge circuit.

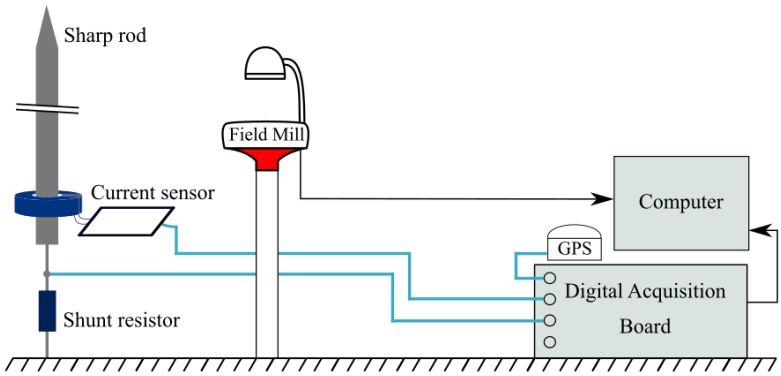


Figure 3.7 - Scheme of the setups for measuring corona discharges.

The sensor provided detections that are correlated to the background electric field, measured by a 10-Hz Previstorm® electric field mill. The indications provided by the Field Mill consider the static component of the electric field. In this way, many lightning strikes occurring within its sample rate cannot be perceived in the measurements individually. Lightning location network was available from LINET (Betz et al., 2009) to monitor the distances of lightning strikes to the sensors' sites.

Figure 3.8 shows pictures of the installations. The first setup was deployed over a shelter in La Tossa d'Alp, near the Eagle Nest Tower, in the Spanish Pyrenees (2525 m above the sea level), where there is also a system for measuring currents of lightning impacts at the tower. At 250 m far from the shelter, the electric field mill was placed over a refugee. The measurements of the ambient electric field do not correspond to the local electric field at the tip of the grounded rod. Nonetheless, they represent the increase in the electric field in the given environment that can lead to local enhancements for different structures in the vicinity.

Figure 3.8 - Sharp grounded rod installed in the two setups: rooftop (left) and flat-ground (right).

The second setup was deployed over the roof of the high voltage laboratory, at LABELEC's facilities in Terrassa, Spain. This is a sub-optimal installation closer to taller metallic structures. That is a typical building from Spanish industrial areas, in which there is a built-up mass exposed to environmental effects. The corona current sensor was coupled to the conductive rod placed over the roof of the shelter. The rod is approximately 1-m long, stands 1.5 m above the roof, and it is the highest structure within a 3-meters radius.

The third setup was deployed in a flat open area at the Observatori de l'Ebre, in Tortosa, Spain. This installation is relatively close to high trees, shrubs, and 50-m far from a VHF transmitting tower, utilized for ionosphere observations. The sensor's tip is 2 m above the ground level.

# 4 Results From the Publications

## 4.1 Observations of Corona Point Discharges from Grounded Rods Under Thunderstorms

### *4.1.1 Introduction and methodology*

This article investigates features of corona point discharges when a grounded conductive rod is subject to a high background electric field. In the laboratory, high voltage is applied to an upper plate in a plane-to-point experiment, and the discharges are observed from a grounded rod using an ultraviolet camera and a photosensor. The current is measured using a shunt resistor, a current transformer, and a high impedance ammeter. In the field, one current sensor coupled to a grounded rod, 1.5 m above a roof, was installed in a site located at an altitude of 2525 m above sea level.

### *4.1.2 Results*

The corona current sensor is optimized for measuring low-level currents through the lightning rod. It consists of a current transformer, able to measure high-frequency current pulses.

It was found that corona current pulses have fast rise time (tens of nanoseconds) and slow decay (hundreds of nanoseconds). For the initial stage of the discharges, above a certain threshold, the frequency of pulses increases with the applied voltage. In the field, under a high background electric field, similar corona pulses were detected using the sensor. The observation of pulses is not related to only nearby lightning activity, but also to the movements of charges in the clouds that can lead to an enhancement of the electric field. The recordings show that the pulses can occur for several seconds after or before lightning strikes in the vicinities. For that specific installation, the frequency of pulses is correlated with the ambient electric field measured 250 meters away. Pulses of positive corona were no longer observed when the electric field magnitude was lower than 1.8 kV/m and pulses of negative corona were more atypical and presented a higher threshold, of about 3.8 kV/m.

Complementary, the same sensor was installed in two other sites, a *rooftop*, and a *flat-ground* installation. The results obtained in these setups were presented at the ICLP conference with the paper depicted in Appendix B2. Due to the enhancement of the E-field caused by lightning strikes in the vicinity of the rod with a sharp tip, positive and negative pulses before or after the strikes were observed. When lightning activity is far from the structure, but the electric field remains high, pulses were still observed.

This study is relevant for understanding the production of corona and space charges in high structures, such as wind turbine blades, towers, and buildings in general.

### *4.1.3 Article and reference*

Arcanjo, M., Montanyà, J., Urbani, M., Lorenzo, V. & Pineda, N. (2021). Observations of corona point discharges from grounded rods under thunderstorms. *Atmospheric Research*, 105238.
doi: 10.1016/j.atmosres.2020.105238.

# Observations of Corona Point Discharges from Grounded Rods under Thunderstorms

Marcelo Arcanjo[a, b, *], Joan Montanyà[a], Michele Urbani[a], Victor Lorenzo[b], Nicolau Pineda[a,c]

[a] Lightning Research Group, Technical University of Catalonia, TR1, Carrer Colom 1, Terrassa, 08222, Spain;

[b] Dena Desarrollos S.L. (Ingesco), Carrer Cardener 5, Terrassa, 08223, Spain;

[c] Meteorological Service of Catalonia, Carrer Berlín 38-46, 08029, Barcelona, Spain.

Correspondence: Marcelo Arcanjo (marcelo.augusto.sousa@upc.edu)

Post-print of paper published with: https://doi.org/10.1016/j.atmosres.2020.105238.

**Abstract:** We investigated features of corona point discharges when a grounded conductive rod is subject to a high background electric field. In the laboratory, high voltage is applied to an upper plate in a plane-to-point experiment, and the discharges are observed from a grounded rod using an ultraviolet camera and a photosensor. The current is measured using a shunt resistor, a current transformer, and a high impedance ammeter. We have found that corona current pulses have fast rise time (tens of nanoseconds) and slow decay (hundreds of nanoseconds). For the initial stage of the discharges, above a certain threshold, the frequency of pulses increases with the voltage applied. In the field, one current sensor coupled to a grounded rod, 1.5 m above a roof, was installed in a site located at an altitude of 2525 m above sea level. The same pulses observed in the laboratory are recorded during periods of electric field enhancement caused by the movement of charged clouds or lightning activity near the sensor. For that specific installation, the frequency of pulses is correlated with the ambient electric field measured 250 meters away. To the best knowledge of the authors, this is the first time in which such correlation is made for outdoor measurements, seeing that other works correlate the electric field with the average current flow. Pulses of positive corona were no longer observed when the electric field magnitude was lower than 1.8 kV/m and pulses of negative corona were more atypical and presented a higher threshold, of about 3.8 kV/m. This study is relevant for understanding the production of corona and space charges in high structures, such as wind turbine blades, towers, and buildings in general.

**Keywords:** corona discharge; point discharge; Trichel pulses; electric field; space charge; lightning protection.

## 1. Introduction

Electrodes or structures subject to high electric fields are likely to favor the ionization of air molecules near their tips and edges, where the local electric field is higher, inducing corona discharges (Moreau et al., 2018). The enhancement of the electric field near sharp grounded structures can generate ions and form a space charge layer that ultimately decreases the magnitude of the electric field at the ground level (Kip, 1938; Chang et al., 1991; Chauzy and Raizonville, 1982).

The discharge current through an insulated point in the field was recorded by Whipple and Scrase (1936). They found an empirical relationship in which the magnitude of the downward current is in the order of a few microamperes and is proportional to the squared electric field. In the following years, several other researchers observed a similar relationship (i.e. Hutchinson, 1951; Chapman, 1955), assessing the increase of the corona current caused by the wind.

Typically, grounded structures can be subject to currents ranging from extremely low values to kiloamperes (as in the case of lightning strikes). A study of discharge currents associated with kite balloons, performed by Davis and Standring (1947), showed that currents ranging from milliamperes to kiloamperes were associated with thundery weather. Chauzy and Soula (1999) simulated the contribution of the point discharges to the convective charging mechanism of thunderclouds. D'Alessandro (2009) conducted a more recent study on corona discharges from a sharp point under a thunderstorm, finding an average current of a few microamperes and electric field thresholds of about 0.5 kV/m to 1.5 kV/m. His experimental data indicated that higher wind speeds may lead to an increase in the average corona current, and a decrease in the electric field threshold for corona onset. Notably, other than the electric field enhancement, the height of the grounded rod and its shape play a considerable role in the corona current generation (Hutchinson, 1951; D'Alessandro, 2009).

The space charge layer created by corona at ground level can attenuate the electric field in the vicinities of grounded conductors. This can affect the initiation of upward leaders and even change the point of lightning impacts (Aleksandrov et al., 2001; Becerra et al., 2007; Bazelyan, 2015; Guo and Zhang, 2017). Investigations have indicated that the corona layer could delay the streamer inception from structures, although this would not cause severe effects, since the lateral development of upward connecting leaders is not strongly influenced by the glow corona space charge (Becerra, 2013 and 2014). In elevated rotating structures, such as wind turbines, observations suggested that the movement of these structures avoids the shielding effect caused by space charges, increasing the probability of lightning strikes (Montanyà et al., 2014). In the case of cloud-to-ground lightning, approaching downward leaders also lead to the rapid enhancement of the electric field and induced currents in grounded structures (Rakov, 2016; Guimaraes et al., 2017; Arcanjo et al., 2019).

Studies conducted in laboratory have shown the different regimes of corona discharges in a gap. In positive corona, the initial stage is a pulsating regime known as burst pulse corona (Chang et al., 1991). As the electric field increases further, the phenomenon reaches a pulseless stage named glow corona, in which the accumulation of space charges leads to a steady-state uniform corona glow around the needle electrode. For an even higher electric field, intense onset streamers develop, constituting a new region called breakdown streamer. These streamers can create an unstable region that can ionize the entire gap and trigger a

spark discharge (Trichel, 1939; Gallo, 1977; Chang et al., 1991). In negative corona, the pulsating regime of the initial stage is known as Trichel Pulse corona (Trichel, 1938). A pulseless stage can develop when the electric field is increased, and the pulses are superimposed one into another. This stage can be unstable at normal temperature and pressure conditions and the discharge can rapidly evolve to a spark (Chang et al., 1991).

Different configurations based on the electrode geometries have been used to perform experiments, the most common being point-to-plane (e.g. Trichel, 1938 and 1939; Gallo, 1977; Dordizadeh et al., 2015). In these cases, the high voltage electrode is typically a needle and the second electrode is a plate grounded through a shunt resistor. The so-called corona current is the current measured through the resistor. For the initial stages of corona discharge (burst corona and Trichel pulse corona), the current is observed as a regular train of pulses with a short rise time (tens of nanoseconds), and time decay in the order of few hundreds of nanoseconds and rather long inter-pulse time (a few microseconds to milliseconds), depending on the configuration of electrodes and the voltage applied (Dordizadeh et al., 2015; Wang et al., 2018).

This work comprises experiments with grounded conductors with sharp tips under high background electric fields. In the laboratory, they are inserted between a grounded plate and an upper plate with a DC high voltage applied. In the field, the rod is installed over a roof, and exposed to thunderstorm conditions. Features of the corona current in both cases are assessed and discussed.

## 2. Methodology and Instrumentation

In the laboratory, two approaches were used to measure the corona current: a current transformer and a shunt resistor. Figure 1 shows a diagram of the connections of the two sensors to the rod within the setup.

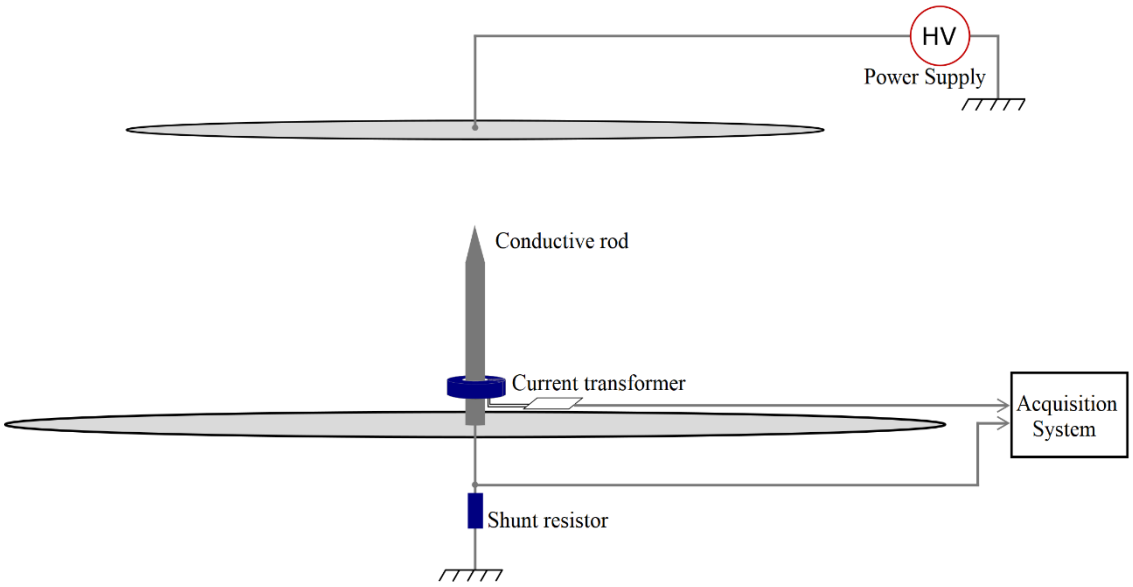


**Figure 1.** Conductive sharp rod in the plane-to-point setup.

The experiments were performed using a grounded conductive rod of 80 cm, placed between two plates (with 1.4 m and 2.0 m of diameter) separated by 100 cm, leading to a gap distance of 20 cm. The high voltage power supply provides up to 20 kV DC at positive or negative polarity, and it is connected to the upper plate. The bottom plate is grounded

through the resistor. This setup reproduces the conditions of sharp grounded structures that are subject to high electric fields when charged clouds are in the vicinity, in such a way, corona emissions are expected from the tip of the rod.

The shunt resistor affects significantly the shape of the waveform, since current pulses are very fast, with a rise time of tens of nanoseconds and decay of a few hundreds of nanoseconds (e.g. Kexin et al., 2015; Wang et al., 2017; Dordizadeh et al., 2017; Wang et al., 2018). If higher values of resistors are used, current pulses have a longer duration. Hence, a resistor with low inductance and low resistance is required. We used a 50-ohm shunt resistor for the characterization of the corona pulse, and after that, the resistor was substituted by an ultra-low-current ammeter that measures the average DC current flow through the grounding cable. The current transformer does not affect the circuit to be measured, and it is composed of a ferrite core with a secondary winding and an auxiliary circuit. Its inductance is 101 µH, and the circuit has cutoff frequencies of 35 kHz and 20 MHz. Within the bandwidth, the circuit presents a flat response and the output voltage is proportional to the current flow through the rod, with a voltage ratio of about 12.3 V/A.

Two optical systems were used for performing detections. Using a low-speed camera with an intensifier for the UV and near-blue range (275-375 nm) it was possible to visualize corona discharges. A secondary system consists of an optical fiber cable pointing to the tip of the rod (as seen in Figure 2) coupled to a filter centered at 375 nm (20 nm bandwidth) and connected to a photosensor tube. The electrical signals emitted by the photosensor correspond to an optical signature of the discharge. Using both systems it was possible to ensure that the signals measured by the photosensor were related to the tip of the rod and not with corona from the tip of the optical fiber.

**Figure 2.** Picture of the optical fiber pointing to the tip of the rod.

In section 3, we show the results of a set of experiments in the laboratory, measuring the corona current with the different probes, increasing the voltage applied to the plate. The amplitude and frequency of the pulses are assessed and synchronized with optical detections.

In section 4, we conduct experiments in the field with a current-transformer prototype. Data records were correlated with the background electric field. This measurement was performed employing a calibrated Electric Field Mill with a 10-Hz time resolution and a form factor adjusted considering waveforms correspondent to fair-weather days compared to the well-known Carnegie Curve (Harrison, 2013). We adopted, by convention, to present the values of the gradient of the electric potential, that correspond to the negative of the electric field vertical component.

We used data of a stand-alone VHF interferometer (Montanyà et al., 2012; Pineda et al., 2018) located at a few kilometers of the sensor, in order to track lightning evolution in the vicinity of the site of installation. We verified the LINET lightning detection network for mapping both intra-cloud and cloud-to-ground lightning strikes during the events analyzed. Wind measurements were gathered by the nearby Tosa d'Alp Automatic Weather Station (AWS), part of the Meteorological Service of Catalonia (SMC) network.

## 3. Features of positive and negative corona point discharges

The shape of one single pulse is shown in Figure 3 when the upper voltage is -16 kV, leading to positive corona (a), and +16 kV, leading to negative corona (b). The signals were digitized at a sampling rate of 2.5 GHz with a bandwidth of 500 MHz. The measurements obtained with the shunt resistor and the current transformer are correlated by applying the V/A ratio (of 12.3) for the current transformer.

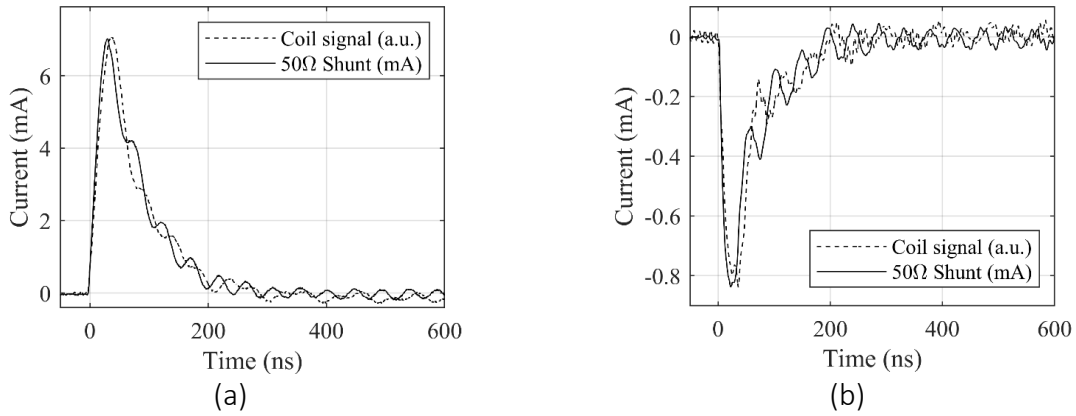


**Figure 3.** Typical corona pulse waveform measured with shunt resistor and current transformer. (**a**) Positive corona; (**b**) Negative corona.

Table 1 presents the rise and decay times of the corona pulses depicted in Figure 3. These parameters do not change significantly with changes for the applied voltage, while their peak amplitude can change considerably even for the same applied voltage. For 16 kV, negative corona pulses (Trichel Pulses) are faster than positive corona bursts, and the amplitude of them is about one order of magnitude lower. The tail of the waveform of the pulses exhibits small oscillations that may be caused by reflections of the fast-current wave in the measuring instrument.

**Table 1.** Corona current pulse (-16 kV / +16 kV applied)

| | Rise time (ns) | Decay time (ns) | Average peak amplitude (mA) |
|---|---|---|---|
| Positive corona pulse | 30 | 400 | 7.0 |
| Negative corona pulse | 20 | 300 | 0.8 |

### *3.1 Optical Detections*

Using the current transformer, corona pulses are synchronized with optical detections measured by a photosensor, as shown in Figure 4. The pulse shape of the optical detection

presents an oscillating behavior and low amplitude. Its time duration is compatible with the current pulse.

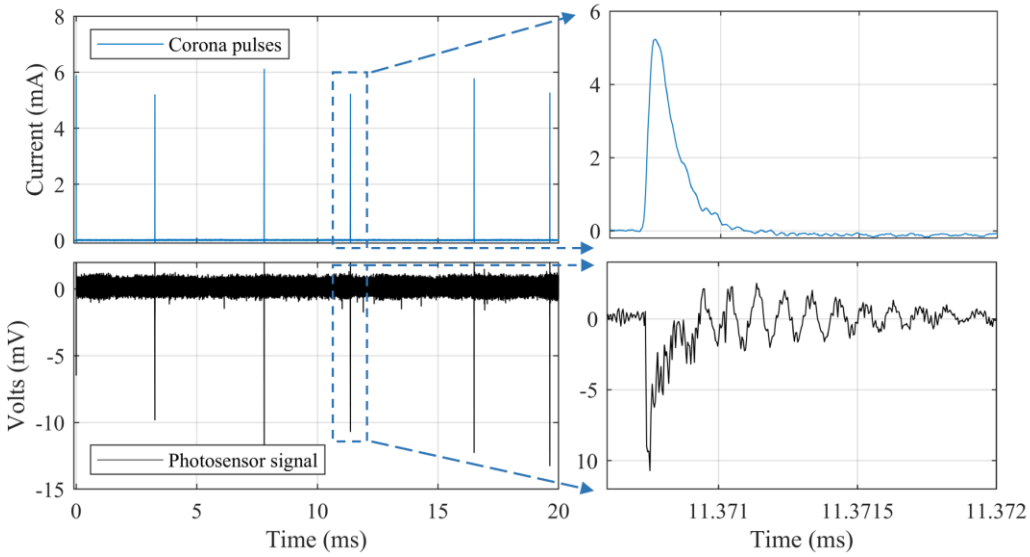


**Figure 4.** Optical detections synchronized with corona current for -15 kV applied in the upper plate.

Figure 5 depicts a picture of the rod taken with the UV-camera when the applied voltage is 16 kV for each of both polarities. The camera is placed at 1.3 m far from the tip of the rod, at the same height. The images were processed to enhance and color the corona region. One can note that the positive corona develops filamentary streamers of around 1.7 cm, while, for the same voltage applied, the negative corona is seen as a glow above the tip of the rod, with a non-clear size.

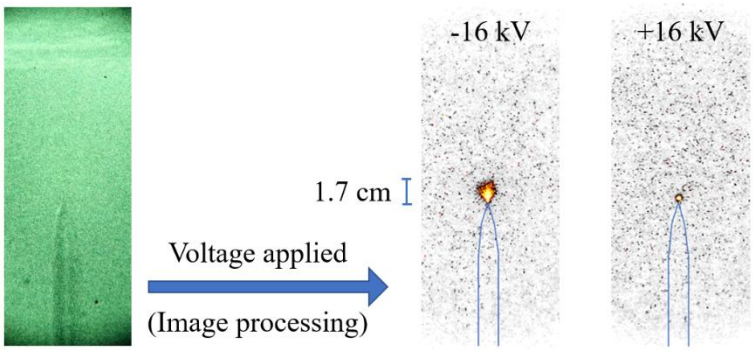


**Figure 5.** Picture of corona discharges from the rod after image processing.

*3.2 Negative corona pulses*

The experiments described in sections 3.2 and 3.3 were performed in a room temperature of 20.7 degrees Celsius, pressure of 980 mbar and humidity of 49%. We replaced the shunt resistor used in the setup shown in Figure 1 by a high impedance ammeter with a low sampling frequency (4 Hz) to measure the average corona current. We used the current transformer to measure the pulse frequency, recording a time window of one second. For each voltage applied, five separate experiments were made, and then we calculate the average current and average pulse frequency obtained. Thereby, we were monitoring simultaneously the upper plate voltage, the average current, and the pulse frequency.

Negative corona is obtained when positive voltage is applied on the upper plate. Figure 6 shows the frequency of pulses detected according to the voltage. For the range of voltages applied in the setup described in section 2, the inception voltage for corona was 8.2 kV. The average current and the pulse frequency increase with the increase of the applied voltage, reaching 6 µA and 35 kHz, respectively, at 18 kV. Closer to the inception voltage, we applied many different voltages in the range from 8 kV to 9 kV. Both the average current and the pulse frequency curves present a knee shape-like rising considerably after the inception.

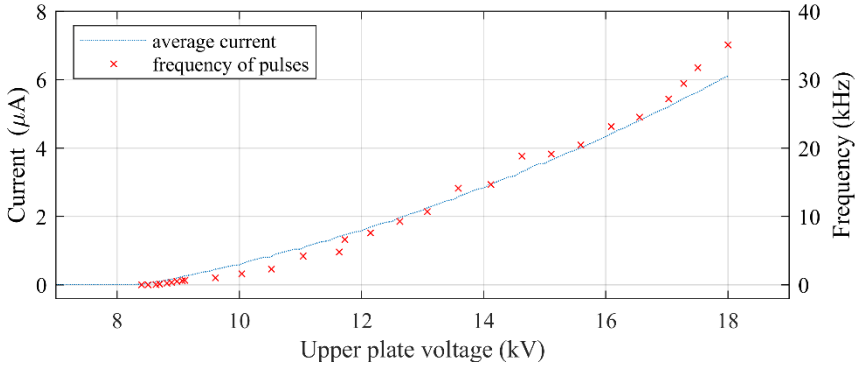


**Figure 6.** Average current (absolute value) and frequency of negative corona pulses.

Figure 7 depicts an interval of 10 milliseconds showing negative corona pulses for an upper plate voltage varying from 9 to 18 kV. We observed considerable dispersion in the amplitude of the pulses. The current peaks reach milliamperes, which is substantially higher than the average current, in the few microamperes range. Visually, using the ultraviolet camera, the shape of the discharges does not change compared to that observed in Figure 5, being a tiny glowing spot with a slight increase of intensity for higher voltages.

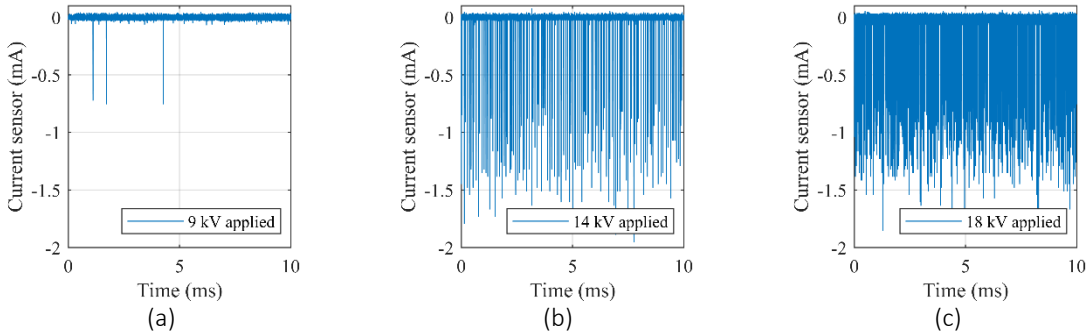


**Figure 7.** Negative corona pulses in a 10-ms time window. (a) 9 kV; (b) 14 kV (c) 18 kV.

### *3.3 Positive corona pulses*

Using the same setup for studying positive corona from the conductive rod, we observed a different behavior of average current and frequency. Figure 8 illustrates how these variables change as the upper plate voltage increases in magnitude. The voltage for inception detected was -9.9 kV. Initially, as the voltage increases, the frequency and current increase, but at around -14.5 kV the frequency reaches a maximum and the current has a slight decrease. Higher voltages cause a decrease in the frequency of pulses until they ultimately disappear at -19 kV, nevertheless, the average current persists to increase, up to a few microamps, reaching similar values to the case of negative corona, and indicating that the discharge has not ceased.

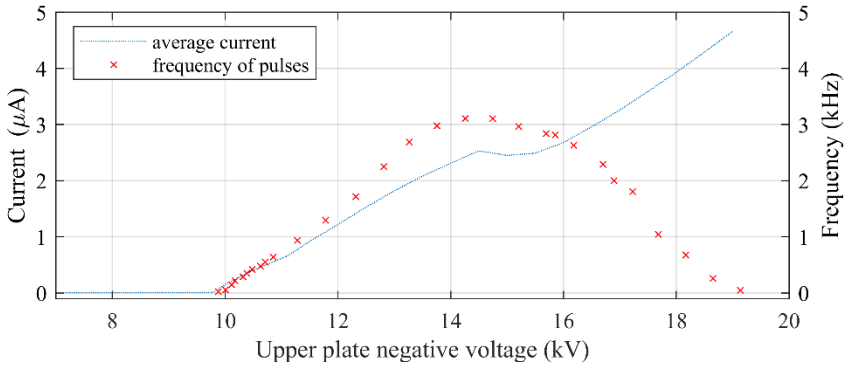


**Figure 8.** Average current and frequency of positive corona pulses.

The behavior of burst pulses observed for positive corona is shown in Figure 9, in a longer time window than the one shown in Figure 7, due to the lower values of pulse frequency for this case. The maximum frequency obtained for the given setup is equal to 3.2 kHz.

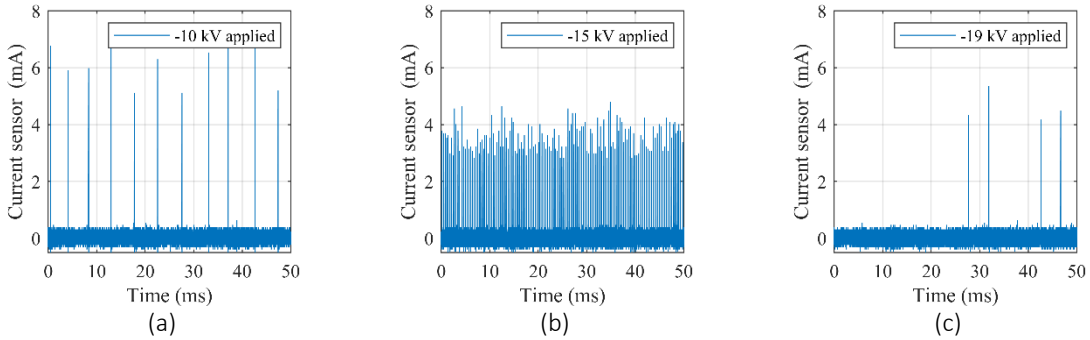


**Figure 9.** Positive corona pulses in a 50-ms time window. (a) -10 kV; (b) -15 kV (c) -19 kV.

Pictures of the three different stages of corona are presented in Figure 10. In (a), when -10 kV is applied, we observed filamentary streamers forming the corona in a conical shape. In (b), streamers are slightly larger and more intense, however, it is possible to identify that they are formed from an onset glow at the tip. In (c), the streamers are barely perceptible, and the tiny glowing spot is formed on the tip of the rod. This stage (for applied voltages between around -14 kV and -19 kV) is a transition between the burst pulse stage and the glow corona stage. At -19 kV, when the corona discharge is pulseless, the glow corona is established.

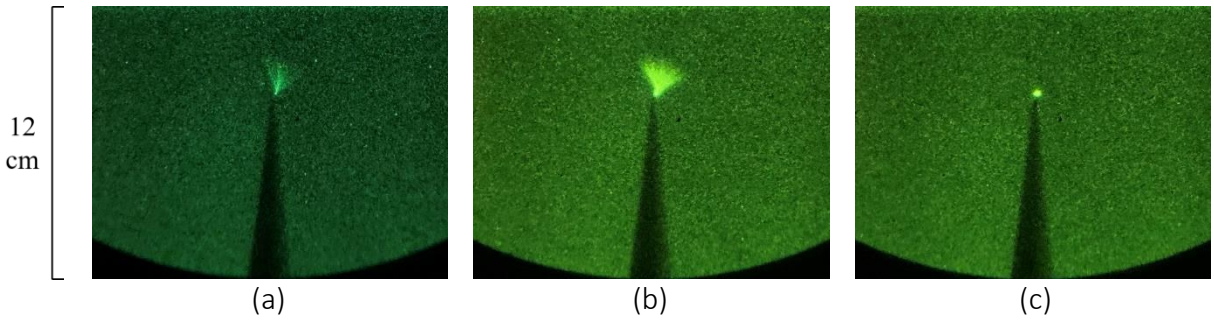


**Figure 10.** Positive corona shape. (a) -10 kV; (b) -15 kV; (c) -19 kV.

## 4. Field experiment

For the outdoor experiment, we installed the current transformer tested in the laboratory over a shelter in La Tossa d'Alp, near the Eagle Nest Tower, in the Spanish Pyrenees (2525 m above the sea level), where there is also a system for measuring currents of lightning impacts at the tower. Figure 11 shows the shelter, the tower and a refugee, 250 m far from the shelter, where the potential gradient was measured using an electric field mill. The measurements of the ambient electric field do not correspond to the local electric field at the tip of the grounded rod, nonetheless, they represent the increase in the electric field in the given environment, which can lead to local enhancements for different structures in the vicinity.

The corona current sensor was coupled to the conductive rod placed over the roof of the shelter. The rod is approximately 1-m long, stands 1.5 m above the roof, and it is the highest structure within a 3-meters radius. We have installed a high-gain flat plate antenna on the roof at about 2.5 meters far from the tip of the rod. The antenna has a time constant of 0.56 second and a lower cutoff frequency of 0.28 Hz. The signals of current and electric field variation were sampled at 20 MHz using a digitizer.

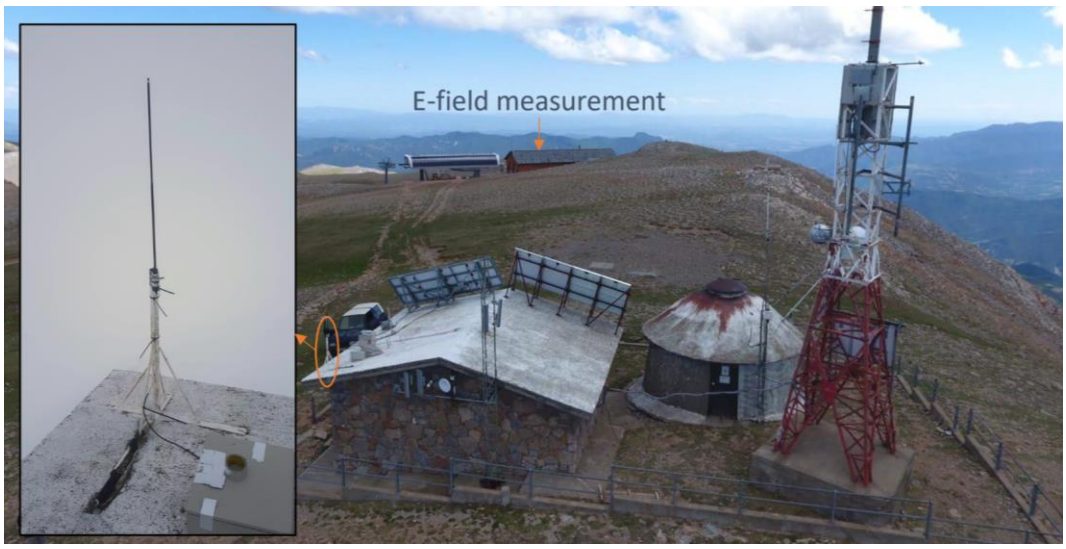


**Figure 11.** Eagle Nest Tower installations in La Tossa d'Alp, Spain.

### *4.1 Typical signals in the field*

Since the system started operating, many events were observed. Each file is recorded in a time window of 200 milliseconds and the acquisition system takes a few seconds to save the data, leading the system to a considerable downtime. For the recordings, the pulse frequency is determined by counting the number of pulses and dividing them by the length of the time window. Figure 12 shows the typical profile of recordings of positive and negative corona pulses in the field, simultaneously with the electric field derivative from the signal measured by the plate antenna. Over the interval considered, a background potential gradient (250 m away from the rod) of -6.3 kV/m was measured for (a) and 4.2 kV/m for (b).

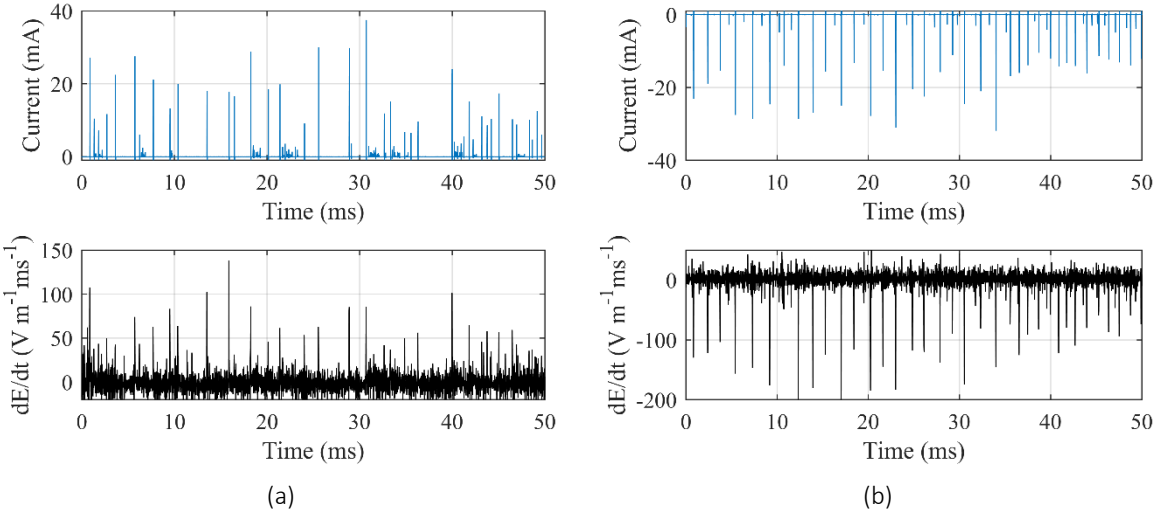


**Figure 12.** Typical recordings obtained in field using the current sensor and electric field derivative measured by the plate antenna. (a) Positive corona; (b) Negative corona.

For the cases shown, an initial high-current pulse (of tens of mA) is followed by a train of less-intense pulses in both polarities. The pulses have similar characteristics of rise and fall time compared to pulses observed in the laboratory. Each pulse introduces a perturbation on the local electric field, measured by the plate antenna. In most of the recordings, negative corona pulses present lower amplitude peaks, but when the pulses are very low in amplitude, the change in the electric field is not distinguishable from the noise level of the plate antenna.

We verified whether the electric field pulses could be associated with VHF pulses recorded during the evolution of lightning leaders inside clouds in the proximities of the sensor. For the events shown in Figure 12, the interferometer installed 3-km far from the tower did not register any VHF source for at least 20 minutes before or after the events. This indicates that the changes in the electric field obtained with the flat plate antenna and the current pulses are associated to discharges from the rod.

The corona pulses that we observed presented some similarities with precursor current pulses of artificially triggered lightning. In both cases, the grounded conductors are subject to high background electric field conditions. Biagi et al. (2012) investigated breakdown processes that occur at the top of upward extending wires. Current pulses have peak amplitudes ranging from 1 to more than 100 A, with polarity depending on the electric field. Zhang et al. (2017) studied in detail the features of precursor pulses for positive upward leaders, presenting a time duration in the order of 0.5 to 6 microseconds. The frequency of precursor pulses can be in the range of tens of hertz to tens of kilohertz, and the entire process can last up to 2 seconds, while the wire is being deployed before the lightning strike.

Comparing these results to corona discharges reported in this work, the peak current and the time duration of precursor pulses are higher, as a consequence of the greater enhancement of the electric field in triggered lightning experiments. Luminosity at the wire tip reveals that precursor pulses can be attributed to aborted leader formations that can extend up to a few meters. The corona discharge is, in turn, related to the inception of streamers over a region that reaches millimeters/centimeters. We believe that corona

discharges would also be detected in triggered lightning experiments by employing current sensors sensitive to lower currents, such as the ones we report in this work.

*4.2 Detection of pulses with lightning occurrences far away from the sensor*

The recordings of pulses were processed and for each file, it was assigned the correspondent timestamp and the pulse frequency (amount of pulses divided by time window). Figure 13 depicts an interval of three hours on Aug 29th, 2019, in which the field mill was continuously acquiring data. The increase in the background electric field can lead to recordings of positive and negative pulses.

Positive corona pulses start to be recorded at 17:33 when the potential gradient was approximately -1.8 kV/m. The highest values of frequency of pulses coincide with peaks in the amplitude of potential gradient indicating a possible correlation between the two quantities. At 17:55, the potential gradient starts decreasing in magnitude and the pulses are no longer observed after 18:15. Its polarity inverts at 18:18, and only a few recordings of negative corona are detected (blue dots) when it reaches its maximum value (around 4 kV/m). For the same value of potential gradient, negative corona pulses present a frequency about 2.5 times higher than the frequency observed for positive corona pulses.

At around 19:23, another inversion of polarity and increase in magnitude leads to recordings of positive corona pulses. The reported potential gradient signature is correspondent to the period of end-of-storm oscillation (Moore et al., 1977), in which the electric field at the ground beneath decaying thunderstorms presents several polarity changes during the transition from foul weather to fair weather.

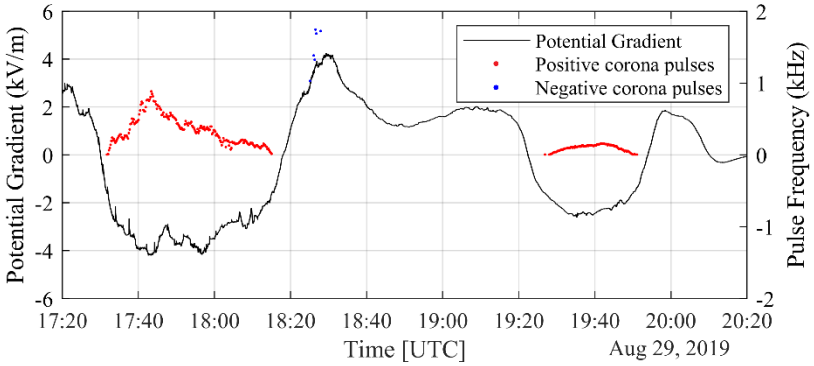


**Figure 13.** Corona pulses detections when no lightning impacts were registered nearby

Using data from the VHF interferometer, we verified storm activity in the vicinity of the sensor for the same period, as it is illustrated in Figure 14, in a large square area with side length equals to 60 km. The current sensor is positioned at the coordinates (0, 0). From the lightning location system (LINET) data, the nearest lightning strike to the sensor was 14 km away from it, at 17:58. In the first hour shown, VHF sources are detected in the vicinity of the sensor. They are related to leader processes of lightning that can extend over a wide area. From the potential gradient shown in Figure 13, these lightning strikes produced very small perturbations in the electric field, and the characteristic step signature is difficult to be distinguished.

As time increases, the core of the storm moved away from the sensor. At 18:30, the signals from VHF were registered at about 30 km. With LINET, we observed that lightning strikes were 65 km far from the sensor at 20:20. Despite the movement of the storm, pulses

were still observed until 19:50, suggesting that the increase in the potential gradient caused by the electrified cloud is enough for corona occurrence.

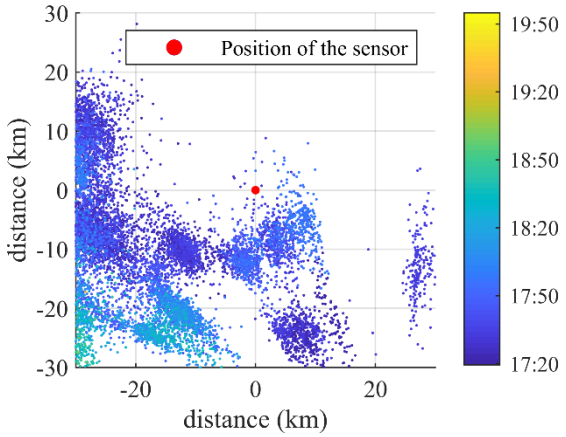


**Figure 14.** VHF sources near the sensor site for the period shown in Figure 13.

*4.3 Detection of pulses during lightning activity near the sensor*

Corona pulses were observed for several thunderstorms near the sensor. Figure 15 depicts a 15-minute interval with several lightning flashes (cloud-to-ground and intracloud) in the 15 km range of the sensor. We verified from the VHF data and with LINET that the nearest return stroke was registered at 18:31:51.642, 1.4 km away from the sensor.

Since the field mill provides a measurement of the quasi-static electric field, the steps observed are usually related to all return strokes of a flash, or even different flashes that happened within a short period. Among some remarkable steps, there are numerous other small steps indicating lightning activity of a storm cell developing tens of kilometers away.

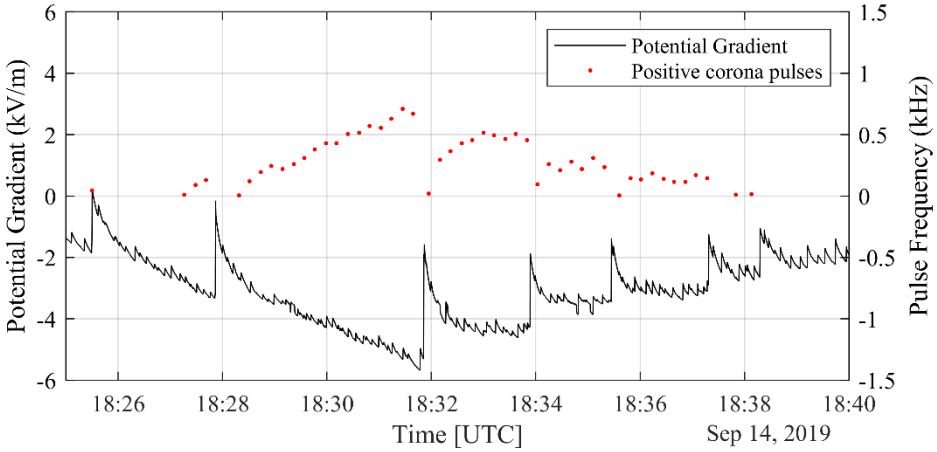


**Figure 15.** Positive corona detections with lightning activity near the sensor

The potential gradient shown in Figure 15 remains mostly negative. One can note that the strong variations caused by near lightning flashes decrease the magnitude of the electric field, and consequently, the frequency of positive corona pulses. For this event, the highest pulse frequency was around 700 Hz, and it was registered when the potential gradient was close to reaching its peak magnitude (around 5.5 kV/m). Figure 16 shows the VHF sources for the period shown in Figure 15, in a square area with a side length of 20 km. One can note that the sources are very dispersed in the vicinity of the sensor during the interval shown.

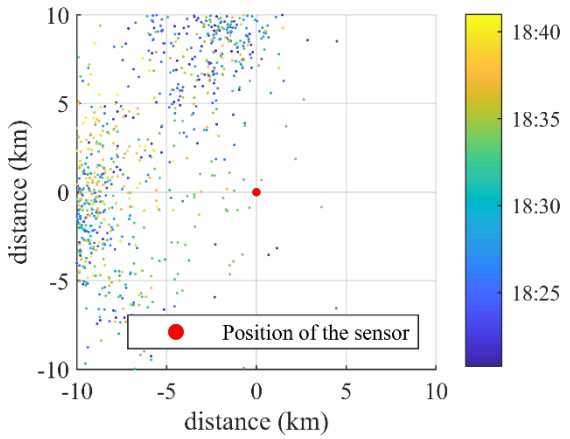


**Figure 16.** VHF sources near the sensor site for the period shown in Figure 15.

On Sep 15th, 2019, more pulses were recorded in a time window of 40 minutes, as seen in Figure 17. The overview of the potential gradient waveform indicates only one remarkable lightning flash detected at 00:35, reported by LINET as a cloud-to-ground lightning strike 4-km far from the sensor. From the negative step in the potential gradient established by the lightning strike, one can infer that this signature is correspondent to a positive cloud-to-ground strike.

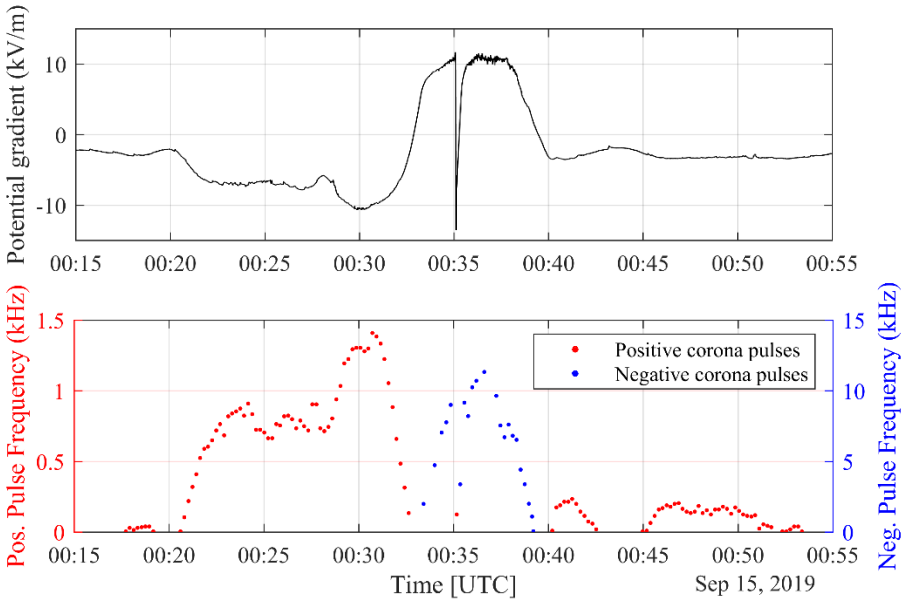


**Figure 17.** Potential gradient and corona pulses in a 40-minute interval.

Positive corona pulses were detected during most of the time interval shown in Figure 17. At 00:33, the potential gradient inverts polarity and increases, negative corona pulses are recorded. One can note that, for the same level of electric field, the frequency of negative pulses is greater than the one for positive pulses (they are plotted in the same graph with one order of magnitude of difference in scale). This is consistent with our observations in the laboratory. Negative corona pulses also seem to present a certain correlation with the background vertical potential gradient, although we did not have many recordings of them. In addition, they present lower amplitudes, which makes it more challenging to count them among the noise level of the digitizer.

Figure 18 shows the VHF detections in the vicinity of the sensor and the location of the only lightning strike detected by Linet at 18:35. At that moment, the inversion of the potential gradient causes the inversion of the polarity of pulses, registered by one single file with positive corona pulses. Considering only the data shown in Figure 17, we can estimate the potential gradient for corona onset from the grounded rod. This value is around -2.5 kV/m for positive corona and 3.8 kV/m for negative corona. The correlation between the electric field intensity and corona pulse frequency will be assessed in more detail in the following section.

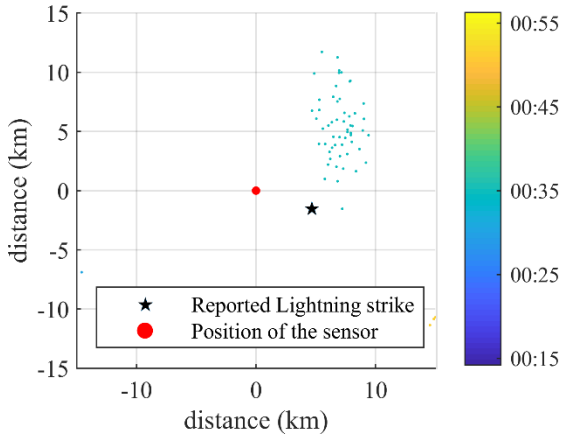


**Figure 18.** VHF sources near the sensor site for the period shown in Figure 17.

## 5. Discussion

For the setup investigated in the laboratory, the background potential gradient between the two plates for corona onset was 10 kV/m (positive corona) and 8.2 kV/m (negative corona). The use of the plane-to-point configuration provides an enhancement of the electric field near the sharp tip of the grounded rod, reaching local levels expected to be in the range of megavolts per meter (Morrow, 1997; Lu et al., 2017), sufficient for ionizing a microregion near the tip and producing the discharges.

Qualitative features of positive and negative corona are very similar to those observed in other studies (i.e. Kexin et al., 2015; Wang et al., 2017; Moreau et al., 2018; Wang et al., 2018). For the same applied voltage, positive corona pulses have higher amplitudes and lower frequency in comparison to negative corona pulses. However, their average current is very similar, in the order of a few microamps, with the precise value depending on the configuration of the geometry of the rod, gap length, presence of wind and several other factors.

### *5.1 Laboratory and Field experiments*

The sensor in La Tossa d'Alp recorded corona pulses, even when lightning activity was observed very far from the region, or not observed at all. Thereby, places located in high mountains are susceptible to corona effects due to the proximity of charged clouds and the consequent increase of the ambient electric field.

From the data points obtained for positive corona pulses, pulse frequency varies from 0 to 1.4 kHz with the measured background electric field, which ranges from 1.8 kV/m to about 12 kV/m. Higher pulse frequencies are associated with higher electric field levels. In the following section, we discuss in more detail the correlation between the two quantities. It is

important to ponder that the electric field measurement was performed at a similar height of the installation of the current sensor, but 250 m away, on a roof of a ski refugee nearby. Since charged clouds can extend horizontally up to a few kilometers, the measurement, performed at such distance, gives representative values for the studies conducted in this work, nevertheless, measurements closer to the sensor could provide an improved correlation. Even with different setups, the values that we report are comparable to the ones obtained by D'Alessandro (2009) that reported a threshold of 1.2 kV/m for positive corona at low wind speeds.

If we compare the frequency of positive pulses obtained in the laboratory (Figure 8) with the values obtained in the field (Figure 13, 15 and 17), we did not observe in the field a reduction in the pulse frequency for higher electric fields. Although the required electric field enhancement may happen for a very short time during close lightning strikes, we speculate that in the laboratory, the configuration of two plates and the grounded rod provides an increase of electric field that is not comparable to the condition of the rod under the ambient electric field. In this way, the current measured in the field is correspondent to the initial stage of corona discharges (burst pulses and Trichel pulses), and for reaching a steady-state glow corona regime, a higher background electric field would be required for a longer period.

Negative corona was more difficult to observe in the field. Due to their lower amplitude, they were more difficult to count among the noise level of the sensor. The lowest electric field observed for their detection was 3.8 kV/m. From his experimental results, D'Alessandro (2009) showed a threshold of 1.5 kV/m for low wind speeds. Evidently, rod geometry, rod height, and the conditions of the installations play a crucial role in these values, making it difficult to compare electric field thresholds for different experiments.

Regarding the pulse frequency from the measured data, one can note that for higher magnitudes of potential gradient, the pulse frequency differs in almost one magnitude for the different corona polarities. For a potential gradient with a magnitude of around -12 kV/m, positive corona has a pulse frequency of about 1.3 kHz, whereas for the same magnitude but positive, the pulse frequency can reach around 11 kHz, with some dispersion (see Figure 17). This is consistent with our observations in the laboratory for the pulsating stage of corona, in which a 12 kV/m average electric field leads to pulse frequencies of 1.3 kHz and 8 kHz, respectively for positive and negative corona.

*5.2. Dependence on wind speed*

In Figure 19, we present three subplots containing the data points obtained in the events discussed in this paper, according to the date of occurrence. D'Alessandro (2009) showed that for the same electric field level, higher wind speeds result in the increase of the corona current magnitude. In our experiments, we use wind speed measurements performed 370 meters away from the current sensor and verified how the pulse frequency is affected by the average wind speed. Each data point corresponds to a recording of 200 milliseconds of the waveform measured by the current sensor. The pulse frequency is estimated by dividing the number of pulses by the time window, the electric field is the average value computed by the field mill at that timestamp, and the wind speed is the one-minute average registered by the weather station.

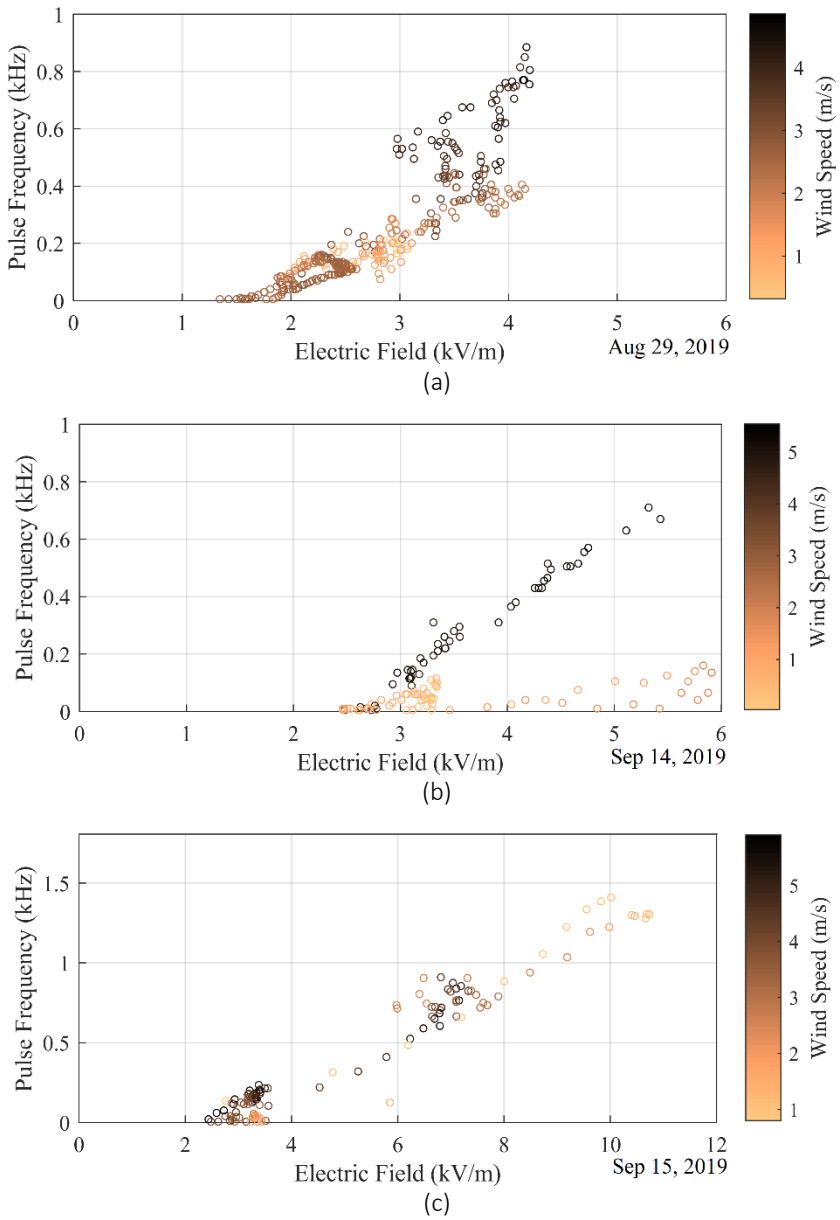


**Figure 19.** Scatter plot of pulse frequency versus electric field magnitude for positive corona on (a) Aug 29, (b) Sep 14, and (c) Sep 15.

In Figure 19a, for data from 29th of August 2019, even with the high number of data points displayed, one can note that for a same electric field level, points with higher pulse frequency are correspondent to higher wind speeds. In Figure 19b, we plotted data from two distinct periods. The period with higher wind speed corresponds to the interval shown in Figure 15, and it reveals a trend line with a slope significantly higher from the second period, recorded later, during the same thunderstorm. In the latter case, the electric field ranges from 2.5 kV/m to 6 kV/m leading to pulse frequencies inferior than 200 Hz.

The dataset of Sep 15th seems to present a more linear correlation, despite the higher variations of pulse frequency, electric field, and wind speed. One can see a high density of data points in the range from 2 to 4 kV/m, in which there is a trend showing a higher slope for higher wind speed. For this range, several points with very low pulse frequency are

recorded when the wind speed is lower than 2.5 m/s. For higher electric fields, the small number of points hinders further correlation of data with the average wind speed.

In several other works (Hutchinson, 1951; Chapman, 1955; D'Alessandro, 2009; Bazelyan et al., 2019), it is discussed the quasi-linear dependence of corona current on wind speed above a certain wind speed onset. The results described in section 3 show that for the initial stage of corona discharges both pulse frequency and average current increase with the electric field. The findings presented in section 5 indicate that higher wind speeds can favor corona discharges, increasing the pulse frequency for the same electric field level. The role of wind in removing ions from a space charge cloud acts as a fuel for the corona current and can also favor the initiation of upward leaders. Mostajabi et al. (2018) conducted an analysis on self-initiated upward lightning finding that among a dataset of 31 events, 30 happened under wind speeds higher than 12 m/s. Very tall structures, that constantly face strong winds, can have the corona shield removed, thus clearing the way for upward leaders (Pineda et al., 2019).

## 6. Summary and Conclusions

This paper presented observations of corona discharges recorded in the laboratory and in the field using a shunt resistor, a high impedance ammeter and a current transformer.

In the laboratory, several features already reported in literature were confirmed, such as the shape of the pulses and the increase of the corona current according to the voltage applied at the upper plate. In the initial stage of corona, regardless the polarity, the frequency of the pulses increases with the applied voltage. Visual detections using a camera with an optical filter and an intensifier for the UV range allowed observations of the difference in shapes of corona for different polarities and intensities. At the same voltage, positive corona visually develops more than the negative corona, presenting higher amplitudes, lower frequency but with a similar, yet slightly lower, average current.

In the field, we used a current transformer coupled to a conductive grounded rod. Current pulses were measured under high background electric fields. We observed that lightning activity can lead to rapid variations of the electric field, which in turn can trigger, cease, or significantly alter the frequency of corona discharges. A correlation between the frequency of positive corona pulses and the ambient electric field indicated a certain dependency between them. Higher wind speeds may contribute to higher pulse frequencies at the same electric field level. Other factors such as humidity and wind speed are well known to affect the discharges.

We observed some similarities between corona current pulses and precursor current registered for triggered lightning. Despite they present different magnitudes of peak current and time duration, both are caused by wire/electrodes under high electric fields. Corona discharges are related to streamer inception while precursor triggered lightning current is related to aborted leader formations.

This work continues under development, with improved prototypes installed in other two different experimental sites, with different orography than the one considered in this paper. We aim to improve the investigation on the behavior of the corona current, and their relation to the inception of upward leaders associated with lightning strikes.

## Acknowledgements

This project has received funding from the European Union's Horizon 2020 research and innovation program under the Marie Sklodowska-Curie grant agreement No. 722337. This work was also supported by research grants from the Ministry of Economy and Competitiveness (MINECO) and the European Regional Development Fund (FEDER): ENE2017-91636-EXP, ESP2017-86263-C4-2-R and ESP2019-109269RB-C42.

## References

Aleksandrov, N., Bazelyan, E., Carpenter Jr, R., Drabkin, M., Raizer, Y., 2001. The effect of coronae on leader initiation and development under thunderstorm conditions and in long air gaps. J. Phys. D: Appl. Phys. 34, 3256. https://doi.org/10.1088/0022-3727/34/22/309.

Arcanjo, M., Guimarães, M, Visacro, S. 2019. On the interpeak interval of unipolar pulses of current preceding the return stroke in negative CG lightning. Elec. Power Sys. Res. 173, 13-17. https://doi.org/10.1016/j.epsr.2019.03.028.

Bazelyan, E., Raizer, Y., Aleksandrov, N., D'Alessandro, F., 2009. Corona processes and lightning attachment: The effect of wind during thunderstorms, Atmos.c Res., 94(3), 436-447. https://doi.org/10.1016/j.atmosres.2009.07.002.

Bazelyan, M., Raizer, Y.P., Aleksandrov, N.L. 2015. The effect of space charge produced by corona at ground level on lightning attachment to high objects. Atmos. Res. 153, 74–86. https://doi.org/10.1016/j.atmosres.2014.07.018.

Becerra, M., Cooray, V., Soula, S., Chauzy, S. 2007. Effect of the space charge layer created by corona at ground level on the inception of upward lightning leaders from tall towers. J. Geophys. Res., 112, D12205. https://doi.org/10.1029/2006JD008308.

Becerra, M. 2013. Glow corona generation and streamer inception at the tip of grounded objects during thunderstorms: Revisited. J. of Physics D: Applied Physics, 46, 135205. https://doi.org/10.1088/0022-3727/46/13/135205.

Becerra, M. 2014. Corona discharges and their effect on lightning attachment revisited: Upward leader initiation and downward leader interception. Atmos. Res., 149, 316-323. https://doi.org/10.1016/j.atmosres.2014.05.004.

Biagi, C. J., Uman, M. A., Hill, J. D., Rakov, V. A., Jordan, D. M. 2012. Transient current pulses in rocket-extended wires used to trigger lightning. Journal of Geophysical Research: Atmospheres, 117(D7). https://doi.org/10.1029/2011jd016161.

Chang, J.S., Lawless, P.A., Yamamoto, T. 1991. Corona discharge processes. IEEE Trans. Plasma Sci., 19(6), 1152-1166. https://doi.org/10.1109/27.125038.

Chapman, S. 1955. Effects of wind and space charge on corona point discharge, particularly from aircraft. Proc. Conf. Atmospheric Electricity. Pap. n. 42, AFCRCTR-55-222. 120-134.

Chauzy, S., Raizonville, P. 1982. Space charge layers created by coronae at ground level below thunderclouds: Measurements and modeling. J. Geophys. Res. 87(C4), 3143– 3148. https://doi.org/10.1029/JC087iC04p03143.

Chauzy, S., Soula, S. 1999. Contribution of the ground corona ions to the convective charging mechanism. Atmos. Res. 51, 279-300. https://doi.org/10.1016/S0169-8095(99)00013-7.

D'Alessandro, F. 2009. Experimental study of the effect of wind on positive and negative corona from a sharp point in a thunderstorm. J. Electrost. 67, 482-487. https://doi.org/10.1016/j.elstat.2008.12.003.

Davis, R., Standring, W.G. 1947. Discharge currents associated with kite balloons. The Royal Soc. pub. 191, 2026. https://doi.org/10.1098/rspa.1947.0117.

Dordizadeh, P., Adamiak, K., Peter Castle, G.S. 2015. Numerical investigation of the formation of Trichel pulses in a needle-plane geometry. J. Phys. D: Appl. Phys. 48, 415203. https://dx.doi.org/10.1088/0022-3727/48/41/415203.

Dordizadeh, P., Adamiak, K., Peter Castle, G.S. 2017. Experimental study of the characteristics of Trichel pulses in the needle-plane negative corona discharge in atmospheric air. J. of Electrostatics. 88, 49-54. https://doi.org/10.1016/j.elstat.2016.12.013.

Gallo, C.F. 1977. Corona-A brief status report. IEEE Trans. Ind. Appl. IA-13, 550–557. https://doi.org/10.1109/TIA.1977.4503458.

Guimarães, M., Arcanjo, M., Murta Vale, M.H., Visacro, S. 2017. Unusual features of negative leaders' development in natural lightning, according to simultaneous records of current, electric field, luminosity, and high-speed video. J. Geophys. Res. Atmos. 122, 2325–2333. https://doi.org/10.1002/2016JD025891.

Guo, X., Zhang, Q. 2017. Effects of geometrical parameters of two height-unequal adjacent objects on corona discharges from their tips during a thunderstorm. Atmos. Res. 190, 113-120. https://doi.org/10.1016/j.atmosres.2017.02.010.

Harrison, R.G. 2013. The Carnegie Curve. Surv. Geophys. 34, 209. https://doi.org/10.1007/s10712-012-9210-2.

Hutchinson, W.C.A. 1951. Point-discharge currents and the earth's electric field. Quar. J. of the Royal Met. Soc. 77, 627-632. https://doi.org/10.1002/qj.49707733406.

Kexin, Z., Yongjun, P., Miao, T., Jingfeng, T., Liqiu, W., Chaohai1, Z. 2015. Mode Transition of Trichel pulses. J. Phys.: Conf. Ser. 652, 012016. https://doi.org/10.1088/1742-6596/652/1/012016.

Kip, A.F. 1938. Positive-Point-to-Plane Discharge in Air at Atmospheric Pressure. Physical Review. 54(2), 139–146. https://doi.org/10.1103/PhysRev.54.139.

Lu, B., Sun, H., Wu, Q. 2017. Characteristics of Trichel Pulse Parameters in Negative Corona Discharge. IEEE Trans. on Pl. Sci. 45(8), 2191-2201. https://doi.org/10.1109/TPS.2017.2713831.

Montanyà, J., Van der Velde, O., Romero, D., March, V., Solà, G., Pineda, N., Soula, S., Hermoso, B. 2012. Two upward lightning at the Eagle Nest tower. at Int. Con. on Lightning Protection (ICLP), Vienna, Austria. https://doi.org/10.1109/ICLP.2012.6344373

Montanyà, J., Van der Velde, O., Williams, E. R. 2014. Lightning discharges produced by wind turbines. J. Geophys. Res. Atmos., 119, 1455-1462. https://doi.org/10.1002/2013JD020225.

Moore, C.B., Voonegut, B. 1977. The thundercloud, in Lightning, vol. 1, edited by R. H. Golde, Elsevier, 51-98.

Moreau, E., Audier, P., Bernard, N. 2018. Ionic wind produced by positive and negative corona discharges in air. J. Electrostatics, 93, 85-96. https://doi.org/10.1016/j.elstat.2018.03.009.

Morrow, R. 1997. The theory of positive glow corona. 1997 J. Phys. D: Appl. Phys.30, 3099. https://doi.org/10.1088/0022-3727/30/22/008.

Mostajabi, A., Sunjerga, A., Azadifar, M., Smorgonskiy, A., Rubinstein, M., Rachidi, F., Diendorfer, G. 2018. On the Impact of Meteorological Conditions on the Initiation of Upward Lightning Flashes from Tall Structures. at 34th Int. Con. on Lightning Protection (ICLP), Rzeszow, Poland. https://doi.org/10.1109/ICLP.2018.8503310.

Pineda, N., Montanyà, J., Romero, D., Bech, J., Casellas, E., Gonzáles, S. 2018. Meteorological aspects of winter upward lightning from an instrumented tower in the Pyrenees. at Int. Con. on Lightning Protection (ICLP), Rzeszow, Poland. https://doi.org/10.1109/ICLP.2018.8503271.

Pineda, N., Figueras i Ventura, J., Romero, D., Mostajabi, A., Azadifar, M., Sunjerga, A., et al. 2019. Meteorological aspects of self-initiated upward lightning at the Säntis tower (Switzerland). J. of Geop. Res. Atmospheres, 124. https://doi.org/10.1029/2019JD030834.

Rakov, V., Fundamentals of Lightning. 2016. Cambridge: Cambridge University Press. https://doi:10.1017/CBO9781139680370.

Trichel, G.W. 1938. The Mechanism of the Negative Point to Plane Corona Near Onset. Physical Review. 54, 1078. https://doi.org/10.1103/PhysRev.54.1078.

Trichel, G.W. 1939. The Mechanism of the Positive Point-to-Plane Corona in Air at Atmospheric Pressure. Physical Review. 55(4), 382–390. https://doi.org/10.1103/PhysRev.55.382.

Wang, Z., Lu, T., Liu, Y., Bian, X., Li, X. 2017. Comparative study of two different measuring methods for corona current pulses. J. Electrost. 88, 134-138. https://doi.org/10.1016/j.elstat.2016.12.018.

Wang, C., Chen, X., Ouyang, J., Li, T., Fu, J. 2018. Pulse Current of Multi-Needle Negative Corona Discharge and Its Electromagnetic Radiation Characteristics. Energies. 11, 3120. https://doi.org/10.3390/en11113120.

Whipple, F.J.W., Scrase F.J. 1936. Point Discharge in the Electric Field of the Earth. Met. Off. of Geo physical Memoirs. 68(7), 20.

Zhang, Y., Krehbiel, P. R., Zhang, Y., Lu, W., Zheng, D., Xu, L., Huang, Z. 2017. Observations of the initial stage of a rocket-and-wire-triggered lightning discharge. Geophys. Res. Lett., 44, 4332– 4340. https://doi.org/10.1002/2017GL072843.

# 4.2 Optical Signatures Associated with Streamers and Leaders of Laboratory Discharges

## *4.2.1 Introduction and methodology*

Lightning is a fast discharge characterized by the propagation of current waves through plasma channels. These surge events produce optical emissions all over the spectra (from ultraviolet to infrared) associated with physical processes of the main components of the lower atmosphere (Nitrogen and Oxygen) and their interaction with the lightning channel. The study of optical signatures from thunderstorms performed in satellites has contributed to a better understanding of processes related to lightning.

This work investigates the strongest optical emissions associated with long laboratory sparks (at the wavelengths of 337 nm and 777 nm) with the aim to understand similar emissions in lightning. The processes of the long-spark formation (long-air gap discharges produced with a Marx Generator) are studied by using optical measurements, current signatures, and short-time exposure images. This work aims to support satellite-based measurements that perform optical measurements in the same wavelength ranges.

## *4.2.2 Results*

Blue optical emissions (337 nm) are associated with streamer development and negative leader stepping, and the optical pulses have good correlation with current pulses. Red optical emissions (777 nm) are mainly associated with stable leader propagation, when this irradiance is predominant over the blue one. The results indicate that formations of stems from positive leaders also produce emissions at 777 nm.

The use of multiple tips for the ground electrode increases the number of current pulses observed during the voltage rise. The correlation between the current and the blue irradiance persists, yet both present significantly lower amplitudes. The stable leader propagation takes place after the peak and collapse of the blue irradiance, with the remarkable increase and acceleration of the current and the red irradiance.

## *4.2.3 Article and reference*

Arcanjo, M., Montanyà, J., Urbani, M. & Lorenzo, V. (2021). Optical Signatures Associated with Streamers and Leaders of Laboratory Discharges. *Geophysical Research Letters*, 48, e2021GL095601.2021.
doi: 10.1029/2021GL095601.

# Optical Signatures Associated with Streamers and Leaders of Laboratory Discharges

M. Arcanjo[1,2], J. Montanyà[1], M. Urbani[1], V. Lorenzo[2]

[1]Electrical Engineering Department, Polytechnic University of Catalonia, Terrassa, Barcelona, Spain.

[2]Dena Desarrollos S.L. (Ingesco), Terrassa, Spain.

Corresponding author: Marcelo Arcanjo (marcelo.augusto.sousa@upc.edu)

Post-print of paper published with: https://doi.org/10.1029/2021GL095601.

## Key points:

- Measurements of 337 nm and 777 nm irradiances in long-gap discharges are acquired simultaneously with current and short-time exposure images
- Blue optical emissions (337 nm) are associated with streamer development and negative leader stepping.
- During stable leader propagation, red optical emissions (777 nm) are predominant over the blue.

## Abstract

This work investigates the strongest optical emissions associated with long laboratory sparks (at the wavelengths of 337 nm and 777 nm) with the aim to understand similar emissions in lightning. The processes of the long-spark formation are studied by using optical measurements, current signatures, and short-time exposure images. Blue optical emissions (337 nm) are associated with streamer development and negative leader stepping, and the optical pulses have good correlation with current pulses. Red optical emissions (777 nm) are mainly associated with stable leader propagation, when this irradiance is predominant over the blue one. The results indicate that formations of stems from positive leaders also produce emissions at 777 nm. This work aims to support satellite-based measurements that perform optical measurements in the same wavelength ranges.

## Plain Language Summary

Lightning is a fast discharge characterized by the propagation of current waves through plasma channels. These surge events produce optical emissions all over the spectra (from ultraviolet to infrared) associated with physical processes of the main components of the lower atmosphere (Nitrogen and Oxygen) and their interaction with the lightning channel. The study of optical signatures from thunderstorms performed in satellites has contributed to a better understanding of processes related to lightning. In this work, we investigate the strongest optical emissions associated with long laboratory sparks (at the wavelengths of 337 nm and 777 nm). Altogether with current signatures and short-time exposure images, we characterized the processes that produce these emissions to support satellite-based measurements.

## 1 Introduction

The advent of new technologies and the improvement of sensors embedded in satellites have allowed optical observations of diverse phenomena associated with lightning. Measurements of radiances from the cloud top consider all types of lightning during day and night, mainly based on the emissions of the oxygen triplet band at 777.4 nm. (e.g. Chern et al., 2003; Christian et al., 1989; Goodman et al., 2013; Kirkland et al., 2001; Neubert et al., 2019). The use of satellite-based instruments, combined with other mapping techniques, provides comprehensive details for lightning investigation. The information obtained by satellites requires careful analysis due to the complexity of lightning-associated phenomena: processes before the return stroke such as the propagation of streamers and leaders inside the clouds, impulsive currents that usually last microseconds during the return strokes, recoil leaders, long continuous currents that can last milliseconds, and subsequent events correlated such as blue jets, sprites, and elves (Rakov & Uman, 2003; Neubert et. al., 2008). Surges in 777.4 nm luminosity were associated with return stroke currents, recoil leaders, and leader branching processes (Montanyà et al., 2021; van der Velde et al., 2019).

In 2018, the Atmosphere-Space Interactions Monitor (ASIM) was launched to obtain information from Transient Luminous Events (TLEs) and Terrestrial Gamma-ray Flashes (TGFs) caused by the activity of thunderstorms. It is equipped with three high-speed photometers at 180–230 nm, 337 nm, and 777.4 nm, with sampling rates up to 100 kHz (Chanrion et al., 2019). Recently, Soler et al. (2020) and Li et al. (2021) reported blue flashes associated with Narrow Bipolar Events (NBEs) with no simultaneous activity

at 777.4 nm; Neubert et al. (2021) showed detections from a blue jet into the stratosphere with emissions in the ultraviolet range and faint and localized emissions in the red spectral band. These studies suggest that the blue flashes and the jet are associated with non-thermal processes of cloud corona and streamer ionization waves.

Laboratory techniques have allowed a better understanding of optical emissions occurring during lightning. A broad review on lightning spectroscopy and the high-speed spectra of meter-long laboratory discharges in a wide range (between 380 nm and 800 nm) were recently explored by Kieu et al. (2021). During the breakdown, they have found several optical emissions similar to those found in natural lightning. Galimberti et al. (1974) and Les Renardiers (1981) showed the similarities between the near UV spectra of first coronas and leader coronas. The spectra are composed mainly by the radiation of the nitrogen second positive system. High-speed photography and imaging systems have also been making progress and revealing details of the formation and propagation of discharges. ICCD cameras have been used for obtaining streak images, taking short-exposure pictures, or full stroboscopic images that can assess rapid streamers' formation (e.g. Bazelyan et al., 2007; Kochkin et al., 2014; Kochkin et al., 2016; Nijdam et al., 2020). Schlieren images use the observation of changes in temperature (i.e. gas density) to distinguish stem channels from streamer filaments that cause a minimal air density change (e.g. Zhao et al. 2021a, 2021b).

Janda et al. (2011, 2012, 2016) conducted several experiments with transient sparks in very short gaps (mm range) for investigating the optical emission spectra associated to streamer-to-spark transition and NOx generation. The discharges were imaged with fast ICCD cameras and characterized with a spectrometer and photometers with narrowband filters centered in the 337 and 777 nm. The streamer development produces strong emissions in the nitrogen second positive system, while the spark phase exhibits strong atomic emissions (such as the oxygen triplet at 777 nm). By increasing the frequency of the discharges, they were able to decrease the intensity of the atomic emissions. They found that the streamer-to-spark transition is governed by the increase in the gas temperature in the plasma channel up to about 1000 K. This stage also presents the emergence of the 777 nm emissions, indicating the production of O species.

To provide a better understanding of satellite-based optical measurements of lightning discharges, this work investigates optical signatures of long-air gap (0.85-1 m) discharges produced with a Marx Generator.

## 2 Methodology

The high voltage experiments were carried out at LABELEC, in Terrassa (Spain). We present unprecedented optical signatures of the aforementioned spectral ranges (near 337 nm and 777 nm) correlated with the applied voltage and ground current during the streamer and leader phases. Additionally, we image the discharges at the moment of strong emissions obtained by the photometers with short-time exposure pictures. The optical emissions associated with the discharges within the response range of our filters can be attributed mainly to the radiation of the second positive system of nitrogen molecules (Galimberti, 1974) in the blue (337 nm) and to the radiation of the neutral O I

line in the red (777 nm), which is in reality a triplet with sublines at 777.19, 777.42, and 777.54 nm (Kieu et al., 2021).

To investigate the streamer and leader inception and their signatures, we employed two different setups. In the first configuration (plate-to-rod), the high voltage was connected to a hanging plate with 2 m of diameter standing 2 m above the floor. The ground electrode stood one meter high, leading to a gap distance of 1 m. We provided an alternative discharge path, which consisted of a sphere-to-sphere configuration, separated by approximately 30 cm. That allows streamers and leaders to develop from the ground electrode in the main gap, but the breakdown can occur in either gap. In the second configuration, there is only one discharge path with a rod-to-rod arrangement and a gap distance of 0.85 m. In both cases, the photomultipliers (PMTs) are located 2.7 m away from the ground electrode and have a wide field of view of the gap. We provide a detailed description of the instrumentation and methods in the supporting information.

## 3 Positive Leaders

When a positive voltage is applied to an electrode providing a certain level of electric field enhancement, avalanche activities in the proximity of the rod may lead to the formation of streamers, namely first coronas. One or more dark periods may follow, and secondary streamer corona bursts can trigger the formation of a thermalized gas channel forming the stem. The corona stem structure is heated up to a threshold level (1200 – 2000 K) that enables the leader development (Galimberti et al., 2002; Jiang et al., 2020). Once established, a brush-like corona zone with positive streamers directs the leader propagation (Rakov and Uman, 2003; Saba et al., 2020).

In our experiments, we used the plate-to-rod setup, applying negative voltage at the upper plate. Since the local electric field thresholds needed for sustained propagation of positive leaders is much lower than for negative leaders (Bazelyan and Raizer 2000), we measured currents and optical signatures solely due to the positive streamer/leader propagation from the grounded rod towards the plate.

In Figure 1, we show signals measured for four positive discharges with corresponding pictures displayed on the right side. A color coding scheme is applied to the original picture to enhance faint streamers (Kochkin et. al, 2014). The time scales presented consider the breakdown occurring at t=0 seconds. Figure 1a shows the last 80 μs of an aborted leader formation. The voltage increases up to 440 kV, and a few current pulses are recorded. At t = -35 μs, a pulse of 1.5 A produces optical emissions detected by both PMTs. The current decays in about 2 μs but a small quasi-DC component of tens of milliamperes is measured. The blue pulses indicate streamers developing in the main gap. At t = -15 μs, the blue irradiance increases smoothly, as well as the current, and the red irradiance starts to increase later, at t = -10 μs. The blue signal reaches another peak at t = -6.5 μs and, after that, reduces intensity substantially. From this moment on, the increase in the current accelerates along with the red signal, characterizing a stable leader development from the ground electrode. When the breakdown occurs (at the spheres adjacent to the main gap) the voltage at the upper plate collapses to zero and the leader development is aborted. The charges stored in the forming leader are rapidly induced back to the electrode. This process is characterized by oscillations in the current and an impulse in the red signal. On the right

side of Figure 1a, the still picture shows the upward leader that propagated over a vertical distance of 28 cm.

Figure 1b depicts pulses from the initial stage of the discharge when the upper plate voltage was in the range of 300-350 kV (negative). The irradiance in the blue is similar to the current, while the irradiance in the red exhibits mild pulses. Using the ICCD camera, an image with a time exposure of 9.5 μs was captured, showing the formation of a stem around the tip of the electrode and a burst of short (15 cm) streamers that emerges from the stem. In the early stage of the voltage rise, several current pulses of low amplitudes did not produce detectable pulses in the red. Our results indicate that red pulses such as shown in Figure 1b might be related to the presence of stems and thermal processes associated to the streamer-to-leader transition.

The initial stage of the leader development is shown in Figure 1c in which an image with a time-exposure of 0.9 μs was taken just before the peak of the blue irradiance. The leader has a vertical length of roughly 15 cm, and one can see that streamers from the leader's tip propagate quite far across the gap, close to reaching the upper plate (about 72 cm). In the remaining microsecond before the breakdown, the current and the intensity of the red continues to increase. On the contrary, the blue irradiance decreases.

Figure 1d shows the later stage of a stable leader propagating upwards with the corresponding image (0.9 μs time-exposure) taken 3.5 μs after the peak of the blue signal. At this point, the red optical emissions completely overcome the blue emissions. Ahead of the leader, one can note a cloud of light immersed in the gap resembling a conical volume. This is part of the corona region in front of the leader and can also be seen in Figure 1a as a purple blur in front of the streamers' tip. In the last 5 μs depicted by Figure 1d, the blue irradiance increases slightly until the breakdown. The peak of the blue signal at the breakdown is much less intense than the peak observed during the streamer burst in the initial stage of the leader. The peak of the red irradiance occurs at the breakdown and saturates the photosensor.

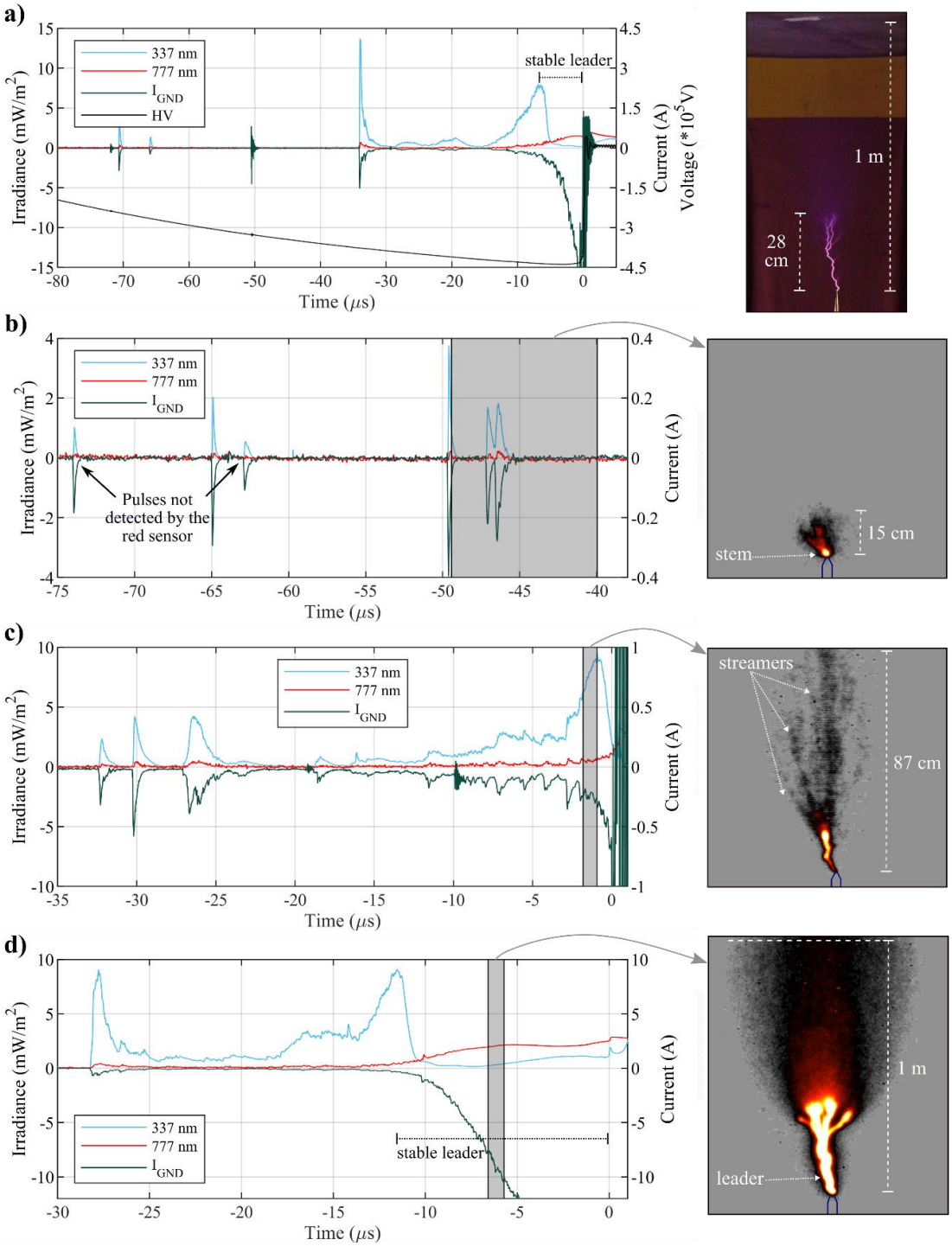


**Figure 1**. Irradiance (blue and red) and current (green) measured for four different discharges. In (a-c), the breakdown takes place in the sphere-to-sphere setup whereas in (d), it occurs in the main gap. (a) Upper plate negative voltage increase, PMTs measurements over 80 µs and 3-s still picture of the development of the aborted upward leader. (b) Pulses of current and irradiances during the formation of a stem with surrounding streamers in a 9.5 µs picture. (c) Streamer burst at the peak of the blue irradiance. The forming leader is observed in a 0.9-µs picture. (d) Optical signals and current signals during the stable leader development toward the upper plate.

We investigated the correlation between the optical irradiances and the current of a single streamer burst. The time duration of each burst varies between 600 ns and 7 µs. In Figure 2a, we show a logarithmic scattered plot of the pulse peak current and the blue peak irradiance. We found a good relationship that can be best fitted to a power-

law function, as indicated in the figure. The largest peak current observed during this regime was 1.2 A. We also calculated the individual charge of each burst, considering the same time segments correlated with the received optical energies by integrating the irradiance measured by the PMT. The results presented in Figure 2b confirm similar agreement between the variables. Comparable findings were reported by Janda et al. (2016) for the streamer stage in short gap transient discharges.

The same analysis was performed for the signals recorded in the red. These results are shown in the supporting information (Figure S3) for the sake of completeness. Compared to the blue, the red radiation does not present a good correlation with the current and charge. Initial streamer bursts that start to heat up the forming plasma channels during the voltage rise did not produce detectable optical pulses in the red.

We grouped the discharges performed with the plate-to-rod setup, classifying them if the stable leader development was detected or not. As indicated in Figures 1a and 1d, this is characterized by the collapse in the blue signal, followed by increasing currents and stronger emissions in the red. All discharges were performed with -650 kV set at the Marx Generator. Figure 2c shows a boxplot with the total charge associated with the discharges of the two groups. For the discharges that did not present the stable leader development (Q1), the total charge is computed from the start of the voltage rise until the breakdown. For the second group (Q2), the charge is calculated until the peak of the blue irradiance is reached. The two groups presented a clear separation between the charge values observed. The obtained averages were 1.3 μC for Q1 and 2.4 μC for Q2. We determined the average ground current at the moment of the peak in the blue for the discharges of Q2, corresponding to 388 mA and standard deviation of 98 mA (excluding one outlier value of 1.9 A).

By using the images obtained with short and long time-exposure for the discharges, the results indicate that the blue peak irradiance is associated with the streamer burst all over the gap, which is a precursor for the stable leader development. Note that our group criterium is different than the concept of streamer-to-leader transition. The minimum amount of charge for a single or successive corona burst required for the thermal transition is estimated in the range of 0.2-1.0 μC (e.g. Arevalo and Cooray, 2017; Galimberti, 1979; Wu et al., 2013). From our analysis, stems and leaders are incepted prior to the peak of blue irradiance, such as the cases shown in Figures 1b and 1c. The individual burst charges in those cases are within the range previously reported. Nevertheless, the group criterium introduced here presents a good agreement with the red irradiance and the current acceleration, features of the sustained leader development.

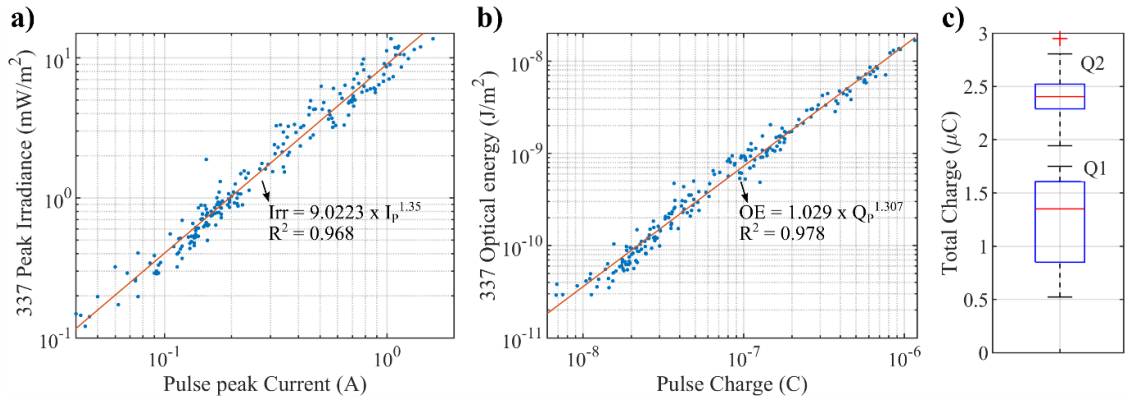


Figure 2. Optical irradiance and energy are associated with pulse peak current and pulse charge of positive discharges from the ground electrode. (a) For pulse peak current ranges from 40 mA to 1.6 A, the peak irradiance is shown for the blue photosensor. (b) The optical energy of each burst with the corresponding charge. (c) Total charge obtained during the voltage rise for two grouped discharges: Q1 when there is no evident blue collapse for increasing current and Q2 otherwise.

## 3.1 Effect of multiple tips at the ground electrode

We explored the effect of multiple tips at the ground electrode on optical emissions and currents. The single sharp tip coupled to the ground electrode was changed for a multiple-tip electrode coupled to a rectangular metallic plate and five tips in total (see Figure S4).

For this experiment, we compared the streamers formed at the two ground electrodes by triggering the camera at the same upper plate voltage levels. The image acquisition was performed with time-exposures of 10 μs (see Figure S4). Discharges with the single tip present fewer pulses, but with greater amplitude (in both current and blue sensor), whereas the discharges produced by multiple tips present more pulses, although weaker. We observe that even very small current pulses (less than 100 mA) emit in the blue range. The irradiance in the red also presents some correspondence with the current pulses, as previously discussed. From the images, we also saw bright spots from the electrodes' tips, which could be an indication of forming stems.

Noteworthy, we have performed discharges using a rod-to-rod setup with a positive voltage applied on the upper electrode. The electric field enhancement provided by this configuration favors the initiation of positive streamers/leaders (Bazelyan and Raizer 2000), as it can be seen from the measurements of irradiances in the blue (see Figure S5 of supporting information for typical waveforms and images). The mechanism of stable leader acceleration (denoted by the increase of red irradiance and decrease of blue irradiance) is the same as discussed for the plate-to-rod setup.

## 4 Negative Leaders

In the laboratory, when a negative voltage is applied to an electrode, the consequent increase in the local electric field provided by the electrode tip can lead to the inception of negative streamers. At a reduced distance from the front of the streamers, a small plasma structure (space stem) can form. Bidirectional streamers originate from this plasma body, according to the local electric field. In the posterior region of the stem, positive streamers are formed, while negative streamers are established at the other end. Upon reaching higher temperatures, the stem evolves into a floating plasma channel (space leader). The propagation of the main negative channel

consolidates after the attachment of the positive portion of the floating leader to the negative electrode streamers. This process leads to an abrupt extension of the length of the channel (step). Following the transfer of potential from the electrode to the end of the newly incorporated floating channel, new negative streamers are formed, and the process repeats, continuing the negative leader propagation (Bazelyan and Raizer 2000; Biagi et al., 2010; Galimberti et al., 2002; Rakov and Uman, 2003).

For these experiments, we used the rod-to-rod setup with a gap of 85 centimeters. It is crucial to acknowledge that the optical signals presented here correspond to discharge developments from both electrodes. Furthermore, the ground current is disturbed by discharges at the high voltage electrode due to capacitive coupling.

Figure 3 shows irradiances and the ground current for negative discharges in switching impulse. The voltage at the upper rod increases up to around 600 kV, and a small number of current pulses are observed. The blue irradiance presented some pulses of low amplitude during the voltage rise, likely related to the negative streamers that are incepted from the upper rod. Negative coronas in the air usually have less current amplitude and are fainter than positive coronas for similar high voltage levels (Arcanjo et al., 2020). We did not observe evident pulses of red irradiance before the last 5 μs of the discharges. Although the charging voltage of the Marx Generator is higher in this case, the rod-to-rod configuration with a negative voltage applied does not favor positive stem/leader inception from the ground electrode, as it occurs for the plate-to-rod setup (See Figure 1).

Figure 3a depicts an interval of 20 μs before the breakdown. At t = -4 μs, a strong pulse is measured by the photometers and the current sensor. This pulse reaches a blue peak irradiance of 38 mW/m2 and a peak current (measured at the ground electrode) of 0.85 A. A 5-μs time-exposure image is taken during the moment indicated by the shaded region shown in Figure 3a, revealing a glowing sphere-like volume around the high voltage electrode. This structure is connected to a secondary volume that is located at about 11.8 cm below the electrode tip, indicating a space stem formation, similar to the ones reported by Les Renardiers (1981), Reess et al. (1995) and Kochkin et al. (2014). From the ground electrode, a dim streamer-like shape can be noticed. A second pulse at t = -2.9 μs, completes the single-step process before the stable leader propagation. The blue peak irradiance is 24 mW/m2 and, after the pulse, the current increases sharply, followed by the collapse of the blue signal and the increase in the red signal until the moment of the breakdown (at t=0).

Figure 3b shows data from another discharge, in which only one large pulse in the blue is observed before the stable leader development. On the right side of the figure, an image taken with time-exposure of 80 ns reveals leaders propagating from both electrodes. At this moment, the current at the ground electrode is 45 A. Although the leaders saturate the image, it is possible to appreciate positive leader branches propagating behind the connecting channel. They are “connected” to the negative leader tip by a glowing zone, similar to the positive upward leader shown in Figure 1d.

For both discharges shown in Figure 3, during the last two microseconds before the breakdown, the red irradiance slowly increases as well as the blue irradiance, although in different levels. The peak irradiances align with the first current peak of about 1.4 kA, but the red signal saturates. After that, the current waveform reaches its peak (roughly

1.6 kA) and decays rapidly, oscillating in both polarities before returning to zero. The blue irradiance observed during the discharge current is drastically lower than the pulses observed during the stepping process.

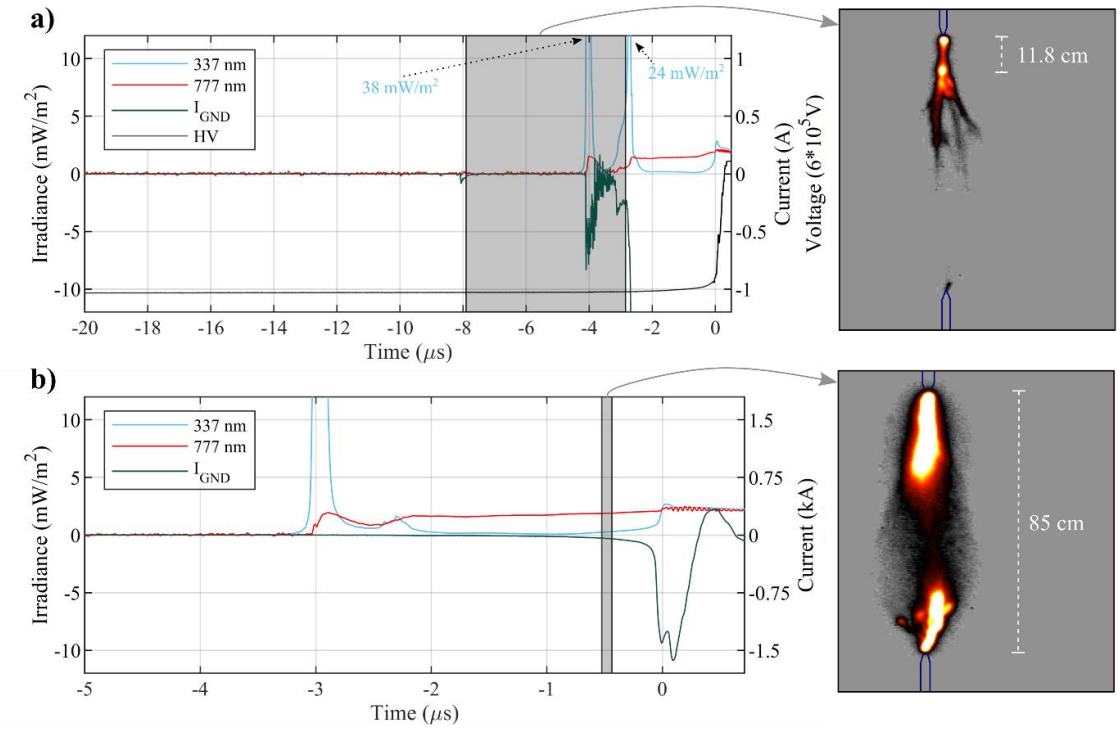


**Figure 3.** Optical emissions and current during the final stage of two negative rod-to-rod discharges. (a) The 4.5 µs time-exposure image shows features of stepping of the negative leader and a space stem formed 11.8 cm below the electrode tip. (b) The leader stage consolidation with stronger red emissions. The negative and positive leader developments are shown in an 80-ns image taken 500 ns before the discharge.

## 5 Discussion and implications for lightning

We observed that the positive leader development is characterized by the increase of the emissions at the 777 nm wavelength. Nevertheless, weaker current pulses during the voltage rise, also produced such emissions when stems are incepted (see Figure 1). That is expected to be related to the thermalization process during the positive streamer-to-leader transition. For initial current pulses measured during the voltage rise, we did not observe 777 emissions, similarly to Janda et al. (2016), who performed transient discharges in a particular setup. Zhao et al. (2021b) showed millimeter-long stems since the first streamer burst, and that later streamer bursts could branch and elongate stems, driving the propagation of positive leaders. Their findings provide valuable contributions to the role of stems heating the precursor leader path. In our experiments, the major emissions in the red starts during the stable leader development (after the streamer burst marked by a peak and collapse of the blue emissions). The red irradiance increases along with the uprising continuous current and a slight increase in the blue irradiance (see Figure 1d) before breakdown.

Blue optical emissions are associated with streamer development, and negative leader stepping, and are expected to be observed in satellite-based observations of activities that involve positive and negative leader propagation. We have found a significant correlation between the peak emissions at the 337 nm wavelength and the peak current of burst streamer pulses (See Figure 2a). Janda et al. (2016) found a similar

agreement comparing the waveforms of detections at 337 nm with the streamer current. We also noted an improved correlation between the optical energy and the pulse charge (See Figure 2b). The use of multiple tips for the ground electrode increases the number of current pulses observed during the voltage rise. The correlation between the current and the blue irradiance persists, yet both present significantly lower amplitudes.

The stable leader propagation takes place with the remarkable increase and acceleration of the current and the red irradiance. That happens after the peak and collapse of the blue irradiance. By grouping the discharges whether they presented the stable leader development, we calculated the total charge "dissipated" from the beginning of the voltage rise. The average total charges found were significantly different: 1.3 μC for the first group (Q1) and 2.4 μC for Q2, calculated up to the moment when the stable leader is detected (see Figure 2c).

We measured blue emissions associated with negative streamers during the voltage rise in the rod-to-rod experiment. They are more difficult to see due to their lower amplitude and shape (Arcanjo et al., 2020). We observed a large pulse in the blue associated with the negative leader inception and step (see Figure 3a). This pulse presents irradiances considerably higher than for the positive leader. We have left for future works a closer-look temporal analysis of emissions during the breakdown, since for now, our PMT saturated.

The development of in-cloud positive leaders with corona brushes leading its propagation is expected to produce emissions content in both blue and red regions. The same should be expected in the stepped fashion propagation of negative leaders, with streamers guiding the connection between the leader tip and the space stems/leaders. That is consistent with similar 337 and 777 nm signatures for several events observed by the ASIM mission (e.g. Heumesser et al., 2020; Neubert et al., 2019; Østgaard et al., 2019).

Blue flashes and other events with an absence of emissions in the red are associated with cold discharges characterized by traveling streamers inside the clouds such as in NBEs (Cooray et al., 2020; Li et al., 2021; Soler et al., 2020). The high currents associated with these events (estimated in the order of tens of kiloamperes) produce narrow but strong irradiating signals (Rison et al., 2016). Using the relationship provided in Figure 2a between peak current and peak irradiance measured in our setup, we extrapolated the irradiance for peak currents such as the ones of fast breakdown. For a peak current value of 55 kA, we estimated irradiances measured at ASIM's distance (400 km) with values of roughly 1 μW/m2 (see supporting information for details). This value is within the order of magnitude of those measured by ASIM, about 10 μW/m2 (Soler et al., 2020). In future works we intend to deepen the calculations of such quantities, considering more events reported by ASIM and atmospheric effects that can interfere on the calculations.

## Acknowledgments

This work has received funding from the European Union Horizon 2020 Framework Programme under the Marie Skłodowska-Curie Grant Agreement SAINT 722337. This

work was also supported by research Grant ESP2017-86263-C4-2-R funded by MCIN/AEI/ 10.13039/501100011033 and by "ERDF A way of making Europe", by the "European Union"; and Grants PIDP2019-109269RB-C42 and ENE2017-91636-EXP funded by MCIN/AEI/ 10.13039/501100011033.

## Data Availability Statement

Measurements and data file supporting the conclusions are available at: https://doi.org/10.7910/DVN/IPC94J.

## References

Arcanjo, M., Montanyà, J., Urbani, M., Lorenzo, V., & Pineda, N. (2020). Observations of corona point discharges from grounded rods under thunderstorms. Atmospheric Research, 247, 105238. https://doi.org/10.1016/j.atmosres.2020.105238

Arevalo L, Cooray V. Unstable Leader Inception Criteria of Atmospheric Discharges. Atmosphere. 2017; 8(9):156. https://doi.org/10.3390/atmos8090156

Bazelyan, E. M., and Y. P. Raizer (2000), Lightning Physics and Lightning Protection, IOP Publishing, Bristol, England.

Bazelyan, E M; Raizer, Yu P; Aleksandrov, N L (2007). The effect of reduced air density on streamer-to-leader transition and on properties of long positive leader. Journal of Physics D: Applied Physics, 40(14), 4133–4144. https://doi.org/10.1088/0022-3727/40/14/007

Biagi, C. J., Uman, M. A., Hill, J. D., Jordan, D. M., Rakov, V. A., & Dwyer, J. (2010). Observations of stepping mechanisms in a rocket-and-wire triggered lightning flash. Journal of Geophysical Research, 115, D23215. https://doi.org/10.1029/2010JD014616

Chern, J. L., R. R. Hsu, H. T. Su, S. B. Mende, H. Fukunishi, Y. Takahashi, & L. C. Lee (2003), Global survey of upper atmospheric transientluminous events on the ROCSAT-2 satellite, J. Atmos. Sol. Terr. Phys.,65, 647–659. https://doi.org/10.1016/S1364-6826(02)00317-6.

Christian, H. J., Blakeslee, R. J.,& Goodman, S. J. (1989). The detection of lightning from geostationary orbit, Journal of Geophysical Research, 94, 13329–13337. https://doi.org/10.1029/JD094iD11p13329

Chanrion, O., Neubert, T., Lundgaard Rasmussen, I., Stoltze, C., Tcherniak, D., Jessen, N. C., et al. (2019). The modular multispectral imaging array (MMIA) of the ASIM Payload on the International Space Station. Space Science Reviews,215, 28. https://doi.org/10.1007/s11214-019-0593-y

Cooray, V., Cooray, G., Rubinstein, M., & Rachidi, F. (2020). Modeling compact intracloud discharge (CID) as a streamer burst. Atmosphere, 11(5), 549.398. https://doi.org/10.3390/atmos11050549

Gallimberti, I; Hepworth, J K; Klewe, R C (1974). Spectroscopic investigation of impulse corona discharges. *J. Phys. D: Appl. Phys.*, 7(6), 880–898. https://doi.org/10.1088/0022-3727/7/6/315

Gallimberti, I. (1979). The mechanism of the long spark formation. Journal de Physique Colloques, 40(C7), 193–250. https://doi.org/10.1051/jphyscol:19797440

Gallimberti, I., Bacchiega, G., Bondiou-Clergerie, A., & Lalande, P. (2002). Fundamental processes in long air gap discharges. Comptes Rendus Physique, 3(10), 1335–1359. https://doi.org/10.1016/S1631-0705(02)01414-7

Goodman, S. J., Blakeslee, R. J., Koshak, W. J., Mach, D., Bailey, J., Buechler, D., et al. (2013). The GOES-R geostationary lightning mapper (GLM). Atmospheric Research, 125, 34–49. https://doi.org/10.1016/j.atmosres.2013.01.006

Heumesser, M., Chanrion, O., Neubert, T., Christian, H. J., Dimitriadou, K., Gordillo-Vazquez, F. J., et al. (2021). Spectral observations of optical emissions associated with Terrestrial Gamma-Ray Flashes. Geophysical Research Letters, 48, e2020GL090700. https://doi.org/10.1029/2020GL090700.

Janda, M., Machala, Z. (2011). Imaging of Transient Spark in Atmospheric Air by Fast iCCD Camera. IEEE Transactions on Plasma Science, 39(11), 2246–2247. https://doi.org/10.1109/TPS.2011.2157175

Janda, M., Machala, Z., Niklová, A., Martišovitš, V. (2012). The streamer-to-spark transition in a transient spark: a dc-driven nanosecond-pulsed discharge in atmospheric air. Plasma Sources Science and Technology, 21(4), 045006. https://doi.org/10.1088/0963-0252/21/4/045006

Janda, M., Martišovitš, V., Hensel, K. et al. Generation of Antimicrobial NOx by Atmospheric Air Transient Spark Discharge. Plasma Chem Plasma Process 36, 767–781 (2016). https://doi.org/10.1007/s11090-016-9694-5

Jiang, R., Qie, X., Li, Z., Zhang, H., Li, X., Yuan, S., et al. (2020). Luminous crown residual vs. bright space segment: Characteristical structures for the intermittent positive and negative leaders of triggered lightning. Geophysical Research Letters, 47(21), e2020GL088107. https://doi.org/10.1029/2020GL088107.

Kieu, N., Gordillo-Vázquez, F. J., Passas, M., Sánchez, J., & Pérez-Invernón, F. J. (2021). High-speed spectroscopy of lightning-like discharges: Evidence of molecular optical emissions. Journal of Geophysical Research: Atmospheres, 126, e2021JD035016. https://doi.org/10.1029/2021JD035016

Kirkland, M. W., Suszcynsky, D. M., Guillen, J. L. L., and Green, J. L. (2001), Optical observations of terrestrial lightning by the FORTE satellite photodiode detector, J. Geophys. Res., 106( D24), 33499– 33509, doi:10.1029/2000JD000190.

Kochkin, P. O., van Deursen, A. P. J., & Ebert, U. (2014). Experimental study of the spatio-temporal development of metre-scale negative discharge in air. Journal of Physics D, 47(14), 145203. https://doi.org/10.1088/0022-3727/47/14/145203.

Kochkin, P., Lehtinen, N., van Deursen, A. P. J., & Østgaard, N. (2016). Pilot system development in metre-scale laboratory discharge. Journal of Physics D, 49, 425203. https://doi.org/10.1088/0022-3727/49/42/425203.

Les Renardieres Group (1981). Negative discharges in long air gaps at Les Renardieres—1978 results and conclusions. Electra,74.67–216.

Li, D., Luque, A., Gordillo-Vázquez, F. J., Liu, F., Lu, G., Neubert, T., et al. (2021). Blue Flashes as Counterparts to Narrow Bipolar Events: The Optical Signal of Shallow In-Cloud Discharges. Journal of Geophysical Research: Atmospheres, 126, e2021JD035013. https://doi.org/10.1029/2021JD035013

Montanyà, J., López, J. A., Morales Rodriguez, C. A., van der Velde, O. A., Fabró, F., Pineda, N., et al. (2021). A simultaneous observation of lightning by ASIM, Colombia-Lightning Mapping Array, GLM, and ISS-LIS. Journal of Geophysical Research: Atmospheres, 126, e2020JD033735. https://doi.org/10.1029/2020JD033735

Neubert, T., Rycroft, M., Farges, T. et al. Recent Results from Studies of Electric Discharges in the Mesosphere. Surv Geophys 29, 71–137 (2008). https://doi.org/10.1007/s10712-008-9043-1

Neubert, T., Østgaard, N., Reglero, V., Blanc, E., Chanrion, O., Oxborrow, C. A., et al. (2019). The ASIM mission on the International Space Station. Space Science Reviews, 215, 26. https://doi.org/10.1007/s11214-019-0592-z

Neubert, T., Chanrion, O., Heumesser, M. et al. (2021). Observation of the onset of a blue jet into the stratosphere. Nature 589, 371–375. https://doi.org/10.1038/s41586-020-03122-6

Nijdam, S., Teunissen, J., Ebert, u. (2020) The physics of streamer discharge phenomena. Plasma Sources Sci. Technol. 29 103001. https://doi.org/10.1088/1361-6595/abaa05

Østgaard, N., Neubert, T., Reglero, V., Ullaland, K., Yang, S., Genov, G., et al. (2019). First 10 months of TGF observations by ASIM. Journal of Geophysical Research: Atmospheres, https://doi.org/10.1029/2019JD031214

Rakov, V. A., & Uman, M. A. (2003). Lightning: Physics and effects. Cambridge, U.K: Cambridge University Press.

Reess, T., Ortega, P., Gibert, P., Domens, P., Pignolet, P. (1995), An experimental study of negative discharge in a 1.3 m point-plane air gap: the function of the space stem in the propagation mechanism. *J. Phys. D: Appl. Phys., 28, 2306.* https://doi.org/10.1088/0022-3727/28/11/011.

Rison, W., Krehbiel, P., Stock, M. et al. Observations of narrow bipolar events reveal how lightning is initiated in thunderstorms. Nat. Commun. 7, 10721 (2016). https://doi.org/10.1038/ncomms10721.

Saba, M. M. F., de Paiva, A. R., Concollato, L. C. et al. Optical observation of needles in upward lightning flashes. Sci Rep 10, 17460 (2020). https://doi.org/10.1038/s41598-020-74597-6.

Soler, S., Perez-Invernon, F. J., Gordillo-Vázquez, F. J., Luque, A., Li, D., Malagón-Romero, A., et al. (2020). Blue optical observations of narrow bipolar events by ASIM suggest corona streamer activity in thunderstorms. J. of Geoph. Res.: Atmospheres, 125, e2020JD032708. https://doi.org/10.1029/2020JD032708

van der Velde, O., Montanyà, J., Neubert, T., Chanrion, O., Lopez, J. A., Fabro, F., et al. (2020), Comparison of high-speed optical observations of a lightning flash from space

and the ground, Earth and Space Science, 7, e2020EA001249. https://doi.org/10.1029/2020EA001249

Wu, C., Xie, S., Qi, F., Li, B., Wan, J., He, J. (2013), Effect of corona discharges on the inception of positive upward leader-streamer system. Int. J. Mod. Phys. B, 27, 1350165. https://doi.org/10.1142/S0217979213501658.

Zhao, X., Liu, X., Yang, Y., Wang, X., Liu, Y., & He, J. (2021a). Observations of the channel illuminations during dark periods in long positive sparks. Geophysical Research Letters, 48, e2020GL091815. https://doi.org/10.1029/2020GL091815

Zhao, X., Becerra, M., Yang, Y. (2021b), Elongation and branching of stem channels produced by positive streamers in long air gaps. Sci Rep 11, 4120. https://doi.org/10.1038/s41598-021-83816-7

# 5 Conclusions

## 5.1 Main conclusions

This PhD thesis presented an investigation on the properties of streamers and leaders mainly related to corona discharges in the laboratory and in the field and the signatures of high voltage discharges. This work followed the propositions established by the SAINT Project Grant Agreement for ESR 14, with objectives, line of investigation and deliverables defined before the beginning of the project. Two journal papers (part of this compendium) were published in relevant journals for the lightning research community (*Atmospheric Research* and *Geophysical Research Letters*). Two conference papers are annexed to this thesis for completeness of the discussions presented.

In the first paper published and the ICLP paper (Appendix B2), it was presented observations of corona discharges recorded in the laboratory and in the field using a shunt resistor, a high impedance ammeter and a current transformer.

In the laboratory, several features already reported in the literature were confirmed, such as the shape of the pulses and the increase of the corona current according to the voltage applied at the upper plate. During the two-month internship performed at TU/e, a broad study of corona discharges from sharp tips in a controlled environment was conducted.

In the field, a current transformer coupled to a conductive grounded rod was used in three different setups: *La Tossa d'Alp*, *Rooftop* and *Flat-ground*. Pulses were measured under high background electric fields. Lightning activity can lead to rapid variations of the electric field, which in turn can trigger, cease, or significantly alter the frequency of corona discharges. A correlation between the frequency of positive corona pulses and the ambient electric field indicated a certain dependency between them. Wind speeds were also found to contribute to higher pulse frequencies at the same electric field level. Other factors such as local humidity and temperature are well known to affect the discharges.

It was observed that the rooftop setup was more susceptible to register corona discharges than the flat-ground setup, presenting steady detections over several seconds. For other grounded structures, such as high towers and wind turbines, the enhancement of the local electric field plays an important role. Consequently, corona discharges are expected to occur more often for lower levels of background electric field, as it was shown in the first paper, for the setup in La Tossa d'Alp.

In a parallel investigation, it was presented some evidence of corona discharges from grounded tethered wires deployed vertically with a drone (paper in Appendix B1). Acquired data are useful for understanding some conditions that tall and elevated structures, such as wind turbine blades and towers are subjected to. Another PhD project is being carried out and conducting more flights to quantitatively assess the data, discussing, with the aid of models, the electric field behavior, and thresholds for corona occurrence.

The second paper part of this compendium was focused on the optical signatures of streamers and leaders in laboratory discharges to support satellite-based measurements that perform optical measurements in the same wavelength ranges. Unprecedent data obtained revealed features of 337 and 777 nm emissions. Blue optical emissions are associated with streamer development, and negative leader stepping, and are expected to be observed in satellite observations of activities that involve positive and negative leader propagation. It was found a significant correlation between the peak emissions at the 337 nm wavelength and the peak current of burst streamer pulses. The stable leader propagation was identified taking place with a remarkable increase and acceleration of the current and the red irradiance. That happens after the peak and collapse of the blue irradiance.

The development of in-cloud positive leaders with corona brushes leading its propagation is expected to produce emissions content in both blue and red regions. The same should be expected in the stepped fashion propagation of negative leaders, with streamers guiding the connection between the leader tip and the space stems/leaders. Blue flashes and other events with an absence of emissions in the red are associated with cold discharges characterized by traveling streamers inside the clouds.

## 5.2 Future work

This thesis provides results that can be applied in future research and on new technology developments for lightning warning/measuring systems. Here, the main work lines for continuation expected with the results obtained by this investigation are listed:

- To optimize the designed current sensor for being the core of a new lightning protection system that acquires information and is able to produce alarms related to lightning/corona activity.
- To investigate the application of the sensor to detect corona emissions from wind turbines. Perform an installation of the sensor with additional instruments to monitor the periods with occurrence of corona, aiming to verify the charging of the blade with measurements of electric field and monitoring related perturbations such as electrostatic discharges.

- In laboratory discharges, optical signatures during the breakdown and the decay of the plasma channel should be deeply explored. Values of irradiances can be used in calculations for estimating and comparing results obtained with satellite-based observation.
- An ongoing investigation on the optical signatures for the wavelengths (337 nm and 777 nm) from natural lightning could reveal many features of leader processes responsible for those emissions. Simultaneous acquisitions have been performed together with electric field, high-speed video, lightning mapping array and VHF broadband interferometer.

## 5.3 Dissemination and further training activities

This section describes the dissemination actions employed in the context of this thesis and training activities received throughout the doctorate. In this way, it was provided a multi-environment platform of academia/industry in which most of the activities were carried out inside Dena Desarrollos, in Spain. The business environment furnished by the company led to research focused on results that can be applied to the interests of the market and the industry.

### *5.3.1 Presentations in conferences and congresses*

Within the SAINT network, several workshops were conducted, and part of the ESRs' individual research projects (IRPs) were presented and discussed. These events also provided opportunity for brainstorming the ongoing research work and results and planning future research and training events.

- SAINT Winter School in Leiden, January/2019.
- Bergen Spring School in Bergen, May/2019.
- SAINT Summer School in Toulouse, July/2019.
- SAINT Online Spring School, throughout 2021.

A list of external presentations made during the development of this work in conferences and congresses are listed below:

- Presentation of conference paper titled *'Corona Discharges from Grounded Rods under High Ambient Electric Field and Lightning Activity'*. At the International Conference on Lightning Protection (ICLP) 2021, online.
- Presentation titled *'Corona point discharges from grounded rods under high background Electric Fields'*. At the EGU General Assembly 2021, online.
- Presentation of conference paper titled *'Experiments with a tethered drone to investigate induced charges on a vertically arranged conductor during fair weather'*. At the GROUND Conference, 2021, online.
- Presentation titled *'Corona point discharges from grounded rods under high background Electric Fields'*. At the European Cooperation in Science and Technology (COST meeting 2021).

- Presentation titled *'Experimental Optical Observations of Streamers and Leaders in Laboratory Discharges and Natural Lightning'*. At the AGU General Assembly 2021, online.

### *5.3.2 Scientific courses and training*

Dedicated scientific courses were performed during the SAINT schools to complement the IRP training. The courses broaden the perspective of the ESRs and increase interactions. Lectures were given by expert scientists, also from outside SAINT in the extended network.

- Optical and electromagnetic signatures of discharges in lightning, high-altitude lightning and in laboratory discharges.
- Collisional plasma physics and chemistry in discharges.
- Satellite mission planning and data management.

The SAINT schools provided transferable skills courses by practicing presentation of research results, communication, collaboration, argumentation, industrial work, and networking. Specific topics aborded in the workshops are listed below:

- Entrepreneurship, business and innovation.
- Project management, PA, QA.
- Proposal and bid writing.

Within the company, apart from several meetings and forming activities, a 20-hour course on 'Occupational Risk Prevention' was provided for the employees in November/2021, certified by Egarsat SP.

### *5.3.3 Awards*

During the joint event of the 35th edition of the International Conference on Lightning Protection (ICLP) and the XVI edition of the Symposium on Lightning Protection (SIPDA), 202 papers were selected to be presented virtually. Young scientists at the beginning of their research career scientists were able to apply for the Young Scientist Award (YSA). The work related to this thesis, titled "Corona Discharges from Grounded Rods under High Ambient Electric Field and Lightning Activity", won one of the four nominations for this award. The award nomination can be checked through the permanent link http://www.iclp-centre.org/awards.php.

### *5.3.4 Other publications*

During this PhD, the collaboration with two other PhD projects resulted in four journal articles that have already been published or are currently under review. These works are branches of the investigation performed by the Lightning Research Group of the UPC and provided insights for the accomplishments of this thesis.

### *Co-authorship in journal articles:*

The first work refers to the application of a broadband VHF interferometer for mapping cloud-to-ground lightning, with X-ray detections during the propagation of approaching negative leaders.

- **Urbani, M., Montanyà, J., van der Velde, O.A., López, J.A., Arcanjo, M., Fontanes, P., et al., 2021. High-energy radiation from natural lightning observed in coincidence with a VHF broadband interferometer. Journal of Geophysical Research: Atmospheres, 126, e2020JD033745.** https://doi.org/10.1029/2020JD033745**.**

*Abstract*: This work presents the first simultaneous X-ray measurements from natural lightning in coincidence with a very high frequency (VHF) broadband interferometer. During an observational campaign in north-central Colombia, five intense X-ray bursts were detected from negative stepped leaders and two X-ray emissions from a dart leader. Thanks to the high angular and time resolution of the interferometer, it was possible to locate the origin of high-energy radiation during the lightning leader propagation. We study the correlation with VHF pulses and the two-dimensional speed of the leader channels. A strong temporal correspondence has been observed between the high-energy emissions and the most intense VHF pulses, which suggests the runaway electrons as a shared mechanism. The observations show that an X-ray burst can have multiple high-energy sources belonging to different leader branches, that can be several hundreds of meters apart. Therefore, from a spatial point of view, not a unique origin has to be searched, but an extensive origin of the X-ray burst should be considered. We hypothesize similar conclusions in particular for downward TGFs and maybe for TGFs in general.

The second work is related to experiments performed in the laboratory with a real wind turbine blade subjected to high background electric field in two configurations (insulated and grounded). A comprehensive study on the effects of polarization and charging of the structure is carried out.

- **Fontanes, P., Montanyà, J., Arcanjo, Guerra-Garcia, C., Tobella, G., 2022. Experimental investigation of the electrification of wind turbine blades in fair-weather and artificial charge-compensation to mitigate the effects, Journal of Electrostatics, Vol. 115, 103669.** https://doi.org/10.1016/j.elstat.2021.103669.

*Abstract:* Wind turbines are tall structures immersed in the electrified Earth's atmosphere. Even in fair-weather, a modern wind turbine can be subjected to several tens of kilovolts of atmospheric potential. In this work, we conduct two series of experiments to investigate the expected electrification of wind turbine blades in fair-weather conditions, as well as the possibility of mitigating this electrification using an artificial charge-compensation system. The first set of experiments is conducted in the laboratory, using a real wind turbine blade tip in a configuration whose down conductor is electrically isolated from the rest of the system. Under the influence of an atmospheric electric field, the isolated blade tip

polarizes. Two main timescales are identified: a fast mechanism attributed to the polarization of the blade down conductor and a slow mechanism attributed to charge accumulation on the insulating blade's glass fiber exterior. The second set of experiments is conducted in the field and uses vertical wires lifted by a multirotor drone. In these experiments, it was shown that a vertical isolated wire of 100 m reached a potential of more than 5 kV due to the effects of the fair-weather electricity. In both sets of experiments, an artificial charge-compensation system is tested to explore the possibility of mitigating blade electrification. It is proposed that charge control of wind turbine blades may mitigate the electrostatic discharge

The third work is associated to the interferometer for mapping positive cloud-to-ground lightning. The main findings are related to the observation of positive lightning with multiple strokes sharing the same channel and the VHF pattern of approaching positive leaders.

- **Urbani, M., Montanyà, J., van der Velde, O.A., Arcanjo, M., López, J.A., 2022. Multi-Stroke Positive Cloud-to-Ground Lightning Sharing the Same Channel Observed with a VHF Broadband Interferometer. (Currently under review in Geophysical Research Letters).**

*Abstract*: This work presents the first observation of a multi-stroke positive cloud-to-ground lightning flash sharing the same channel to ground with a VHF broadband interferometer and a Lightning Mapping Array. This phenomenon is rarely observed and it is currently unclear how frequent it is and even under what conditions it occurs. We reconstructed development of the entire ash, the cloud charge structure, and identified the origin of the downward positive leader (DPL). We provide a detailed comparison between the first positive cloud-to-ground stroke and the subsequent stroke, investigating the temporal and spatial propagation, leader velocities, and VHF waveforms. In the first DPL, we observed a clear intermittent pattern of bursts of VHF pulses located on the positive leader tip and an increase in the burst frequency as the DPL approaches ground. The subsequent DPLs have similar velocities as negative dart leaders and do not present an analogous pattern of VHF burst.

The fourth work is related to the experiments with drones to study wind turbine-induced currents. This collaboration was very significant for sharing experiences related to the emergence of corona discharges from grounded structures and how they can affect those.

- **Fontanes, P., Montanyà, J., Arcanjo, M., Urbani, M., Asensio, C., Guerra-Garcia, C., 2022. Experiments using drones to study wind turbine-induced currents. (Currently under review in IEEE Access).**

*Abstract*: The wind energy sector is constantly striving to increase performance. To that end, wind turbines are being fitted with multiple sensors that monitor their status and are exposed to harsh environmental conditions, including wind turbine-induced electrical currents. This paper presents a novel experiment

using vertical wires lifted by a drone to study those currents under fair-weather conditions. Based on the experimental results, a model for predicting induced currents on wind turbines under fair-weather conditions is proposed and estimates for thunderstorm conditions are made. Results from these experiments are useful for predicting base current noise levels for wind turbine sensors as well as determining environmental conditions that could lead to their failure once installed. Additionally, the proposed experiments are a low cost and reliable method for measuring atmospheric currents.

### *Co-authorship in congress papers:*

The collaborations already mentioned and other activities developed during the PhD led to four papers presented at important congresses. The titles and abstracts are depicted in the following.

- **Fontanes, P., Montanyà, J., Arcanjo, M., Urbani, M., 2021. Experiments lifting vertical wires with drones to study wind turbines current induction and charging. Presented at the 35th International Conference on Lightning Protection (ICLP).**

*Abstract*: A series of experiments lifting vertical wires with drones under fair weather conditions have been performed in order to study induced currents on tall structures such as wind turbines and charging phenomena on floating conductors like wind turbines with spark-gap isolated blades. Results show that blade tips altitude change at certain speed along with point discharge are key factors for the current induction on wind turbines. Additionally, deployment of vertical conductors in an electrified environment shares some similarities with bidirectional lightning leaders and the return stroke processes when they contact ground.

- **Montanyà, J., López, J.A., van der Velde, O., Solà, G., Romero, D., Arcanjo, M. et al., 2021. On the use of space-based lightning detection in electric power systems. Presented at the 35th International Conference on Lightning Protection (ICLP).**

*Abstract*: Information about lightning activity and its parameters is necessary to design and evaluate the lightning protection of a power system. Most extended lightning detection networks provide mainly information on cloud-to-ground lightning strikes covering areas up to global scale, whereas high-resolution ground-based total lighting (cloud-to-ground and intracloud) networks are restricted to small regions. In addition, real-time lightning detection makes it possible to provide warnings and actions to ensure safety and power quality. Recently, the first satellite-based lightning optical detectors are operating continuously from geostationary orbits. These imagers observe the luminosity escaping from clouds to detect and locate total lightning activity. This allows to delineating the initiation and propagation (sometimes over tens to hundreds of kilometers before striking the ground) not observable by the ground-based networks. In this paper, we explore the use of this new technology for lightning protection in power systems.

- **Costa, K., Guimaraes, M., Alipio, R., Arcanjo, M., 2021. Striking distance to flat ground estimated from the bipolar leader model and the influence of the lightning channel radius. Presented at the 35th International Conference on Lightning Protection (ICLP).**

*Abstract*: This paper proposes a physically consistent method to estimate the lightning striking distance to flat ground as a function of the return stroke charge, as well as a function of the prospective return stroke peak current. This method is based on an axisymmetric electrostatic model of charges in thunderstorm clouds used to initiate a vertical bipolar leader that develops bidirectionally from the region of maximum electrical field inside the cloud towards the ground. The leader is assumed as a perfect conductor whose potential is equal to the average cloud potential over its length. The charge simulation method is applied to calculate the leader charge distribution by the numerical solution of the Poisson equation. The striking distance to flat ground is computed when the average potential gradient between the leader tip and the ground is equal to 500 kV/m. This analysis is extended to different leader radius values, in order to evaluate its effect on striking distance, since there are some uncertainties regarding the leader radius reported in literature. Furthermore, the obtained results are compared to models from different authors.

- **Urbani, M., Montanyà, J., Arcanjo, M., López J.A., van der Velde, O.A., 2021. Strong temporal correlation between high-energy emissions and the most intense VHF pulses in negative cloud-to-ground lightning, Presented at URSI GASS 2021, Rome, Italy, August/2021.**

*Abstract*: In order to investigate the high-energy emissions in cloud-to-ground lightning strikes, a measurement campaign was conducted in north-central Colombia in 2019 and 2020. In several natural lightning events, it was possible to detect high-energy emissions in coincidence with a lightning imaging obtained from a VHF broadband interferometer. A strong temporal correlation was observed between the high energy emissions and the most intense VHF pulses during the negative downward leader propagation. In this summary paper, we present, through a case study, the evidence of this temporal correlation and a possible interpretation.

# 6 Bibliography


Aleksandrov, N., Bazelyan, E., Carpenter Jr, R., Drabkin, M., Raizer, Y., 2001. The effect of coronae on leader initiation and development under thunderstorm conditions and in long air gaps. J. Phys. D: Appl. Phys. 34, 3256. https://doi.org/10.1088/0022-3727/34/22/309.

Arcanjo, M., Guimaraes, M., Visacro, S., 2019. On the interpeak interval of unipolar pulses of current preceding the return stroke in negative CG lightning. Elec. Power Sys. Res. 173, 13-17. https://doi.org/10.1016/j.epsr.2019.03.028.

Arevalo L, Cooray V., 2017. Unstable Leader Inception Criteria of Atmospheric Discharges. Atmosphere; 8(9):156. https://doi.org/10.3390/atmos8090156.

Bartnikas, R. e McMahon, E. J., 1979. Engineering Dielectrics – Volume I – Corona measurement and Interpretation. Baltimore: ASTM.

Bazelyan, E.M., Raizer, Y.P., 1998. Spark Discharge (1st ed.). Routledge. https://doi.org/10.1201/9780203739075.

Bazelyan, E.M., Raizer, Y.P., 2000. Lightning Physics and Lightning Protection, IOP Publishing, Bristol, England.

Bazelyan, E.M., Raizer, Y.P., Aleksandrov, N.L., 2007. The effect of reduced air density on streamer-to-leader transition and on properties of long positive leader. Journal of Physics D: Applied Physics, 40(14), 4133–4144. https://doi.org/10.1088/0022-3727/40/14/007.

Bazelyan, E., Raizer, Y., Aleksandrov, N., D'Alessandro, F., 2009. Corona processes and lightning attachment: The effect of wind during thunderstorms, Atmos.c Res., 94(3), 436-447. https://doi.org/10.1016/j.atmosres.2009.07.002.

Bazelyan, M., Raizer, Y.P., Aleksandrov, N.L., 2015. The effect of space charge produced by corona at ground level on lightning attachment to high objects. Atmos. Res. 153, 74–86. https://doi.org/10.1016/j.atmosres.2014.07.018.

Becerra, M., Cooray, V., Soula, S., Chauzy, S., 2007. Effect of the space charge layer created by corona at ground level on the inception of upward lightning leaders from tall towers. J. Geophys. Res., 112, D12205. https://doi.org/10.1029/2006JD008308.

Becerra, M., 2013. Glow corona generation and streamer inception at the tip of grounded objects during thunderstorms: Revisited. J. of Physics D: Applied Physics, 46, 135205. https://doi.org/10.1088/0022-3727/46/13/135205.

Becerra, M., 2014. Corona discharges and their effect on lightning attachment revisited: Upward leader initiation and downward leader interception. Atmos. Res., 149, 316-323. https://doi.org/10.1016/j.atmosres.2014.05.004.

Berger, K., Anderson, R.B., Kroninger, H., 1975. Parameters of lightning flashes. Electra, vol. 80, pp. 223-237.

Betz, H. D., Schmidt, K., Laroche, P., Blanchet, P., Oettinger, W. P., Defer, E., et al., 2009. Linet–an international lightning detection network in Europe. Atmospheric Research, 91(2–4), 564–573. https://doi.org/10.1016/j.atmosres.2008.06.012

Biagi, C., Jordan, D.., Uman, M., Hill, J., Beasley, W., Howard, J., 2009. High- speed video observations of rocket-and-wire initiated lightning. Geophys. Res. Lett., 36(15), n/a-n/a, https://doi.org/10.1029/2009GL038525.

Biagi, C., Uman, M., Hill, J., Jordan, D., Rakov, V., Dwyer, J., 2010. Observations of stepping mechanisms in a rocket-and-wire triggered lightning flash. J. Geophys. Res. Atmos., 115(23), 2–7, https://doi.org/10.1029/2010JD014616.

Biagi, C. J., Uman, M. A., Hill, J. D., Rakov, V. A., Jordan, D. M., 2012. Transient current pulses in rocket-extended wires used to trigger lightning. Journal of Geophysical Research: Atmospheres, 117(D7). https://doi.org/10.1029/2011jd016161.

Chang, J.S., Lawless, P.A., Yamamoto, T., 1991. Corona discharge processes. IEEE Trans. Plasma Sci., 19(6), 1152-1166. https://doi.org/10.1109/27.125038.

Chanrion, O., Neubert, T., Lundgaard Rasmussen, I., Stoltze, C., Tcherniak, D., Jessen, N. C., et al., 2019. The modular multispectral imaging array (MMIA) of the ASIM Payload on the International Space Station. Space Science Reviews,215, 28. https://doi.org/10.1007/s11214-019-0593-y.

Chapman, S., 1955. Effects of wind and space charge on corona point discharge, particularly from aircraft. Proc. Conf. Atmospheric Electricity. Pap. n. 42, AFCRCTR-55-222. 120-134.

Chauzy, S., Raizonville, P., 1982. Space charge layers created by coronae at ground level below thunderclouds: Measurements and modeling. J. Geophys. Res. 87(C4), 3143– 3148. https://doi.org/10.1029/JC087iC04p03143.

Chauzy, S., Soula, S., 1999. Contribution of the ground corona ions to the convective charging mechanism. Atmos. Res. 51, 279-300. https://doi.org/10.1016/S0169-8095(99)00013-7.

Chern, J. L., Hsu, R.R., Su, H.T., Mende, S.B., Fukunishi, H., Takahashi, Y., Lee, L.C., 2003. Global survey of upper atmospheric transientluminous events on the ROCSAT-2 satellite, J. Atmos. Sol. Terr. Phys.,65, 647–659. https://doi.org/10.1016/S1364-6826(02)00317-6.

Chilingarian, A., Chilingaryan, S., Karapetyan, T. et al., 2017. On the initiation of lightning in thunderclouds. Sci Rep 7, 1371. https://doi.org/10.1038/s41598-017-01288-0.

Christian, H.J., Blakeslee, R.J., Goodman, S.J., 1989. The detection of lightning from geostationary orbit, Journal of Geophysical Research, 94, 13329–13337. https://doi.org/10.1029/JD094iD11p13329.

Cooray, V., Cooray, G., Rubinstein, M., Rachidi, F., 2020. Modeling compact intracloud discharge (CID) as a streamer burst. Atmosphere, 11(5), 549.398. https://doi.org/10.3390/atmos11050549.

Costa, K., Guimaraes, M., Alipio, R., Arcanjo, M., 2021. Striking distance to flat ground estimated from the bipolar leader model and the influence of the lightning channel radius. Presented at the 35th International Conference on Lightning Protection (ICLP).

da Silva C.L., and Pasko, V.P., 2013. Dynamics of streamer-to-leader transition at reduced air densities and its implications for propagation of lightning leaders and gigantic jets. J. Geophys. Res. Atmos., 118, 13,561– 13,590, https://doi.org/10.1002/2013JD020618.

Davis, R., Standring, W.G., 1947. Discharge currents associated with kite balloons. The Royal Soc. pub. 191, 2026. https://doi.org/10.1098/rspa.1947.0117.

D'Alessandro, F., 2009. Experimental study of the effect of wind on positive and negative corona from a sharp point in a thunderstorm. J. Electrost. 67, 482-487. https://doi.org/10.1016/j.elstat.2008.12.003.

Diendorfer, G., Mair, M., Schulz, W., Hadrian, W., 2000. Lightning current measurements in Austria-experimental setup and first results, in 25th ICLP (International Conference on Lightning Protection), Rhodes, Greece, pp. 44-47.

Dordizadeh, P., Adamiak, K., Peter Castle, G.S., 2015. Numerical investigation of the formation of Trichel pulses in a needle-plane geometry. J. Phys. D: Appl. Phys. 48, 415203. https://dx.doi.org/10.1088/0022-3727/48/41/415203.

Dordizadeh, P., Adamiak, K., Peter Castle, G.S., 2017. Experimental study of the characteristics of Trichel pulses in the needle-plane negative corona discharge in atmospheric air. J. of Electrostatics. 88, 49-54. https://doi.org/10.1016/j.elstat.2016.12.013.

Dubinova A., Rutjes C., Ebert U., Buitink S., Scholten O., Trinh T.N.G., 2015. Prediction of lightning inception by large ice particles and extensive air showers Phys. Rev. Lett. 115 015002. https://doi.org/10.1103/PhysRevLett.115.015002.

Dwyer, J.R., Uman, M.A., 2014. The physics of lightning. Physics Reports, Vol 534 (4), 147-241. https://doi.org/10.1016/j.physrep.2013.09.004.

Gallimberti, I., Hepworth, J.K., Klewe, R.C., 1974. Spectroscopic investigation of impulse corona 381 discharges. J. Phys. D: Appl. Phys., 7(6), 880–898. https://doi.org/10.1088/0022-3727/7/6/315.

Gallimberti, I., 1979. The mechanism of the long spark formation. Journal de Physique Colloques, 40(C7), 193–250. https://doi.org/10.1051/jphyscol:19797440.

Gallimberti, I., Bacchiega, G., Bondiou-Clergerie, A., Lalande, P., 2002. Fundamental processes in long air gap discharges. Comptes Rendus Physique, 3(10), 1335–1359. https://doi.org/10.1016/S1631-0705(02)01414-7.

Gallo, C.F., 1977. Corona-A brief status report. IEEE Trans. Ind. Appl. IA-13, 550–557. https://doi.org/10.1109/TIA.1977.4503458.

Goodman, S.J., Blakeslee, R.J., Koshak, W.J., Mach, D., Bailey, J., Buechler, D., et al., 2013. The GOES-R geostationary lightning mapper (GLM). Atmospheric Research, 125, 34–49. https://doi.org/10.1016/j.atmosres.2013.01.006.

Guimaraes, M., Araujo, L., Pereira, C., Mesquita, C., Visacro, S., 2014. Assessing currents of upward lightning measured in tropical regions. Atmospheric Research, 149, 324–332. https://doi.org/10.1016/j.atmosres.2014.01.005.

Guimaraes, M., 2017. Observação e modelagem dos processos físicos envolvidos na formação das descargas atmosféricas. PhD thesis presented at the Federal University of Minas Gerais (UFMG), Engineering School.

Guimaraes, M., Arcanjo, M., Murta Vale, M.H., Visacro, S., 2017. Unusual features of negative leaders' development in natural lightning, according to simultaneous records of current, electric field, luminosity, and high-speed video. J. Geophys. Res. Atmos. 122, 2325–2333. https://doi.org/10.1002/2016JD025891.

Guo, X., Zhang, Q., 2017. Effects of geometrical parameters of two height-unequal adjacent objects on corona discharges from their

tips during a thunderstorm. Atmos. Res. 190, 113-120. https://doi.org/10.1016/j.atmosres.2017.02.010.

Gurevich, A.V., 1961. On the theory of runaway electrons, Sov. Phys. JETP Engl. Transl., 12, 904 – 912.

Gurevich, A.V., Milikh, G.M., Roussel-Dupre, R., 1992. Runaway electron mechanism of air breakdown and preconditioning during a thunderstorm, Phys. Lett. A, 165, 463 – 468.

Gurevich, A.V., Zybin, K.P., 2001. Runaway breakdown and electric discharges in thunderstorms, Phys. Usp., 44, 1119 – 1140.

Harrison, R.G., 2011. Fair weather atmospheric electricity. J. Phys.: Conf. Ser. https://doi.org/10.1088/1742-6596/301/1/012001.

Harrison, R.G., 2013. The Carnegie Curve. Surv. Geophys. 34, 209–232. https://doi.org/10.1007/s10712-012-9210-2

Heidler, F., Zischank, W., and Wiesinger, J., 2001. Current Parameters of Lightning Discharges Measured at the Peissenberg Telecommunication Tower," SAE Technical Paper 2001-01-2879. https://doi.org/10.4271/2001-01-2879.

Heumesser, M., Chanrion, O., Neubert, T., Christian, H.J., Dimitriadou, K., Gordillo-Vazquez, F.J., et al., 2021. Spectral observations of optical emissions associated with Terrestrial Gamma-Ray Flashes. Geophysical Research Letters, 48, e2020GL090700. https://doi.org/10.1029/2020GL090700.

Hutchinson, W.C.A. 1951. Point-discharge currents and the earth's electric field. Quar. J. of the Royal Met. Soc. 77, 627-632. https://doi.org/10.1002/qj.49707733406.

Hill, J., Uman M., Jordan, D., 2011. High-speed video observations of a lightning stepped leader, J. Geophys. Res. Atmos., 116(16), 1–8, https://doi.org/10.1029/2011JD015818.

Hussein, A.M., Janischewskyj, W., Chang, J.S., Shostak, V., Chisholm, W.A., Dzurevych, P., Kawasaki, Z.I., 1995. Simultaneous measurement of lightning parameters for strokes to the Toronto Canadian National Tower. Journal of Geophysical Research, vol. 100, pp. 8853-61.

Janda, M., Machala, Z., 2011. Imaging of Transient Spark in Atmospheric Air by Fast iCCD Camera. IEEE Transactions on Plasma Science, 39(11), 2246–2247. https://doi.org/10.1109/TPS.2011.2157175.

Janda, M., Machala, Z., Niklová, A., Martišovitš, V., 2012. The streamer-to-spark transition in a transient spark: a dc-driven nanosecond-pulsed discharge in atmospheric

air. Plasma Sources Science and Technology, 21(4), 045006. https://doi.org/10.1088/0963-0252/21/4/045006.

Janda, M., Martišovitš, V., Hensel, K. et al., 2016. Generation of Antimicrobial NOx by Atmospheric Air Transient Spark Discharge. Plasma Chem Plasma Process 36, 767–781. https://doi.org/10.1007/s11090-016-9694-5.

Jiang, R., Qie, X., Li, Z., Zhang, H., Li, X., Yuan, S., et al., 2020. Luminous crown residual vs. bright space segment: Characteristical structures for the intermittent positive and negative leaders of triggered lightning. G. Research Letters, 47(21), e2020GL088107. https://doi.org/10.1029/2020GL088107.

Karunarathna, N., Marshall, T., Karunarathne, S., Stolzenburg, M., 2017. Initiation locations of lightning flashes relative to radar reflectivity in four small Florida thunderstorms. J. Geophysical Research: Atmospheres, 122, 6565-6591. https://doi.org/10.1002/2017JD026566.

Kasemir, H., 2012. Static discharge and triggered lightning, In: Mazur, V.; Ruhnke, L. (Ed.). Heinz-Wolfram Kasemir: His collected works. 1. ed. Wash. DC: American Geophysical Union, chap. 4.3, p.418-428. ISBN 978-0-87590-737-6.

Kasemir, H., 1950. Qualitative Ubersicht uber Potential-, Feld- und Ladungsverhaltnisse bei einer Blitzentladung in der Gewitterwolke, H. Israel, Ed. Leipzig: Akad. Verlagsges, pp. 112–126.

Kasemir, H., 1960. A Contribution to the Electrostatic Theory of a Lightning Discharge. J. Geophys. Res., v. 65, no. 7, pp. 1873–1878.

Kexin, Z., Yongjun, P., Miao, T., Jingfeng, T., Liqiu, W., Chaohai1, Z., 2015. Mode Transition of Trichel pulses. J. Phys.: Conf. Ser. 652, 012016. https://doi.org/10.1088/1742-6596/652/1/012016.

Kieu, N., Gordillo-Vázquez, F. J., Passas, M., Sánchez, J., Pérez-Invernón, F. J., Luque, A., et al., 2020. Submicrosecond spectroscopy of lightning-like discharges: Exploring new time regimes. Geophysical Research Letters, 47, e2020GL088755. https://doi.org/10.1029/2020GL088755.

Kieu, N., Gordillo-Vázquez, F. J., Passas, M., Sánchez, J., & Pérez-Invernón, F. J., 2021. High-speed spectroscopy of lightning-like discharges: Evidence of molecular optical emissions. Journal of Geophysical Research: Atmospheres, 126, e2021JD035016. https://doi.org/10.1029/2021JD035016.

Kip, A.F., 1938. Positive-Point-to-Plane Discharge in Air at Atmospheric Pressure. Physical Review. 54(2), 139–146. https://doi.org/10.1103/PhysRev.54.139.

Kirkland, M.W., Suszcynsky, D.M., Guillen, J.L.L., and Green, J.L., 2001, Optical observations of terrestrial lightning by the FORTE satellite photodiode detector, J. Geophys. Res., 106(D24), 33499– 33509, https://doi.org/10.1029/2000JD000190.

Kochkin, P. O., van Deursen, A.P.J., Ebert, U., 2014. Experimental study of the spatio-temporal development of metre-scale negative discharge in air. Journal of Physics D, 47(14), 145203. https://doi.org/10.1088/0022-3727/47/14/145203.

Kochkin P.O., van Deursen A.P.J., Ebert U., 2015. Experimental study on hard x-rays emitted from meter-scale negative discharges in air. J. Phys. D: Appl. Phys. 40 025205. https://doi.org/10.1088/0022-3727/47/14/145203.

Kochkin, P., Lehtinen, N., van Deursen, A. P. J., Østgaard, N., 2016. Pilot system development in metre-scale laboratory discharge. Journal of Physics D, 49, 425203. https://doi.org/10.1088/0022-3727/49/42/425203.

Kostinskiy, A. Y., Syssoev, V. S., Bogatov, N. A., Mareev, E. A., Andreev, M. G, Bulatov, M. U., Makal'sky, L.M., Sukharevsky, D.I., Rakov, V.A., 2016. Observations of theconnection of positive and negativeleaders in meter-scale electricdischarges generated by clouds ofnegatively charged water droplets, J. Geophys. Res. Atmos., 121, 9756–9766. https://doi.org/10.1002/2016JD025079.

Kostinskiy, A. Y., Marshall, T. C., Stolzenburg, M., 2020. The mechanism of the origin and development of lightning from initiating event to initial breakdown pulses (v.2). Journal of Geophysical Research: Atmospheres, 125, e2020JD033191. https://doi.org/10.1029/2020JD033191.

Krzewiński, S., Frącz, P., Urbaniec, I., Turba, T., 2017. Comparative Analysis of Optical Signals Emitted by Corona on a Laboratory Model of Transmission Lines Made of Various Materials", Journal of Spectroscopy, Article ID 8423797, 9 pages. https://doi.org/10.1155/2017/8423797.

Kozyrev, A.V., Kozhevnikov, V.Y., Kostyrya, I.D. et al., 2012. Radiation from a diffuse corona discharge in atmospheric-pressure air. Atmos Ocean Opt 25, 176–183. https://doi.org/10.1134/S102485601202008X.

Les Renardieres Group, 1981. Negative discharges in long air gaps at Les Renardieres—1978 results and conclusions. Electra, 74.67–216.

Li, D., Luque, A., Gordillo-Vázquez, F.J., Liu, F., Lu, G., Neubert, T., et al., 2021. Blue Flashes as Counterparts to Narrow Bipolar Events: The Optical Signal of Shallow In-Cloud Discharges. Journal of Geophysical Research: Atmospheres, 126, e2021JD035013. https://doi.org/10.1029/2021JD035013.

López, J. A., Pineda, N., Montanyà, J., van der Velde, O., Fabró, F., Romero, D., 2017. Spatio-Temporal dimension of lightning flashes based on

Three-Dimensional Lightning Mapping Array, Atmospheric Research. http://dx.doi.org/10.1016/j.atmosres.2017.06.030.

López, J. A., Montanyà, J., van der Velde, O. A., Pineda, N., Salvador, A., Romero, D., et al., 2019. Charge structure of two tropical thunderstorms in Colombia. Journal of Geophysical Research: Atmospheres, 124, 5503–5515. https://doi.org/10.1029/2018JD029188.

Liu, L., 2017. Physics of Electrical Discharge Transitions in Air. PhD thesis from the KTH Royal Institute of Electrical Engineering.

Lu, W., Chen, L., Ma, Y., Rakov, V. A., Gao, Y., Zhang, Y., Yin, Q., Zhang, Y., 2013. Lightning attachment process involving connection of the downward negative leader to the lateral surface of the upward connecting leader, Geophys. Res. Lett., 40, 5531– 5535. https://doi.org/10.1002/2013GL058060.

Lu, B., Sun, H., Wu, Q., 2017. Characteristics of Trichel Pulse Parameters in Negative Corona Discharge. IEEE Trans. on Pl. Sci. 45(8), 2191-2201. https://doi.org/10.1109/TPS.2017.2713831.

Lyu, F., Cummer, S. A., Qin, Z., Chen, M., 2019. Lightning initiation processes imaged with very high frequency broadband interferometry. Journal of Geophysical Research: Atmospheres, 124, 2994–3004. https://doi.org/10.1029/2018JD029817.

Loeb, L.B., 1948. Recent Developments in Analysis of the Mechanisms of Positive and Negative Coronas in Air. Appl. Phys. 19, 882.

Marshall, T.C., and Rust, W.D., 1991. Electric field soundings through thunderstorms, J. Geophys. Res., 96 (D12), 22297–22306, https://doi.org/10.1029/91JD02486.

Mazur, V., Ruhnke, L., 1998. Model of electric charges in thunderstorms and associated lightning. J. Geophys. Res., v. 103, no. D18, pp. 23299–23308.

Mazur, V., Taylor, C.D., Petersen, D.A., 2015. Simulating electrodeless discharge from a hydrometeor array. J. Geophys. Res. Atmos., 120, 10,879– 10,889, https://doi.org/10.1002/2015JD023466.

Mazur, V., 2016. Principles of Lightning Physics, IOP Publishing.

Miki, M., Miki, T., Asakawa A., Shindo, T., 2014. Characteristics of Negative Upward Stepped Leaders in Positive Upward Lightning, XV International Conference on Atmospheric Electricity, 15-20 June 2014, Norman, Oklahoma, U.S.A.

Montanyà, J., van der Velde, O., Romero, D., March, V., Solà, G., Pineda, N., Soula, S., Hermoso, B., 2012. Two upward lightning at the Eagle Nest tower.

at Int. Con. on Lightning Protection (ICLP), Vienna, Austria. https://doi.org/10.1109/ICLP.2012.6344373.

Montanyà, J., van der Velde, O., Williams, E.R., 2014. Lightning discharges produced by wind turbines. J. Geophys. Res. Atmos., 119, 1455-1462. https://doi.org/10.1002/2013JD020225.

Montanyà, J., van der Velde, O., Williams, E.R., 2015. The start of lightning: Evidence of bidirectional lightning initiation. Sci Rep 5, 15180. https://doi.org/10.1038/srep15180.

Montanyà, J., López, J.A., Morales Rodriguez, C.A., van der Velde, O. A., Fabró, F., Pineda, N., et al., 2021. A simultaneous observation of lightning by ASIM, Colombia-Lightning Mapping Array, GLM, and ISS-LIS. Journal of Geophysical Research: Atmospheres, 126, e2020JD033735. https://doi.org/10.1029/2020JD033735.

Moore, C.B., Voonegut, B., 1977. The thundercloud, in Lightning, vol. 1, edited by R. H. Golde, Elsevier, 51-98.

Moore, C.B., Rison, W., Mathis, J., Aulich, G., 2000. Lightning rod improvement studies, J. Appl. Meteorol., 39, 593 – 609. https://doi.org/10.1175/1520-0450-39.5.593.

Moore, C.B., Aulich, G., Rison, W., 2003. The Case for Using Blunt-Tipped Lightning Rods as Strike Receptors, J. Appl. Meteorol., 42(7), 984–993. https://doi.org/10.1175/1520-0450-39.5.593.

Moreau, E., Touchard, G., 2008. Enhancing the mechanical efficiency of electric wind in corona discharges. J. Electrost. 66, 39-44. https://doi.org/10.1016/j.elstat.2007.08.006.

Moreau, E., Audier, P., Bernard, N., 2018. Ionic wind produced by positive and negative corona discharges in air. J. Electrostatics, 93, 85-96. https://doi.org/10.1016/j.elstat.2018.03.009.

Morrow, R., 1997. The theory of positive glow corona. J. Phys. D: Appl. Phys.30, 3099. https://doi.org/10.1088/0022-3727/30/22/008.

Mostajabi, A., Sunjerga, A., Azadifar, M., Smorgonskiy, A., Rubinstein, M., Rachidi, F., Diendorfer, G., 2018. On the Impact of Meteorological Conditions on the Initiation of Upward Lightning Flashes from Tall Structures. at 34th Int. Con. on Lightning Protection (ICLP), Rzeszow, Poland. https://doi.org/10.1109/ICLP.2018.8503310.

Nag, A., Rakov, V.A., 2012. Positive lightning: An overview, new observations, and inferences. J. Geophys. Res., 117, D08109, https://doi.org/10.1029/2012JD017545.

Nag, A., Cummins, K., Plaisir, M., Wilson, J., Crawford, D., Brown, R., Noggle, R.C., Rassoul, H., 2021. Inferences on upward leader characteristics from measured currents, Atmospheric Research, 251, 105420, https://doi.org/10.1016/j.atmosres.2020.105420.

Neubert, T., Rycroft, M., Farges, T. et al., 2008. Recent Results from Studies of Electric Discharges in the Mesosphere. Surv Geophys 29, 71–137. https://doi.org/10.1007/s10712-008-9043-1.

Neubert, T., Østgaard, N., Reglero, V., Blanc, E., Chanrion, O., Oxborrow, C. A., et al., 2019. The ASIM mission on the International Space Station. Space Science Reviews, 215, 26. https://doi.org/10.1007/s11214-019-0592-z.

Neubert, T., Chanrion, O., Heumesser, M. et al., 2021. Observation of the onset of a blue jet into the stratosphere. Nature 589, 371–375. https://doi.org/10.1038/s41586-020-03122-6.

Nijdam, S., Teunissen, J., Ebert, U., 2020. The physics of streamer discharge phenomena. Plasma Sources Sci. Technol. 29 103001. https://doi.org/10.1088/1361-6595/abaa05.

Nna-Mvondo, D., Navarro-González, R., Raulin, F. et al., 2005. Nitrogen Fixation by Corona Discharge on The Early Precambrian Earth. Orig Life Evol Biosph 35, 401–409. https://doi.org/10.1007/s11084-005-1972-9.

Østgaard, N., Neubert, T., Reglero, V., Ullaland, K., Yang, S., Genov, G., et al., 2019. First 10 months of TGF observations by ASIM. Journal of Geophysical Research: Atmospheres, https://doi.org/10.1029/2019JD031214.

Petersen, D., Bailey, M., Hallett, J. and Beasley, W., 2008. A brief review of the problem of lightning initiation and a hypothesis of initial lightning leader formation. J. Geophys. Res.,113, D17205, https://doi.org/10.1029/2007JD009036.

Petersen, D., Bailey, M., Hallett, J. and Beasley, W., 2015. Laboratory investigation of corona initiation by ice crystals and its importance to lightning. Q.J.R. Meteorol. Soc., 141: 1283-1293. https://doi.org/10.1002/qj.2436.

Pineda, N., Montanyà, J., Romero, D., Bech, J., Casellas, E., Gonzáles, S., 2018. Meteorological aspects of winter upward lightning from an instrumented tower in the Pyrenees. at Int. Con. on Lightning Protection (ICLP), Rzeszow, Poland. https://doi.org/10.1109/ICLP.2018.8503271.

Pineda, N., Figueras i Ventura, J., Romero, D., Mostajabi, A., Azadifar, M., Sunjerga, A., et al., 2019. Meteorological aspects of self-initiated upward lightning at the Säntis tower (Switzerland). J. of Geop. Res. Atmospheres, 124. https://doi.org/10.1029/2019JD030834.

Qie, X., Yuan, S., Zhang, H., Jiang, R., Wu, Z., Liu, M., Sun, Z., Pu, Y., Li, J., Srivastava, A., Ma, Z., Lu, G., 2019. Propagation of positive, negative, and recoil leaders in upward lightning flashes. Earth and Planetary Physics, 3: 102-110. https://doi.org/10.26464/epp2019014.

Rakov, V.A., Uman, M.A., 2003. Lightning: Physics and Effects. Cambridge University Press.

Rakov, V., Fundamentals of Lightning. 2016. Cambridge: Cambridge University Press. https://doi:10.1017/CBO9781139680370.

Rakov, V.A., Tran, M.D., 2019. The breakthrough phase of lightning attachment process: From collision of opposite-polarity streamers to hot-channel connection. Electric Power Systems Research, 173, (122-134). https://doi.org/10.1016/j.epsr.2019.03.018.

Reess, T., Ortega, P., Gibert, P., Domens, P., Pignolet, P., 1995. An experimental study of negative discharge in a 1.3 m point-plane air gap: the function of the space stem in the propagation mechanism. J. Phys. D: Appl. Phys., 28, 2306. https://doi.org/10.1088/0022-3727/28/11/011.

Riousset, J. A., Pasko, V. P., Krehbiel, P. R., Thomas, R. J., and Rison, W., 2007. Three-dimensional fractal modeling of intracloud lightning discharge in a New Mexico thunderstorm and comparison with lightning mapping observations, J. Geophys. Res., 112, D15203. https://doi.org/10.1029/2006JD007621.

Rison, W., Krehbiel, P., Stock, M. et al., 2016. Observations of narrow bipolar events reveal how lightning is initiated in thunderstorms. Nat Commun 7, 10721. https://doi.org/10.1038/ncomms10721.

Robinson, M., 1961. Movement of air in the electric wind of the corona discharge. IEEE Trans. Am. Inst. of Elec. Eng. Com. and Elec. 80(2), 143-150.

Romero, C., Paolone, M., Rubinstein, M., Rachidi, F., Rubinstein, A., Diendorfer, G., Schulz, W., Daout, B., Kälin, A., Zweiacker, P., 2012. A system for the measurements of lightning currents at the Säntis Tower, Electric Power Systems Research, 82 (1), 34-43, https://doi.org/10.1016/j.epsr.2011.08.011.

Romero, C., Rachidi, F., Rubinstein, M., Paolone, M., Rakov, V., Pavanello, D., 2013. Positive lightning flashes recorded on the Santis tower from May 2010 to January 2012. J. Geophys. Res. Atmos.,118, 12,879–12,892, https://doi.org/10.1002/2013JD020242.

Saba, M. Schumann, C., Warner, T., Helsdon, J., Orville, R., 2015. High-speed video and electric field observation of a negative upward leader connecting a downward positive leader in a positive cloud-to-ground flash. Electric Power Systems Research, https://doi.org/10.1016/J.EPSR.2014.06.002.

Saba, M., Paiva, A., Schumann, C., Ferro, M., Naccarato, K., Silva, J., Siqueira, F., Custódio, D.M., 2017. Lightning attachment process to common buildings. Geophys. Res. Lett., 44, 4368–4375. https://doi.org/10.1002/2017GL072796.

Saba, M. M. F., de Paiva, A. R., Concollato, L. C. et al., 2020. Optical observation of needles in upward lightning flashes. Sci Rep 10, 17460. https://doi.org/10.1038/s41598-020-74597-6.

Schumann, C., Saba, M.M.F., Warner, T.A. et al., 2019. On the Triggering Mechanisms of Upward Lightning. Sci Rep 9, 9576. https://doi.org/10.1038/s41598-019-46122-x.

Soler, S., Perez-Invernon, F. J., Gordillo-Vázquez, F. J., Luque, A., Li, D., Malagón-Romero, A., et al., 2020. Blue optical observations of narrow bipolar events by ASIM suggest corona streamer activity in thunderstorms. J. of Geoph. Res.: Atmospheres, 125, e2020JD032708. https://doi.org/10.1029/2020JD032708.

Soler, S., Gordillo-Vázquez, F. J., Pérez-Invernón, F. J., Luque, A., Li, D., Neubert, T., et al., 2021. Global frequency and geographical distribution of nighttime streamer corona discharges (BLUEs) in thunderclouds. Geophysical Research Letters, 48, e2021GL094657. https://doi.org/10.1029/2021GL094657.

Soula, S., Pineda, N., Georgis, J., Leroy, A., Vanpoucke, I., Montanyà, J., Casellas, E., Gonzalez, S., Bech, J., 2021. On the conditions for winter lightning at the Eagle Nest Tower (2537 m asl) during the Cerdanya 2017 field experiment, Atmospheric Research, 247, 105208, https://doi.org/10.1016/j.atmosres.2020.105208.

Stekolnikov, I., Valeev, C., 1937. L'etude de la foudre dans un laboratoire decampagne, CIGRE Report no. 30.

Stolzenburg, M., Marshall, T.C., 2008. Charge Structure and Dynamics in Thunderstorms. Space Sci Rev 137, 355–372. https://doi.org/10.1007/s11214-008-9338-z.

Stolzenburg, M., Marshall, T., 2009. Electric field and charge structure in lightning-producing clouds. In H.-D. Betz. Lightning: principles, instruments and applications, pp. 57-82. https://doi.org/10.1007/978-1-4020-9079-0_3.

Stolzenburg, M., Marshall, T.C., Bandara, S. et al. 2021. Ultra-high speed video observations of intracloud lightning flash initiation. Meteorol Atmos Phys 133, 1177–1202. https://doi.org/10.1007/s00703-021-00803-3.

Tianyu, H., Huang, S., Cheng, D., Fu, Y., Fu, Z., Bian, K., 2020. Relationship Between Brightness and Current of the Propagating Positive Leaders in Laboratory High Voltage

Atmospheric Discharges. IEEE Access, vol. 8, pp. 158559-158567. https://doi.org/10.1109/ACCESS.2020.3015849.

Tran, M., Rakov, V., 2016. Initiation and propagation of cloud-to-ground lightning observed with a high-speed video camera. Nature, Scientific Reports, http://dx.doi.org/10.1038/srep39521.

Trichel, G.W., 1938. The Mechanism of the Negative Point to Plane Corona Near Onset. Physical Review. 54, 1078.

Trichel, G.W., 1939. The Mechanism of the Positive Point-to-Plane Corona in Air at Atmospheric Pressure. Physical Review. 55(4), 382–390.

Uman M. 1969. Lightning, Westinghouse Research Laboratories. Pitsburgh, Pennsylvania.

van der Velde, O., Montanyà, J., 2013. Asymmetries in bidirectional leader development of lightning flashes, J. Geophys. Res. Atmos., 118, 13,504–13,519, https://doi.org/10.1002/2013JD020257.

van der Velde, O., Montanyà, J., Neubert, T., Chanrion, O., Lopez, J. A., Fabro, F., et al., 2020. Comparison of high-speed optical observations of a lightning flash from space and the ground, Earth and Space Science, 7, e2020EA001249. https://doi.org/10.1029/2020EA001249.

Wang, Z., Lu, T., Liu, Y., Bian, X., Li, X., 2017. Comparative study of two different measuring methods for corona current pulses. J. Electrost. 88, 134-138. https://doi.org/10.1016/j.elstat.2016.12.018.

Wang, C., Chen, X., Ouyang, J., Li, T., Fu, J., 2018. Pulse Current of Multi-Needle Negative Corona Discharge and Its Electromagnetic Radiation Characteristics. Energies. 11, 3120. https://doi.org/10.3390/en11113120.

Warner, T., Saba, M., Schumann, C., Helson Jr., J., Orville, R., 2016. Observations of bidirectional lightning leader initiation and development near positive leader channels. J. Geophys. Res. Atmos., 121, 9251–9260, https://doi.org/10.1002/2016JD025365.

Whipple F.J.W., Scrase F.J., 1936. Point Discharge in the Electric Field of the Earth. Met. Off. of Geo physical Memoirs. 68(7), 20.

Wu, C., Xie, S., Qi, F., Li, B., Wan, J., He, J., 2013. Effect of corona discharges on the inception of positive upward leader-streamer system. Int. J. Mod. Phys. B, 27, 1350165. https://doi.org/10.1142/S0217979213501658.

Wu, S., Cheng, W., Huang, G., Wu, F., Liu C., Liu, X., Zhang, C., Lu, X., 2018. Positive streamer corona, single filament, transient glow, dc glow, spark, and their transitions in atmospheric air", Physics of Plasmas 25, 123507. https://doi.org/10.1063/1.5042669.

Zhang, Y., Krehbiel, P. R., Zhang, Y., Lu, W., Zheng, D., Xu, L., Huang, Z., 2017. Observations of the initial stage of a rocket-and-wire-triggered lightning discharge. Geophys. Res. Lett., 44, 4332– 4340. https://doi.org/10.1002/2017GL072843.

Zhang, N., Yuan, P., ting An, T., Zhang, M., rong Chen, R., 2020. The conductivity and propagation property of lightning leader tip. Atmospheric Research, 245, 105099. https://doi.org/10.1016/j.atmosres.2020.105099.

Zheng, Y., Zhang, B., He, J., 2015. Self-sustained criterion with photoionization for positive dc corona plasmas between coaxial cylinders. Physics of Plasmas. 22, 063514. https://doi.org/10.1063/1.4923283.

Zhao, X., Liu, X., Yang, Y., Wang, X., Liu, Y., He, J., 2021a. Observations of the channel illuminations during dark periods in long positive sparks. Geophysical Research Letters, 48, e2020GL091815. https://doi.org/10.1029/2020GL091815.

Zhao, X., Becerra, M., Yang, Y., 2021b. Elongation and branching of stem channels produced by positive streamers in long air gaps. Sci Rep 11, 4120. https://doi.org/10.1038/s41598-021-83816-7.

# Appendix A: Applications

## A.1. Introduction

In this appendix, a few applications derived from the results obtained in this thesis are described. The Grant agreement of project SAINT stipulated as one deliverable of this investigation a design for a new lightning rod that could integrate information for lightning protection and lightning warning.

Appendix A2 describes the general aspects of the sensor and how it fits within the scope of SAINT. In Appendix A3, the results of a 3-month internship performed at the Eindhoven University of Technology (TU/e) are presented. These results, on corona discharges from very sharps tips in a controlled environment were valuable for the investigation developed during this project. Appendix A4 introduces the use of photometers for determining the leader inception in laboratory long spark discharges. That study is mainly focused on the same spectral lines (337 nm and 777 nm) investigated in the second article of this compendium.

## A.2. Corona current sensor

The current sensor presented in this thesis will be the core of a new lightning protection system that integrates information on corona/streamers, leaders and current of lightning strikes.

The system under implementation includes sensors for a great range of electric current that can flow through the lightning rod. A computer runs an algorithm to monitor the state of the sensors. Warnings are produced when there is a high level of electric field or when the system detects currents along the rod. Currents and charges of positive and negative downward lightning that strike the lightning rod, as well as upward lightning, are calculated by the computer using information acquired by the sensors.

### *A.2.1 Patent*

The concepts for the device for detecting and measuring electrical currents associated with corona discharges during storm activity were written in a patent submitted at the beginning of 2021, and the undisclosed document is currently under evaluation.

The invention refers to a sensor for low amplitude electrical currents of atmospheric origin optimized for corona discharges in conductors, providing advantages and characteristics described in the patent.

## A.3 Streamer inception from very sharp tips

As part of the SAINT network, this internship project (secondment) was meant to establish a collaborative work between the Early-Stage Researchers (ESRs). The activities performed in this investigation were performed at the Eindhoven University of Technology (TU/e) over two months. The obtained results are presented and discussed in this section.

Unlike what was performed in the main scope of this thesis, this work aimed to investigate the streamer inception from very sharp tips in a controlled environment. For a point-to-plane setup with a fixed gas mixture, pressure, and gap distance, the following are investigated:

- streamer inception time delay.
- discharge current.
- pulse frequency with the variation of applied voltage and the electrode's radius.

The results revealed that under a steady pulsating regime, with the increase of the voltage, the frequency of the pulses and the average current increase, whereas the time delay decreases. For a constant applied voltage, sharper electrodes have higher pulse density, higher current, and shorter time delay. Using short-time exposure images, it is noticed that the first discharges are stronger (in intensity) for sharper electrodes. For negative corona, the behavior of a pulsating glow corona is studied.

Using a point-to-plane setup, the streamer inception for very sharp tips with different tip radius was studied. The experiments were performed in a vessel with dry air (80% Nitrogen and 20% Oxygen) at a pressure of 500 mbar. The tip is placed 5 cm far from the ground plate. Figure A.1 shows a schematic of the setup for the experiments and how the electrode is placed in the vessel.

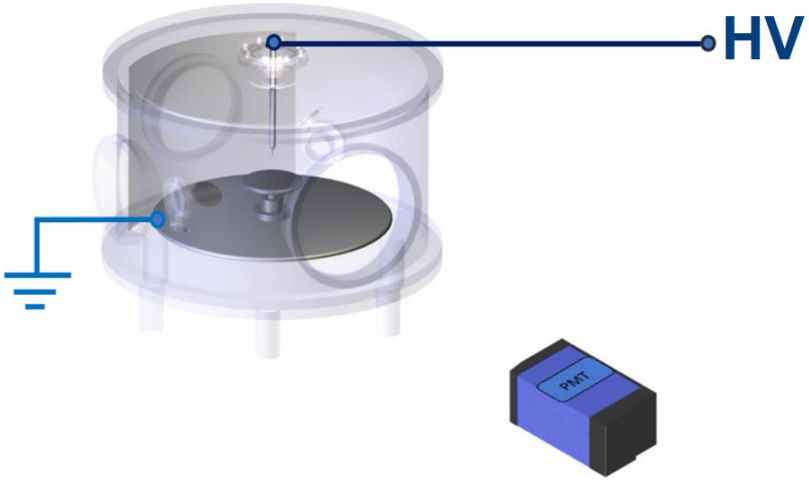


Figure A.1 - Scheme of installation for point-to-plate setup for testing sharp electrodes.

### A.3.1 Short-pulse test

A high voltage pulse with a duration of 10 milliseconds is applied to the needle. The photomultiplier signal is measured and the time delay for inception ($t_D$) is calculated using the rising of the high-voltage pulse and the signal from the PMT, as depicted in Figure A.2. In this experiment, the $t_D$ distributions for the different tips are compared.

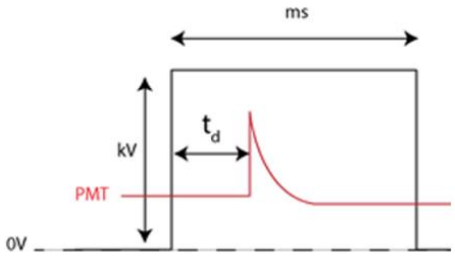


Figure A.2 - High voltage pulse and PMT detection for the first discharge.

### A.3.2 Long-pulse test

The efficiency of the tips in the production of space charges is verified with a long-pulse test. With the waveforms of current from both needle and plate, a longer pulse (1∼2 seconds) is applied; the discharge pulses are counted to determine the average frequency of pulses ($f$) and the total charge transferred ($Q$) to calculate the average current ($I$). Using a Pearson coil (1 V/A), the current is measured following the steps:

- The signals of the PMT and the coil are synchronized, and for each PMT pulse, the correspondent current pulse is integrated.
- For a given time window, the total charge is determined, and then, the average current.

In this way, the Pearson coil does not allow accounting for DC currents of the discharges.

### A.3.3 Laboratory facilities

The experimental setup uses gas cylinders, and the gas mixture is placed in the vessel with controlled pressure. Contamination levels are very low. After opening the vessel for doing any maintenance or changing the electrodes, it has to be emptied with a vacuum pump and filled with fresh gas from the cylinders.

Two independent DC high voltage power supplies are used for negative and positive voltage. Using a function generator, it is possible to control a switch that applies to the electrode pulses with controllable width and repetition frequency.

Data acquisition is performed using a LeCroy oscilloscope controlled by a MATLAB script. The application communicates with the function generator and the

oscilloscope, thus the waveform applied to the electrodes and the parameters of acquisition (number of pulses, sampling rate, basic processing) are embedded within this tool.

A 4Pico camera is triggered by the oscilloscope in order to capture (in the microsecond range) pictures of the electrode subject to high voltage. In this way, the detections of the PMT are synchronized with images of the discharges. The StreamerTools, developed by Prof. Sander Nijdam, is used for visualizing and processing raw files of images obtained in the experiments.

### *Electrodes*

To test a wide range of electrodes' radii, very sharp tips were coupled to steel electrodes. Table A.1 shows the nominal values of radii and the type of tests performed.

Table A.1 – Test conditions for different electrodes

| Electrode | Radius | Voltages | Test type |
|---|---|---|---|
| Steel | 1000 µm | 5 different positive voltages | Short pulse (10 ms – 2 Hz) N=600 pulses |
| | 500 µm | | |
| | 100 µm | 5 different negative voltages | Long pulse (1 s – 1 Hz) |
| | 30 µm | | |

Figure A.3 shows a picture and a scheme of the steel electrode, with approximately 12 cm of length and 1 cm of diameter. Electrodes' radii varied from 30 µm to 1000 µm.

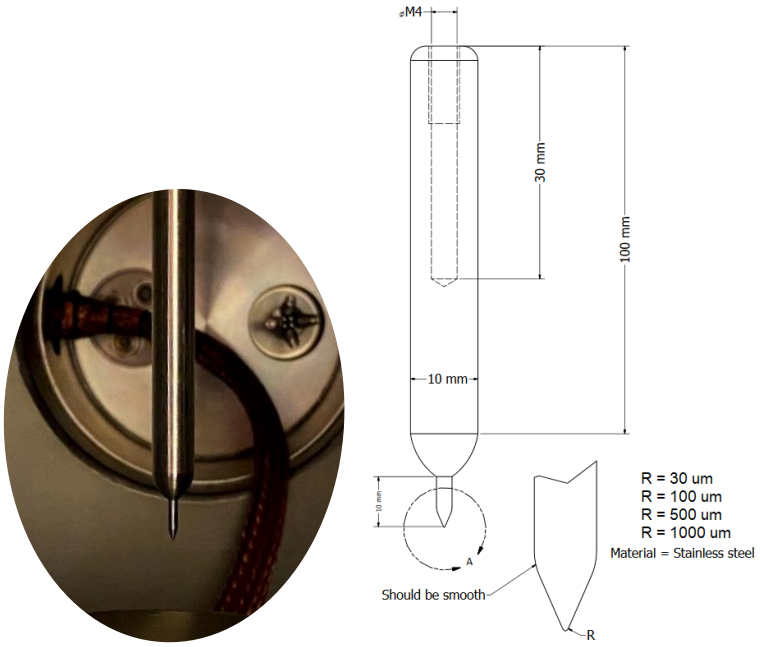


Figure A.3 - Steel electrode picture and scheme.

## *A.3.4 Results*

The first set of experiments were performed with the steel electrodes. The vessel was filled with dry air at 500 millibars, the gap separation between the needle and the grounded plate was 5 cm.

### *Positive corona*

The time delay for inception ($t_D$) is determined using the rising edge of the high voltage pulse and of the PMT signal. Figure A.4 depicts the results obtained for different voltages applied to the electrodes in linear and logarithmic scales. Each data point is an average of 600 high voltage pulses applied to the electrode.

First, as expected, the voltage inception for the discharges increases with the radius. The results show that the time delay is also greater for higher radii, which is consistent with the increase of the ionization region. In general, the average time delay decreases with voltage. For the 30 μm electrode, the values of time delay are in the range of 10 to 100 microseconds, and the magnitude of the standard deviation is comparable to these values. Therefore, the decrease of time delay with a higher voltage is more difficult to be observed.

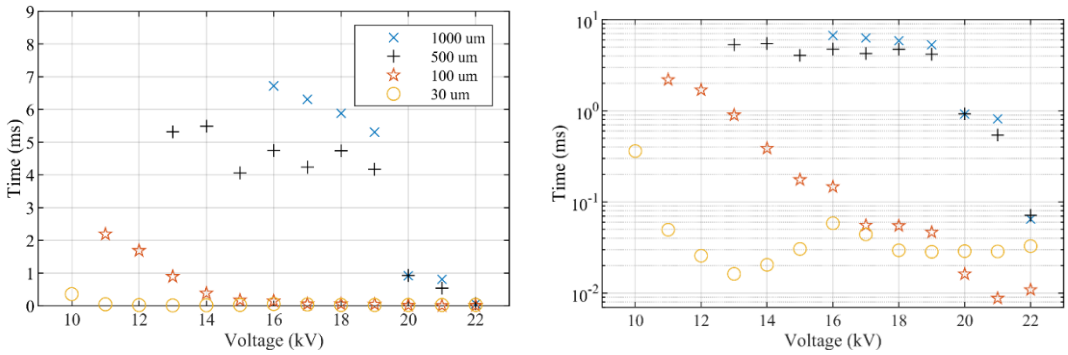


Figure A.4 - Time delay for inception (Positive Corona).

A high voltage pulse of a few seconds is applied, and the pulses are counted in a 1-s time window. Only higher voltages were considered for this analysis to ensure that the discharges reached a steady state. Figure A.5 shows the frequency of pulses and average current for different radii of electrodes and different voltages applied. A sharper electrode is subject to a greater enhancement of electric field and, as a result, a higher current. The 30 μm electrode shows clearly a higher frequency and higher current when compared to the other electrodes. On the other hand, the 1000 μm electrode presented a higher onset voltage and lower frequency and current.

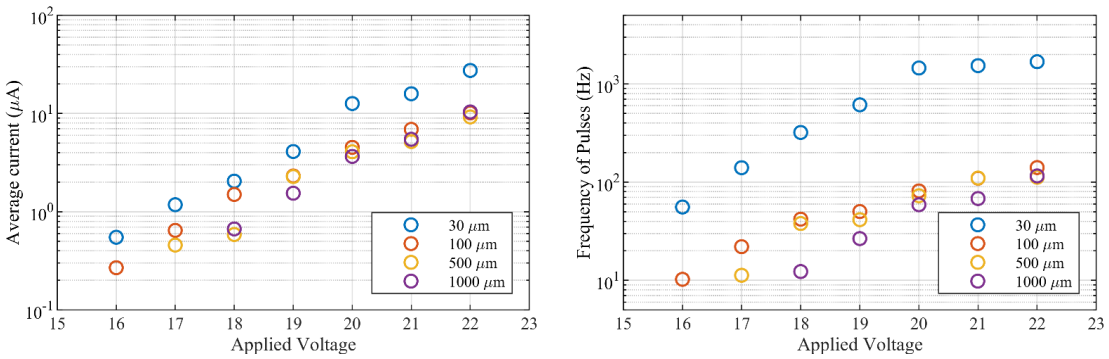


Figure A.5 - Frequency of pulses and average current for different radii in positive corona.

The frequency of the pulses varies from tens of hertz to almost 2 kHz for the range of voltages applied, growing exponentially, as well as the current, that ranges from hundreds of nanoamperes to tens of microamperes. The shape of a single discharge is shown in Figure A.6. Initially, a fast pulse of 20 nanoseconds is observed from both signals of current and optical detection. The discharge lasts for about 1 microsecond, with a fast rising (of about 70 nanoseconds), and a time decay of about 900 nanoseconds.

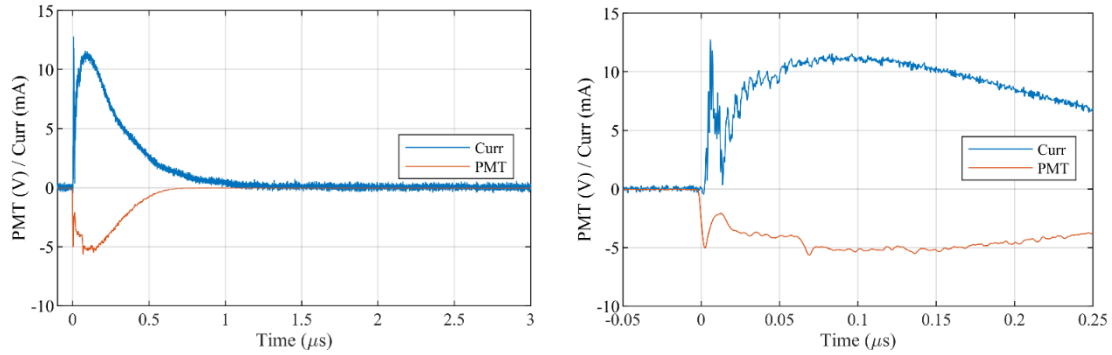


Figure A.6 - Pulse profile for positive corona.

For voltages ranging from 18 kV to 22 kV, the waveforms of the PMT for the different electrodes were recorded, aiming to compare the regime of the discharges. In Figure A.7, a 250-millisecond time window shows the increase in the number of pulses according to the voltage applied. For the 30 μm electrode, one can note a burst composed of a train of pulses with decreasing amplitude. The pulse train frequency also increases, and they appear to be close to superposition at higher voltages. The amplitude of the PMT reaches a few volts without major differences between different electrodes and various voltages applied.

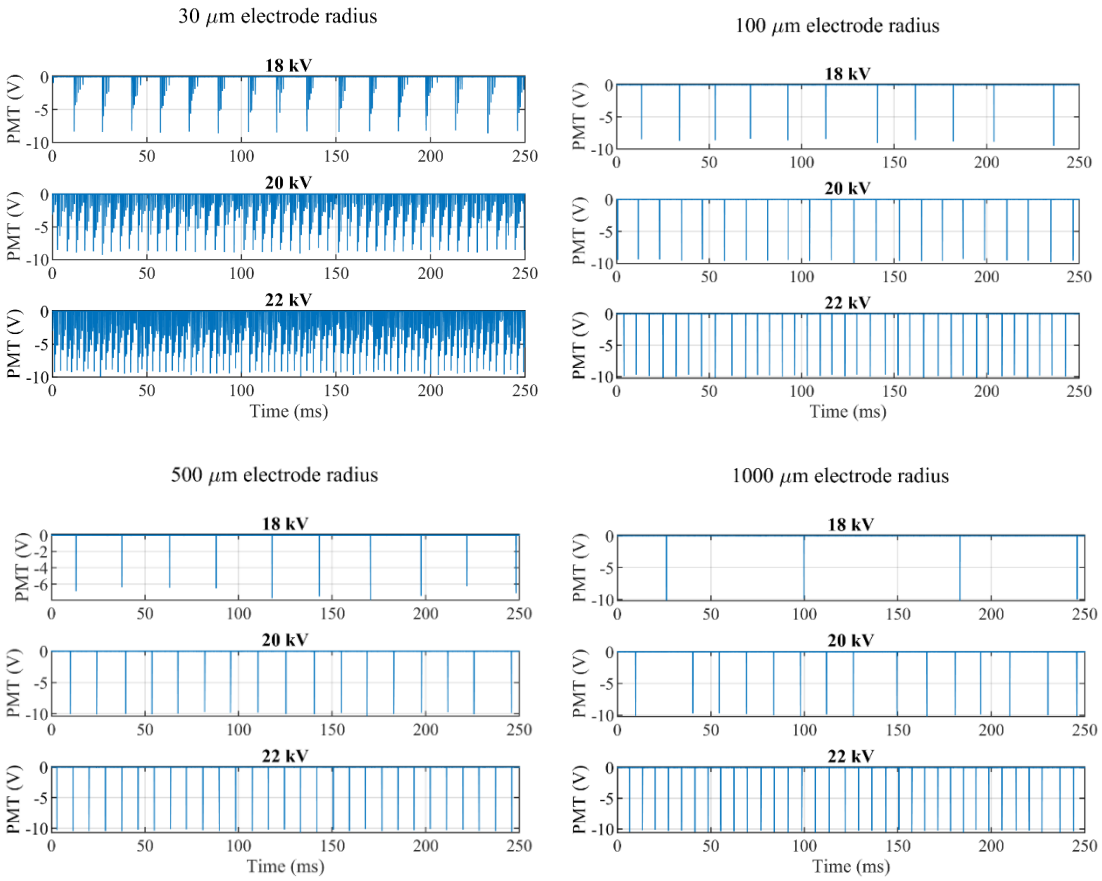


Figure A.7 - Regime of the discharges for positive corona.

### *Negative corona*

The experiments with negative corona used an analogically controlled high-voltage power supply; hence, the applied values were not round. A 10-ms negative pulse was applied to the electrodes and the time delays for inception determined. However, the electrodes of 500 µm and 1000 µm, most of the applied pulses resulted in no discharge. Figure A.8 shows the time delays for the other electrodes. The inception voltage is considerably higher for negative corona, as well as the time delay that varies from hundreds of microseconds to several milliseconds.

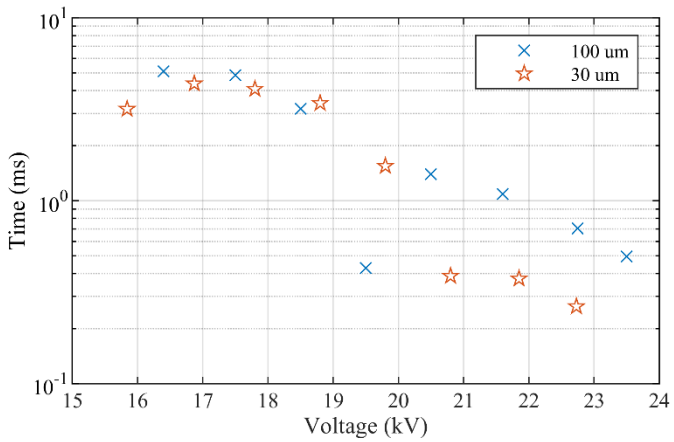


Figure A.8 - Time delay for inception (Negative Corona).

The shape of a single negative discharge is shown in Figure A.9. The negative pulse is shorter than the positive (total duration of 500 nanoseconds), the rise time is considerably low (about ten nanoseconds). The pulses do not change shape much for the different rods and different applied voltages. The PMT signal shows that one single discharge seems to be composed of multiple visual discharges.

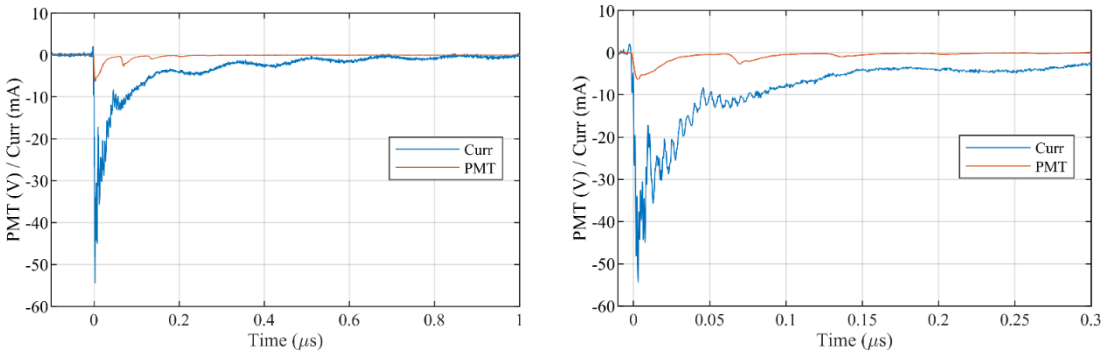


Figure A.9 - Pulse profile for negative corona (19 kV applied - 500 μm electrode).

For counting pulses, a long high voltage pulse was applied. It was expected that the corona discharges would reach the steady state with Trichel pulses. Figure A.10 shows the frequency of pulses and average current obtained. The data for current was found to be very dispersive.

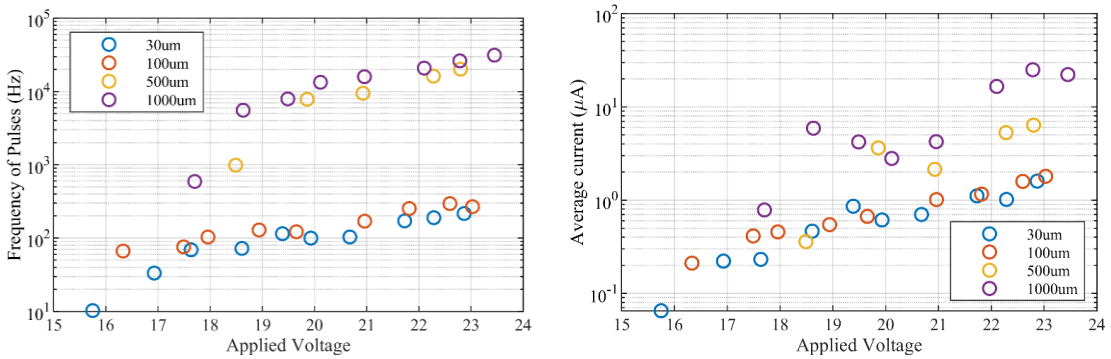


Figure A.10 - Frequency of pulses and average current for different radii in negative corona.

The data shown in Figure A.10 shows that the frequency of the pulses is lower for shorter electrodes, which is not consistent with previously reported findings. It was observed that the electrodes of 500 μm and 1000 μm have a much higher pulse frequency (reaching tens of kilohertz) than the 30 μm and 100 μm electrodes (tens of hertz). The pulses obtained in a 200-millisecond time interval for different voltages and electrodes are depicted in Figure A.11.

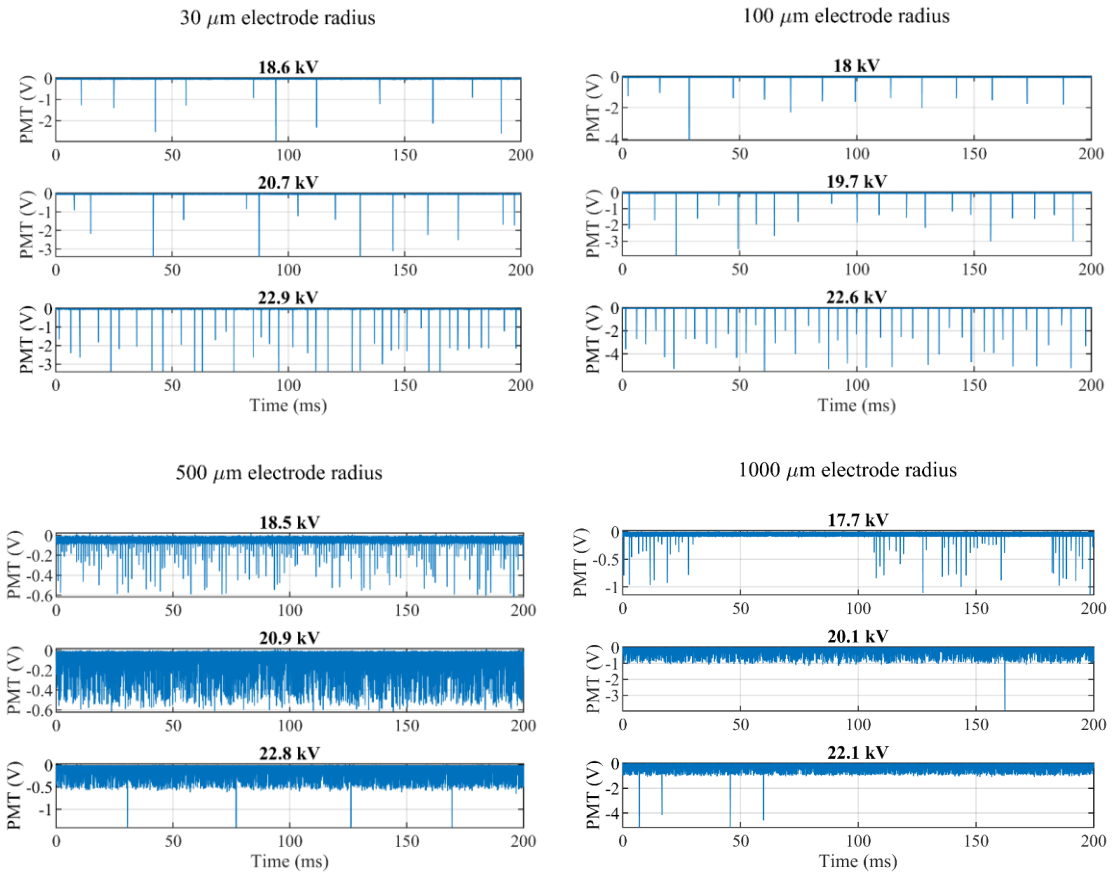


Figure A.11 - Regime of the discharges for negative corona.

In Figure A.11, one can see a few pulses that are very dispersive in amplitude for the 30 µm and 100 µm electrodes. For higher voltages, the 500 µm and 1000 µm electrodes produce numerous pulses of low amplitude. At about 22 kV, there are only a few pulses with high signal and many low-amplitude pulses. This behavior is different than what is shown in Figure A.7. Disregarding the corona polarity, it is expected that sharp tips produce higher corona currents and pulse densities, for the same voltage level.

It was suspected that the discharges in the electrodes of 30 µm and 100 µm were reaching the glow corona regime, in which the number of pulses reduces, and a continuous glow (and current) can be observed. The DC regime of negative corona discharges is very unstable at atmospheric pressure, but in the case of the experiments, the pressure at 500 mbar could allow this regime. A preliminary analysis with the camera was performed, as it is described in the following.

### *30-µm and 100-µm electrodes*

Figure A.12 depicts two different pulses applied to the high voltage electrode in which the camera images at 100 µs exposure. Both cases correspond to a 10-ms high voltage pulse of 20 kV applied to the electrode in which the PMT signal is inverted just for convenience. In the first pulse (left), the camera exposure coincides with the discharge pulse. The shape of the discharge, as expected, is a strong glow around the tip

of the electrode and a diffuse glow typical of the streamers from negative corona discharges. During the second pulse (right), the image is captured after the first discharge. In this case, a tiny glow can be observed, corresponding to a DC discharge that is not measured by the Pearson coil and from the PMT signal, it can be misinterpreted with the noise level.

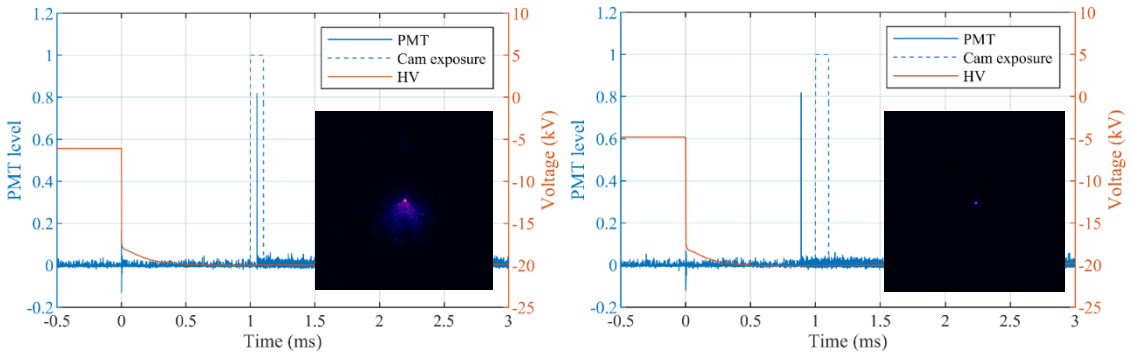


Figure A.12 - First discharge imaged in 100 µs (left) and subsequent period of first discharge (right).

Figure A.13 shows the same analysis performed for the 100-µm electrode. In this case, two remarks for the images captured: although they have the same gain-level adjusted, they correspond to a 500-µs exposure picture, and they were taken in a moment when the lights of the laboratory were not completely turned off, leading to a blue background. One can note that during the 10 milliseconds of the 21 kV high voltage pulse, one single discharge is captured in both experiments. The first discharge presents the diffuse shape observed, and after the first discharge, the glow is present in the electrode.

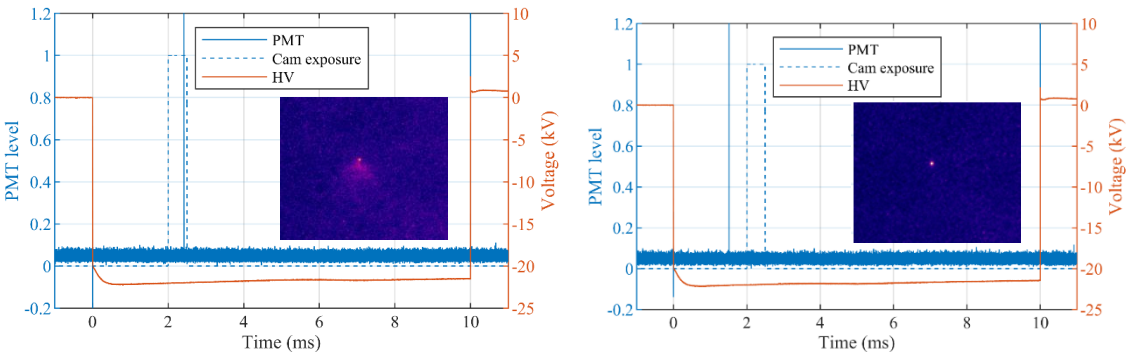


Figure A.13 - First discharge imaged with 500 µs (left) and subsequent period of first discharge (right).

Although the glow shown in Figure A.13 has a higher time exposure than the one shown in Figure A.12, it is clear that its size is smaller for the sharpest tip. Further investigation is required on that. Figure A.14 depicts an interval of a longer pulse (total time of one hundred milliseconds) and shows a picture taken during the third discharge pulse. It is possible to notice that this pulse did not trigger a diffuse discharge, yet it enhanced the glow formed around the tip if compared to the continuous glow shown in Figure A.13.

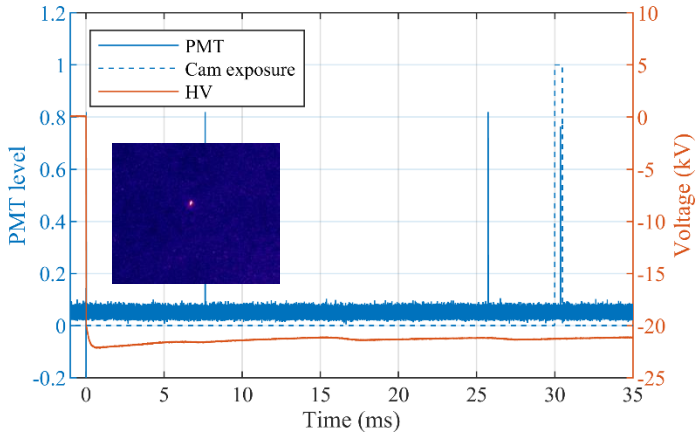


Figure A.14 - 500 µs capture of the third pulse of a negative discharge.

This finding confirms that the regime of the discharges at these conditions (pressure, gap distance, air mixture and voltage applied) are enough for producing glow corona from the 30-µm and the 100-µm electrode. Therefore, since we used the pulses measured by the Pearson coil for determining the average current, the results shown in Figure A.10 for average current and frequency of pulses are not consistent.

### *500-µm and 1000-µm electrodes*

Now, the waveforms of the discharges with low-exposure imaging for the electrodes of 500 µm and 1000 µm are compared. Figure A.15 shows a long frame with several discharges when -20 kV was applied to the electrode. The behavior for the first discharge is diffuse with a high amplitude for the PMT, as it was observed for the other electrodes. The subsequent discharges also seem to be diffuse, with less intensity than the first one. When the camera captured the interval between pulses, no glow was observed, indicating that the discharges were likely still under the Trichel pulse regime.

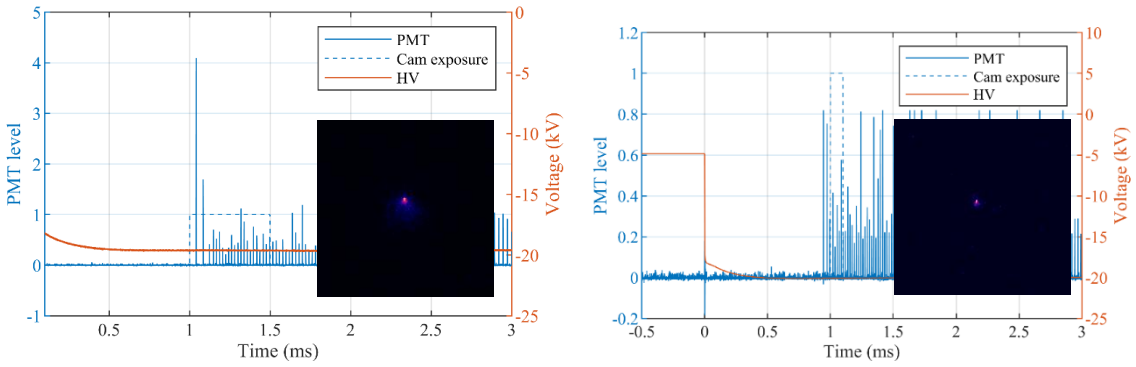


Figure A.15 - First discharges imaged with 500 µs (left) and subsequent discharges with 100 us exposure (right) for the 500 µm electrode.

With the 1000 µm electrode, a similar behavior to the 500 µm electrode was observed. As shown in Figure A.16, both the first and the subsequent discharges are diffuse, and they seem to be more intense. No glow was observed when the capture was performed between pulses.

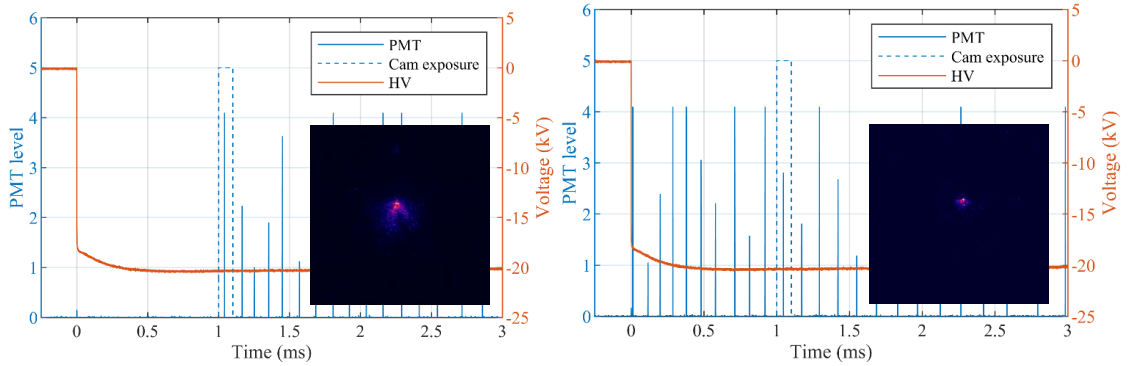


Figure A.16 - First discharges imaged with 500 µs (left) and subsequent discharges (right) for the 1000 µm electrode.

For the transition from the steady Trichel pulse regime to a glow discharge, the electric field enhancement should be enough to increase the frequency of the pulses in a way that negative ion clouds produced by the discharges get closer and closer to each other until they merge and form the glow. It is believed that the electric field enhancement provided by the sharper tips could be enough for achieving this stage.

An investigation with imaging of negative discharges for the low voltage range (12-18 kV) is required to verify if the steady stage of Trichel pulses is achievable with this setup conditions (pressure, gas, electrode, and gap distance). At atmospheric pressure, it is known that a pulseless stage is difficult to be reached in negative corona, with the discharges rapidly evolving into a spark. Possibly, the pressure used for this experiment may lead directly to the glow-pulsating regime.

### *A.3.5 Conclusions*

This section summarized the findings obtained in two months of activities performed at TU/e, in an investigation of streamer inception and characteristics for different sharp tips ranging from 30 µm to 1000 µm. The main findings for positive corona are listed below:

- The average time delay ($t_D$) for inception decreases with the increase of the voltage. At the same voltage, sharper electrodes tend to present a short time delay. The 30-µm electrode presents very low $t_D$ values, but its standard deviation is comparable to the values obtained.
- The frequency of pulses and the current present a coherent relationship with the voltage applied. Sharper electrodes have a higher frequency and higher current at the same voltage.
- Imaging of the discharges could provide additional clarification, mainly on the shape of the current (and the PMT signal) of a single pulse, as well as to ensure if any Hermstein glow is observed after the pulses.

For negative corona, the main results are listed below:

- Since the inception voltage for discharges is higher, a 10-millisecond time window was not enough for getting consistent results of time delay for the rounder electrodes with the voltages that we could reach without changing anything on the setup. For the sharper electrodes, it was observed the same features of positive corona.
- It was found that, for the range of voltages applied, the sharper electrodes have lower pulse density, which was clarified after performing imaging of the discharges, and confirming that a glow stage was reached (and consequently a superimposed continuous current occurred).
- Imaging discharges at lower voltages is required to verify whether it is possible to reach a stage of steady Trichel pulse.

The results shown with these experiments are useful on the object of investigation of this thesis. The work presented in this section can be preliminary of a complete picture of corona discharges from sharp electrodes with a great range of tip radii. It can also provide experimental background for other investigations associated with streamer/leader inception from lightning rods, wind turbines, and aircraft.

## A.4 Use of photometers to determine the leader inception

The investigation described in this section was performed to determine the leader inception using the photometers employed for 337 and 777 nm wavelengths. The main idea of this work is to compare the leader initiation of three structures with one solidly grounded rod, assigned as “reference rod” (PR). The setup consists in a plate-to-rod setup with 1 m of gap distance (d) and the tip standing 1 m above the ground (h). The configurations for the rods should follow the scheme proposed in Figure A.17.

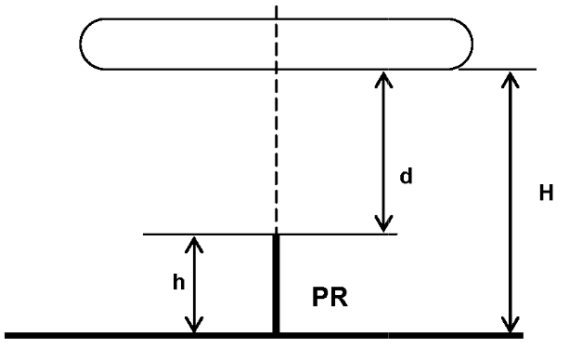


Figure A.17 - Reference Rod (PR) and Test Unit (PDC) evaluated in the same setup.

At the upper plate, a negative high voltage is applied for polarization simulating the background electric field (EF) before the inception of an upward positive leader. In the experiments performed, HV was set to -40 kV (i.e., electric field of -20 kV/m).

To represent the phenomena, the electric field enhancement at the electrode’s tip is emulated using a switching impulse waveform with rise time between 100 μs and 1000 μs. For the validation of lightning rods, at the leader inception, the waveform’s derivative should lay between $2x10^8$ to $2x10^9$ V/m/s.

The applied voltage at the Marx Generator is found using, firstly, the up and down method for 50% ($U_{50}$) and then, the final voltage is calculated for 100% of the discharges ($U_{100}$). One test consists of 50 discharges, that will give an average $T_{init}$ for the reference rod (PR) and the units to be tested.

### *A.4.1 Determining the leader initiation*

Figure A.18 shows the typical discharge waveforms when no polarization is applied to the upper plate. During the voltage rise, several small pulses can be noticed before the breakdown measured with the Pearson coil.

At the beginning of the rising voltage (-103 μs), two strong optical pulses correspond to the discharges of the Marx Generator’s spheres. The initial pulses, such as the one seen at -83 μs, are correspondent to initial streamer and stem formation before the actual leader inception. At t=-12 μs, there is a strong pulse in the 337 nm as well as in the 777 nm. These pulses can be attributed to the stable leader propagation.

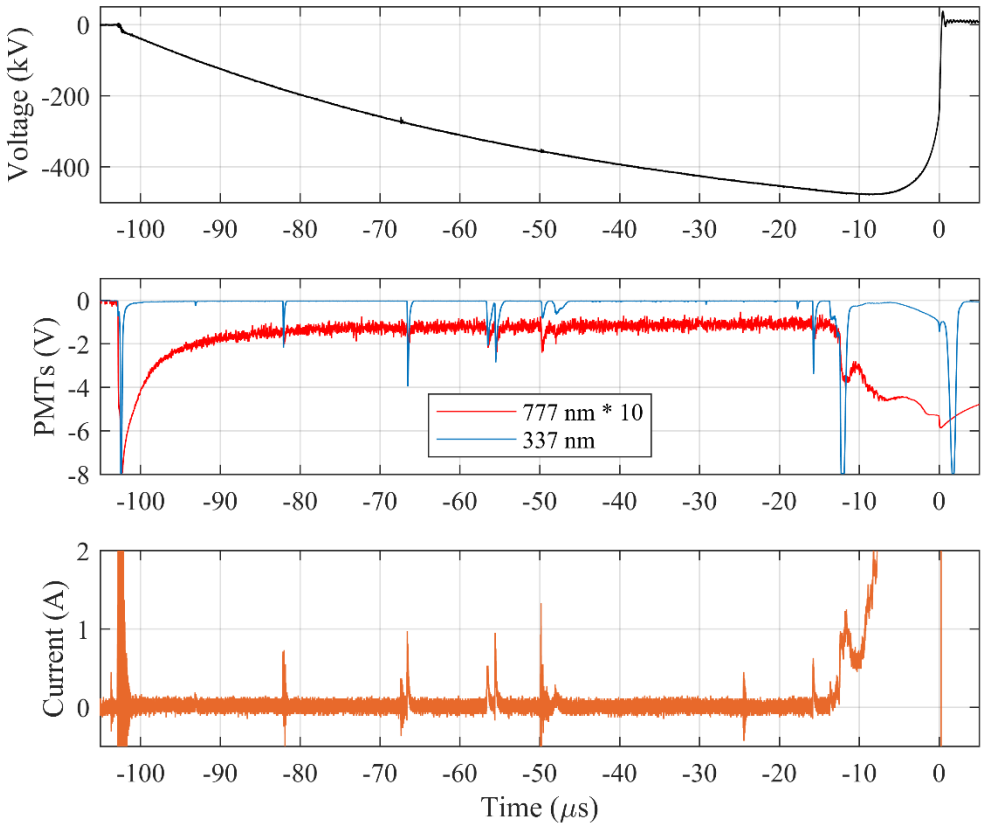


Figure A.18 - Typical current pulses measured during voltage rise.

When the polarization is applied, one circuit with two gaps is introduced in the system, as it is depicted in Figure A.19. The high voltage upper plate has approximately the HVN voltage (-40 kV). The two spark gaps produce an open circuit to the Ground and the Marx Generator. Therefore, ideally, no power is dissipated because there is no current through the 1 MOhm resistor.

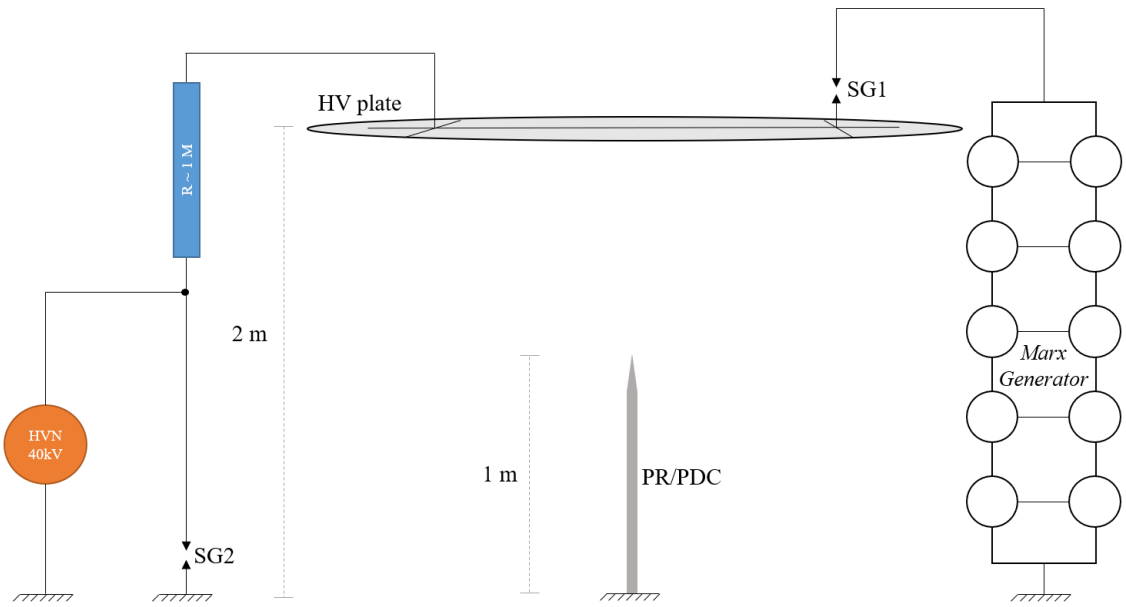


Figure A.19 - Setup scheme for DC polarization.

When the Marx is switched on, and the negative voltage is applied, a preliminary breakdown happens at SG1, for a certain voltage level. At this moment, the voltage measured by the HV capacitors steps to a value of lower magnitude since the upper plate has already -40 kV. Later on, the increase in the Marx voltage and some current flowing through SG2 makes a second breakdown. Figure A.20 shows the typical waveform of one intercomparison test performed, in which one can see clearly only distinctive optical pulses corresponded to electrical activity outside the main gap.

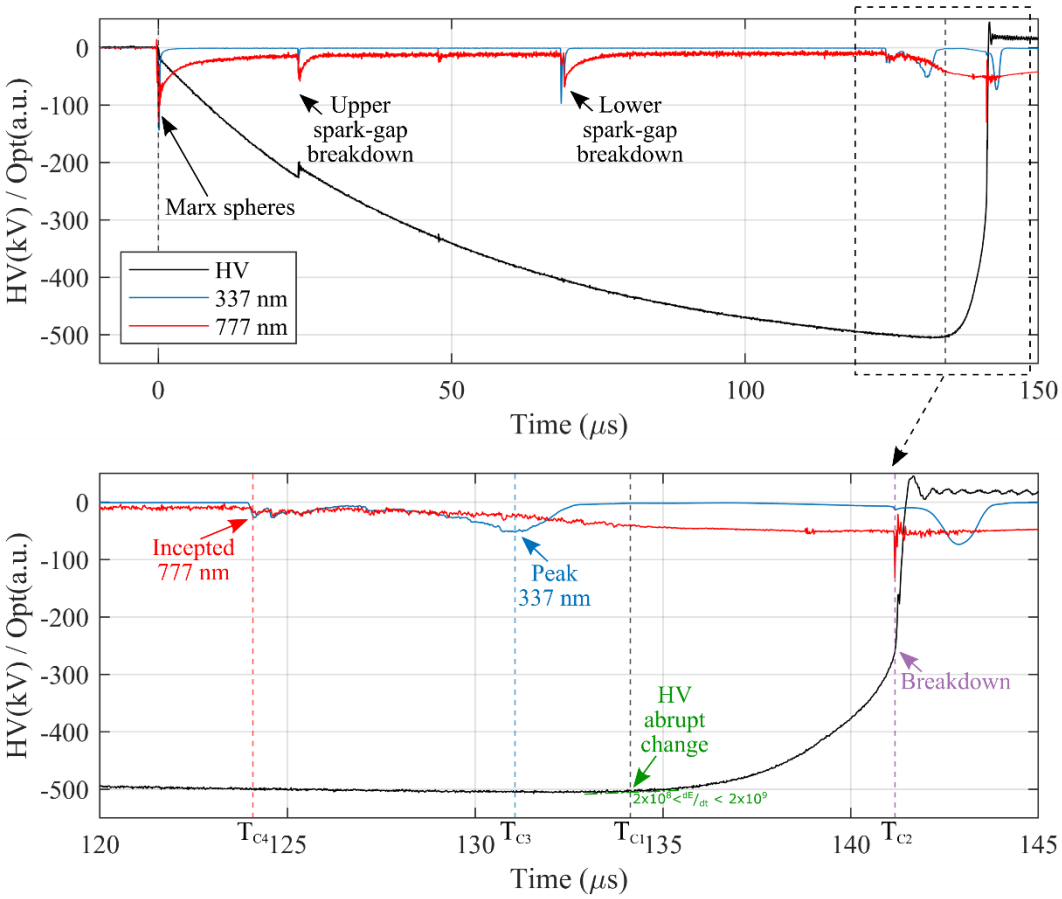


Figure A.20 - Typical waveform obtained when there is DC polarization.

In this study, four criteria for leader initiation were considered ($T_{C1}$, $T_{C3}$ and $T_{C4}$). The time of the breakdown was also verified as a criterion ($T_{C2}$). The criteria are described in the following:

- *Abrupt Change* ($T_{C1}$): This criterion adopts what is proposed in the typical standards for lightning protection, in which the HV should be evaluated for the "abrupt change". Following what is proposed, we adopt a point in the voltage rise that produces an Electric field derivative between the range of $2x10^8$ and $2x10^9$. In Figure A.20, $T_{C1}$ is presented as a black dashed line.
- *Breakdown* ($T_{C2}$): We detect the breakdown by looking for VHF oscillations in the 777 nm signal. This moment also coincides with another abrupt change from the high voltage, as it can be notice by the purple dashed line in Figure A.20.

- *Peak 337* ($T_{C3}$): This is taken at the maximum 337 nm irradiance before the breakdown. As it is observed in the second paper of this compendium, this can also be adopted as a criterion for stable leader propagation, as it is correspondent to a burst of long streamers all over the gap. In Figure A.20, $T_{C3}$ is shown as a blue dashed line.
- *Incepted 777* ($T_{C4}$): This is the leader/stem inception from the grounded rod that actually evolves into a stable leader. Usually, it can happen significantly before the 337 nm peak. In Figure A.20, $T_{C4}$ is shown as the red dashed line.

### *A.4.2 Tests performed using photometers*

We performed **three different experiments** to compare three structures used as a lightning captor. In these experiments, the units to be tested were:

a. Test 1 (Spark Gap Tip): One electrode connected to the ground through a spark gap.
b. Test 2 (HV Prototype): Electrically floating electrode, connected to a negative power supply (-15 kV) that allows positive charging of the tip.
c. Test 3 (Horizontal cable): Straight horizontal cable placed at the same height of the other units (1 m above ground), to simulate cables used in faraday cages built over high structures.

For 50 discharges, the average $T_C$ for each of the criteria is calculated, for both the units to be tested (PR and UNITx). The average times ($<T_{UNIT}>$) obtained are used to evaluate if the leader initiation occurs before or after than the times obtained for the reference unit ($<T_{PR}>$).

### *A.4.3 Results*

Table A.2 depicts the results of the calculations performed for each of tests. One can notice that the spark gap tip and the HV Prototype produces a considerable advance time following either criterion. The horizontal cable, conversely, produces a negative advance time.

Table A.2 – Advance time following different methodologies for leader initiation

| | | $T_{C1}$ (µs) | $T_{C2}$ (µs) | $T_{C3}$ (µs) | $T_{C4}$ (µs) |
|---|---|---|---|---|---|
| **Test 1 Spark Gap Tip** | $<T_{PR}>$ | 132.31 | 140.30 | 129.35 | 126.66 |
| | $<T_{UNIT1}>$ | 120.80 | 128.22 | 118.72 | 116.15 |
| **Test 2 HV prototype** | $<T_{PR}>$ | 147.71 | 156.71 | 144.14 | 142.47 |
| | $<T_{UNIT2}>$ | 122.07 | 130.11 | 119.96 | 117.20 |
| **Test 3 Horizontal cable** | $<T_{PR}>$ | 135.42 | 142.75 | 133.30 | 131.04 |
| | $<T_{UNIT3}>$ | 151.99 | 159.42 | 150.43 | 148.08 |

The difference between the criteria is considerable but not major. The methodologies can produce advance times higher or lower, depending on each test. In addition, these values are within the uncertainties of the typical validation procedures of lightning rods, which can range to up to 15% of the measured values.

Figure A.21 shows one of the waveforms of the photometers with the high voltage for the unit in test 1. For that discharge, we used the Xybion camera to image the discharge with a time exposure of 10 μs. The picture was taken 40 μs before the breakdown, and the photometers confirm the optical signals corresponding to a leader-formation attempt from the grounded rod. The optical signals cease before the stable leader inception that takes place at about 10 μs before the discharge.

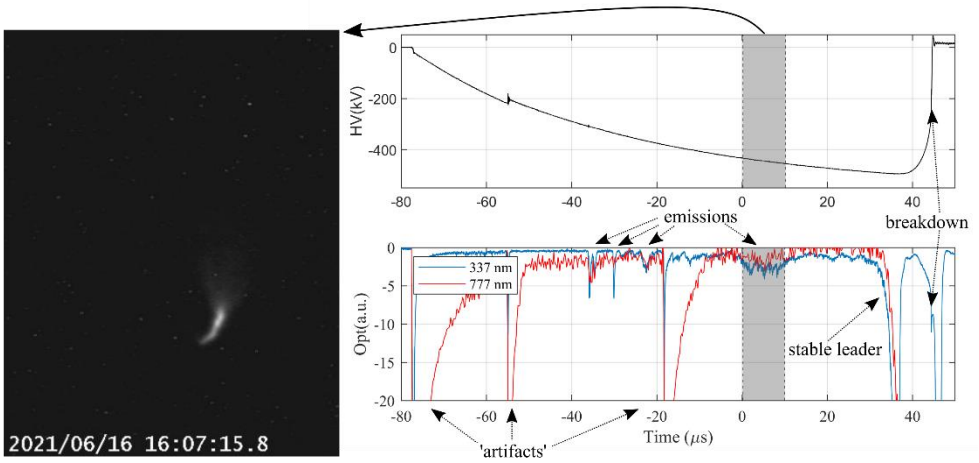


Figure A.21 - Typical image obtained during leader formation attempts that occur before the breakdown.

The criteria $T_{C1}$-$T_{C4}$ performed for leader initiation only consider the stable leader and not the earlier emissions that correspond to streamers and leader-formation attempts. It is important to consider that these emissions would not follow typical standards when it is mentioned the “abrupt change” in the voltage and the required voltage derivatives.

It is observed that the artifacts indicated in Figure A.21 are associated with the breakdown outside of the main gap (in the Marx Generator and the spark gaps). From the results, the horizontal cable, standing at the same height as the reference rod (PR), did not produce time advance for the leader inception.

Figure A.22 shows the signals of the photometers and the upper plate voltage during the discharge process. Many pulses in the 337 suggest streamer activity from the horizontal cable, which is confirmed from the Xybion image, taken with a time exposure of 10 μs. The red arrow indicates which streamer zone was responsible for the breakdown.

Although not producing advance times, the horizontal cable produced more corona discharges due to providing more surface than the single PR sharp tip subject to the enhancement of the electric field. Since the cable was kept at the same height of the

PR's tip, and pretty much horizontal, the breakdown took place in different sections of it during the numerous discharges performed.

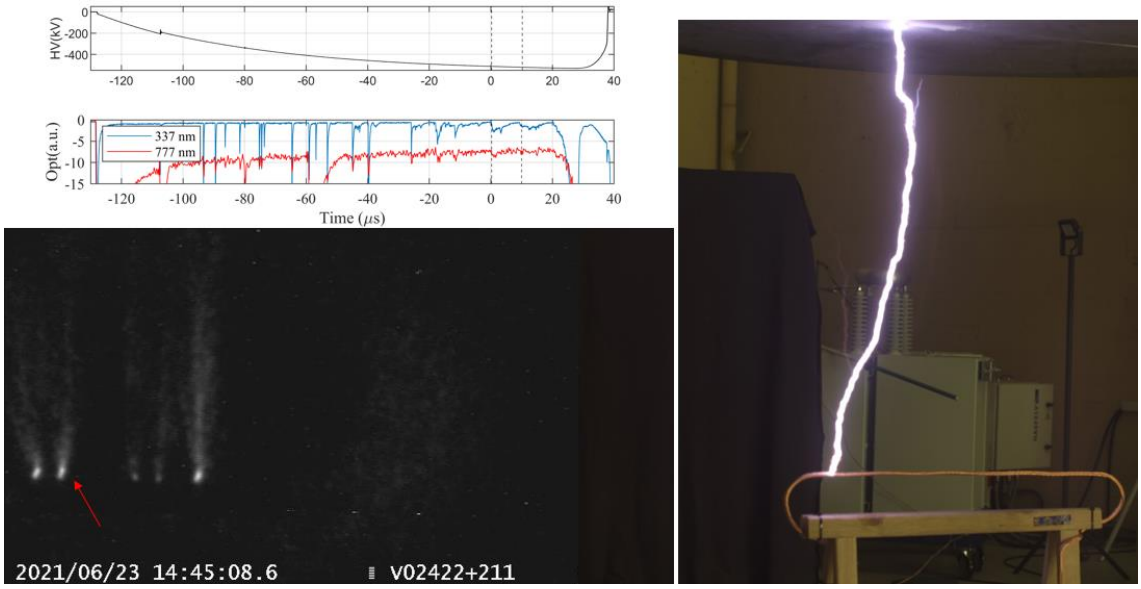


Figure A.22 - Leader formation attempts for the horizontal cable.

## *A.4.4 Conclusions*

This section summarizes the results obtained with the investigation of the use of narrow-band photometers for blue (337) and red (777.4) emissions associated with long air laboratory discharges. Three different tests were performed to compare the performance of the devices with a reference rod (PR) with four different methodologies.

The time of leader initiation must be taken under the following conditions:

- $U_{100}$ switching impulse voltage with rise time between 100 and 1000 μs.
- In the initiation zone of the upward leader, EF derivative between $2x10^8$ and $2x10^9$ V/m/s.
- The time should be correspondent to the abrupt change in the slope of the voltage corresponding to an emission.

The results obtained here for the first methodology proved to be consistent with the requirements of the standards. In addition, all $T_{C1}$s correspond to moments where the leader is already incepted (as it is seen from the photometers).

The other criteria were performed to validate $T_{C1}$ and check if the photometer signals would produce a significantly different result for the times determined. In fact, even though from the photometers it was found out that the leaders are incepted before the "abrupt change", the results do not produce significant changes for the advance times.

# Appendix B: Other Publications

## B.1 Conference paper: Experiments with a tethered drone to investigate induced charges on a vertically arranged conductor during fair weather

This section presents the results of one collaboration performed during this PhD project. They are experiments using tethered drones for investigated induced charges on vertically arranged conductors.

To better understand the phenomena associated with electrostatic charges and potential distribution over vertical conductors, preliminary results were obtained with a tethered drone that is used to lay vertically a 100-m long-stranded copper wire. Several flights were conducted in fair weather conditions. In the first configuration, a conductive spherical shell with a spool for the wire is placed in a Teflon holder and used for ensuring that the charges inducted on the conductive body do not produce any corona from the bottom of the system. A field mill is placed below the sphere at a fixed distance, and its measurement can be used as a reference to the charge distribution over the sphere during the flights. The second configuration consists of grounding the bottom sphere, taking the null potential up to the tip of the wire that is deployed. In this setup, several approaches for measuring currents were explored.

The post-print paper presented at the International Conference on Grounding & Lightning Physics and Effects (GROUND 2020/21 and 9th LPE) in the following pages.

### *B.1.1 Main results*

Laboratory experiments were conducted to represent the situation when the system is composed of the sphere connected to a vertical wire and insulated from the ground. For that, a small electric field mill near the sphere gives an indication of the distribution of charges over the sphere.

In the field, three flights were performed in different configurations for observing qualitatively how the potential rises and the charge separation. In the first

flight, most of the charges were concentrated in the wire, and the sphere presented some positive charge after the rupture of the wire. In the second flight, the drone altitude was acquired simultaneously with the readings of the electric Field Mill, and the system gets charged after collecting the wire. In the third flight, in a different weather condition, some possible evidence of corona current is observed, obtained when the drone altitude is higher than 80 meters.

The data presented in this paper are useful for understanding some conditions that tall and elevated structures, such as wind turbine blades and towers are subject to.

# Experiments with a tethered drone to investigate induced charges on a vertically arranged conductor during fair weather

M. Arcanjo[1,2], P. Fontanes[1,2], M. Urbani[1], J. Montanyà[1]

[1]Lightning Research Group (LRG), Polytechnic University of Catalonia, Terrassa, Barcelona, Spain.

[2]Dena Desarrollos S.L. (Ingesco), Terrassa (Barcelona), Spain.

Corresponding author: Marcelo Arcanjo (marcelo.augusto.sousa@upc.edu)

Post-print of paper presented at the International Conference on Grounding & Lightning Physics and Effects (GROUND 2020/21 and 9th LPE).

**Abstract:** To better understand the phenomena associated with electrostatic charges and potential distribution over vertical conductors, this work describes preliminary results obtained with a tethered drone that is used to lay vertically a 100-m long-stranded copper wire. Several flights were conducted in fair weather conditions. In the first configuration, a conductive spherical shell with a spool for the wire is placed in a Teflon holder and used for ensuring that the charges inducted on the conductive body do not produce any corona from the bottom of the system. A field mill is placed below the sphere at a fixed distance, and its measurement can be used as a reference to the charge distribution over the sphere during the flights. The second configuration consists of grounding the bottom sphere, taking the null potential up to the tip of the wire that is deployed. In this setup, several approaches for measuring currents were explored.

## 1 – Introduction

The background electric field can reach a few hundred volts per meter on the earth's surface during fair weather conditions. Tall and elevated structures effectively distort their surrounding electric field and can, eventually, accumulate surface charges. Modern wind turbine blades, as an example, can get charged, reach a potential of several kilovolts, and cause electrostatic discharges (ESD) that stress the wind turbine's rotor bearings and other parts of its mechanical systems.

On the investigation of induced currents in stormy weather, Davis and Standring [1] conducted in 1947 an experiment with tethered balloons, reporting currents in the range of milliamperes to the kiloamperes (when the balloon was effectively struck by lightning). The measurement of the electric potential at different altitudes using a wire tethered balloon was performed by Vonnegut et al. [2]. At altitudes of 1000 m, they reported values close to 100kV. Holzworth [3] used a high impedance device for measuring the potential and reported values of 150kV at altitudes near 600 m. In addition to effects caused by potential differences, the mechanical movement of wind turbines can avoid the shielding effect caused by space charges. Observations made by Montanyà et al. [4] support the hypothesis that the blade rotation contributes to the existence of stronger local electric fields at the blade's tip. These observations are aligned with previous works [5-7] that relate the wind turbine blade rotation to an increase in its susceptibility to receive lightning strikes.

López et al. and Montanyà et al. measured induced voltages and currents in conductive tethered kites [8] and drones [9], respectively. The deployment of a vertical conductive wire causes a current flow due to induced charges. The high potential difference between the grounded cable and the local potential at certain altitudes may also lead to corona point discharges. Recently, Hong et al. [10] indicated evidence of corona discharges observed in fair weather in an experiment with a tethered grounded balloon and a sharp tip. Currents in the order of a few hundreds of nanoamps were obtained when the balloon exceeded heights of about 65 meters. They estimated the potential difference for the environment and calculated an average electric field at the ground level of 115 V/m.

In this work, we discuss preliminary results obtained for flights with a tethered drone to investigate charges induced in a system composed of an insulated sphere and a vertical wire. In a secondary approach, the system is grounded, and we observe possible indications of corona discharges. This study reveals important contributions to the understanding of corona discharges from grounded and floating conductors, that may be associated with upward leaders' formation from different structures.

## 2 – Experiments in the laboratory

We performed experiments in the laboratory aiming to represent the situation when the system is composed of the sphere connected to the vertical wire and insulated from the ground. For that, we used a small electric field mill near the sphere. Its output voltage could give an indication of the distribution of charges over the sphere.

### *2.1 Charging a floating sphere with corona discharges*

With this experiment, we propose to charge the sphere by producing corona discharges in the tip of a wire connected to it. Figure 1 shows the setup used for this investigation. A spherical shell with a diameter of 30 cm is placed between two plates with 2 m of diameter, electrically floating and supported on a Teflon structure. On the top of the sphere, a straight insulated wire is connected with its tip exposed. The gap distance between the tip of the wire and the upper plate is about 4 cm.

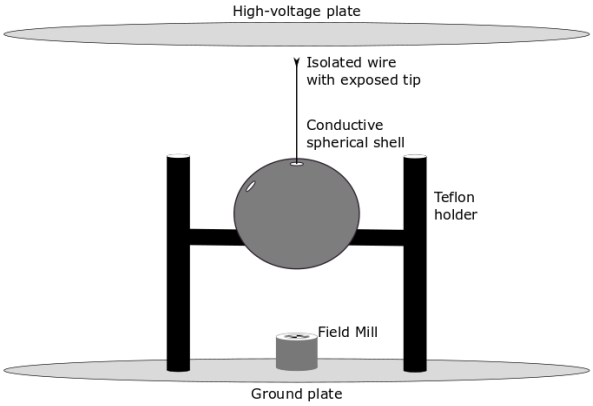


**Figure 1** - Insulated sphere-wire subject to high electric field.

The measurements of the Field Mill (FM) provide a qualitative idea of the charge distribution in the setup. The experiment performed consists of increasing the upper plate voltage from zero to a high-voltage level (6 kV, 9 kV, 12 kV, or 15 kV), with a slope of 10kV/s. For three seconds, the voltage remains constant and returns to zero, with the same rate of change.

The output of the Field Mill indicates the electric field due to the upper voltage applied. We are interested in the values obtained when the upper plate voltage returns to zero. This indication should be zero if the sphere-wire returns to the initial conditions.

Figure 2 shows the data obtained during the experiment, when positive (a) and negative (b) voltage were applied. For the positive voltage, we observed that when 6 kV or 9 kV were applied, the sphere did not get electrically charged, and the Field Mill readings were the same as at the beginning of the experiment. However, when 12 kV or 15 kV were applied, the sphere gets charged. In the laboratory, we measured the corona current using both a shunt resistor and a current transformer. Figure 1 shows the diagram of connections of the sensors in the setup.

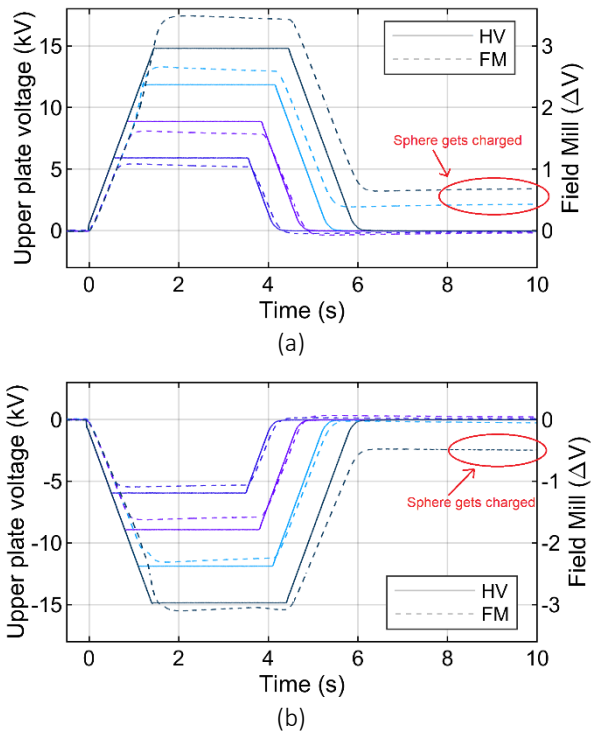


**Figure 2** – Charging the sphere with positive (a) and negative (b) net charges by producing corona at the tip of the wire.

We were able to prove this condition by discharging the sphere with a grounded cable and using a camera with an enhancement for the ultraviolet, which let us able to see tiny corona discharges from the tip of the wire. When negative voltage is applied, only in the condition of -15 kV we could charge the sphere.

When the upper plate voltage increases positively, the charges in the wire-sphere system are rearranged (polarized). Negative charges are concentrated on the tip of the wire, and positive on the bottom of the sphere. That explains the reading of positive values on the Field Mill. If the enhancement of the local electric field at the tip of the wire is high enough (for this setup, when the voltage is about 11 kV), negative corona discharges occur, and the sphere gets charged positively.

The opposite happens when the voltage applied is negative. Positive corona is observed only for higher magnitudes if compared with negative (Figure 2b). For this setup, we observed a threshold voltage of about -13.5 kV. In this work, we did not measure the net charge of the sphere after the experiments.

## 3 – Experiments in the field

For the experiments in the field, a multicopter drone is used to deploy and keep a vertically stable conductive wire, as shown schematically in Figure 3. A conductive spherical shell with a spool for the wire is used for making sure that the separation of charges in the conductive body does not produce any corona from the bottom of the system. The Field Mill is placed below the sphere at a fixed distance, and its measurement can be used as a reference of the charge distribution over the sphere during the flights. A current sensor is positioned on the top of the sphere to detect corona pulses.

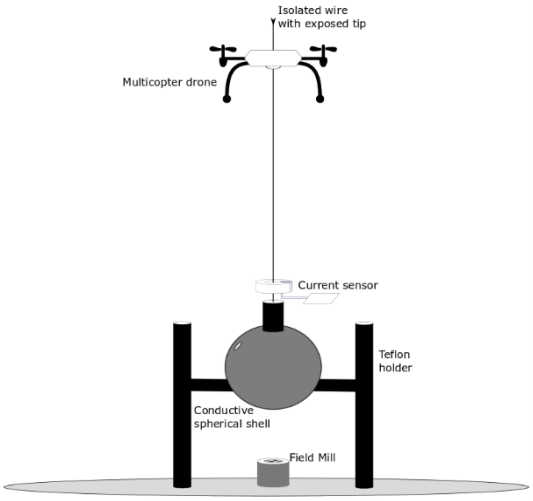


**Figure 3** – Floating sphere with vertical wire connected.

Figure 4 shows a picture of the site where the flight reported in section 3.1 took place (on 11th Nov 2019). The sky was very clear with no clouds nearby. The experiment was performed in the morning to avoid windy conditions.

**Figure 4** – Picture of the site where flight 1 took place.

As discussed in [9], the potential $\phi$ of a vertical perfect conductive wire is the average potential of the atmosphere $\phi(z)$. In fair weather, the average potential gradient is about 100 V/m [11]. Thus, a 100-meter vertical wire will be subjected to a potential difference of about 10 kV and will develop an average potential of 5 kV. Negative charges will be attracted to the upper tip of the wire, and its bottom part will have positive charges.

Figure 5 shows schematically the potential of the induced charges on an electrically floating wire and its potential. We follow the idea proposed in [12], considering the wire a perfect conductor, negative and positive charges would be induced on it, and this potential, added to the background potential, corresponds to the average potential expected (in our case, 5 kV).

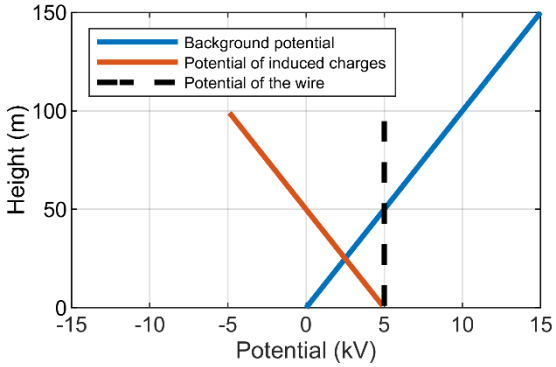


**Figure 5** – Potential of a 100-m floating wire deployed vertically. The dashed line is the sum of the background potential and the potential of the induced charges.

### *3.1 Flight 1: Insulated sphere with wire-disruption*

With this experiment, we tried to detect corona pulses from the wire and measure the electric field from the bottom of the sphere to observe the distribution of charges on the sphere-wire system.

When the maximum altitude (110 meters for this case) was reached, the wire breaks at the point of connection with the sphere. Figure 6 shows the indications of the FM (measured in volts and not converted to electric field). During the fast-rising of the drone (from 0 to 55 seconds), the voltage increases, indicating that the bottom of the sphere is positively charged. When the wire breaks from the sphere, the FM indication suddenly drops.

Most of the charges of the system appear to be accumulated along the wire, since, when it breaks from the system, the level indicated by the field mill is not much higher than before the experiment. However, to verify if the sphere presented any remaining charge, the sphere is grounded at t = 180 seconds. One can note a small step in the FM signal at that moment, indicating that the sphere was positively charged. The results obtained with this experiment suggests that the separation of charges intensifies the higher the wire extends while being deployed vertically.

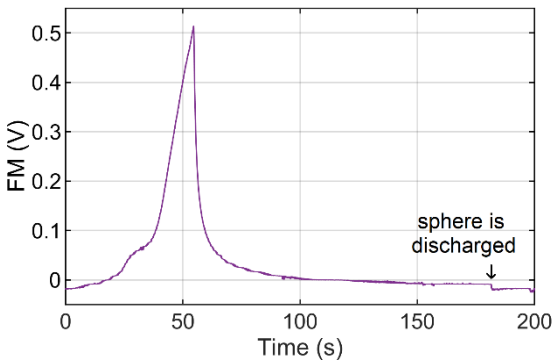


**Figure 6** – Electric Field Mill uncalibrated measurement for Flight 1.

Figure 7 depicts the waveform of the discharge of the sphere using a 50-ohm shunt resistor, with a typical oscillating waveform. For this measurement, the peak current saturates the scale of the digitizer used when it reaches more than 20 milliamperes. The total duration of the discharge is less than 800 nanoseconds, and the charge transferred

(calculated with the saturated signal) was 160 pC. This value is much lower than the one reported in [9], indicating that most of the charges were distributed along the wire.

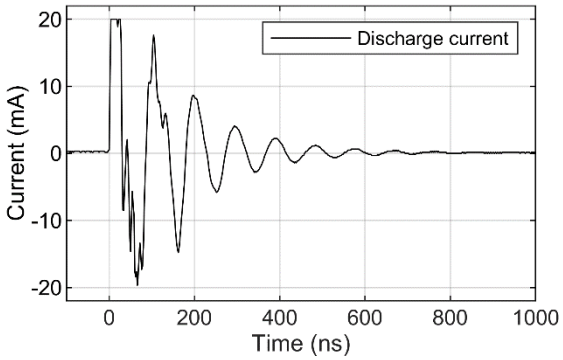


**Figure 7** – Discharge current of the charged sphere.

*3.2 Flight 2: Insulated sphere with vertical wire*

Flight two was performed on 21st Feb 2020. For this test, the drone rose with a lower speed than in the case reported in flight 1. Figure 8 shows the measurement of the Field Mill and the simultaneous altitude of the drone. The wire does not touch the ground at any moment of this experiment, and during the descent of the drone, the wire is collected by a motor installed inside the spherical shell.

From 0 to 100 seconds the drone rises to an altitude of 115 m. Similar to Figure 6, the voltage indicated by the Field Mill also increases due to the polarization of charges. After 100 seconds, the drone starts to descend, and the wire is spooled back inside the sphere. At 400 seconds, the drone is back to the initial position, and one can see that the potential measured by the Field Mill is negative and slowly returns towards zero.

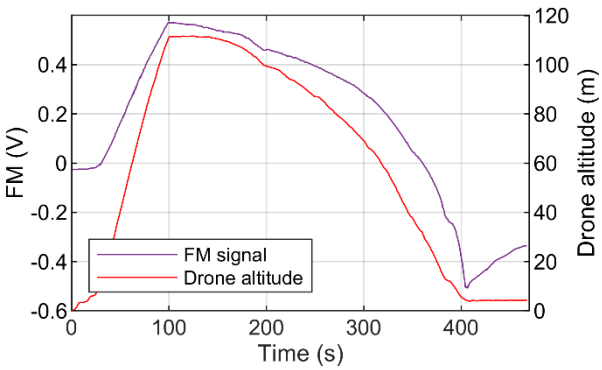


**Figure 8** – Drone altitude and FM signal.

From these results, it is evident that some mechanism charged the sphere-wire system. However, the polarity obtained after the drone descends was the opposite of what we obtained in the laboratory experiments (section 2.1). Therefore, the residual net charge of the sphere was negative, and it was not possible to ensure that corona discharges occurred and were responsible for charging the system.

*3.2 Flight 3: Measuring currents with grounded sphere*

Figure 9 shows a picture of the site where the third flight was performed (on 19th Dec 2019). On this day, the weather was cloudy with some fog, but not thundery. In order to increase the probability of corona current, we grounded the sphere, in this way, the zero potential was taken to the tip of the wire. In this case, a supposed 100

V/m potential gradient would subject the wire to a potential difference of 10 kV. We used a low-sensitivity current ammeter that allows measurements of the average current from the picoamperes scale.

**Figure 9** - Picture of the site where the flight reported in 3.3 took place.

The total time to reach 100 meters was 5 minutes (300 seconds), during this interval, the drone was kept steady several times to verify the behavior of the current. Figure 10 shows the measurements of current and the drone altitude, Figure 11 depicts the detail of the current correlated with the drone speed.

One can note from Figure 10 that the experiment starts at t = 0, and the drone rises to about 33 meters (at t = 110 seconds), for a few seconds, the drone is kept steady, and the current decreases. The current resumes increasing when the drone is pushed up, until 170 seconds, when it stops again. In Figure 11, the drone speed presents a strong correlation with the current through the wire when the drone is rising. When the drone is steady, it is possible to see a steady "background" current in the range of a few nanoamps.

At t = 250 seconds, the drone rises from 60 meters to 100 meters, and when it reaches 80 meters, the current inverts its polarity and increases abruptly comparing with the previous values. The correlation observed with the drone speed no longer exists. When the drone is steady at 100 meters, the current is about -150 nanoamperes.

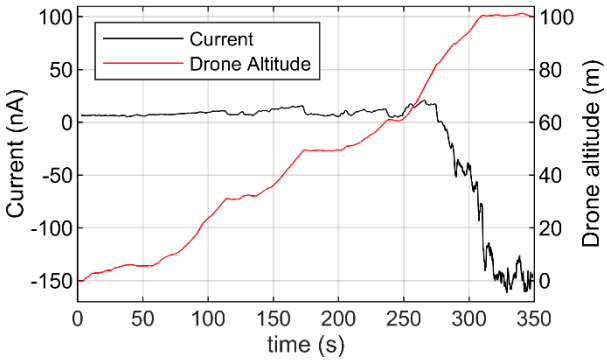


**Figure 10** – Measured current compared with drone altitude.

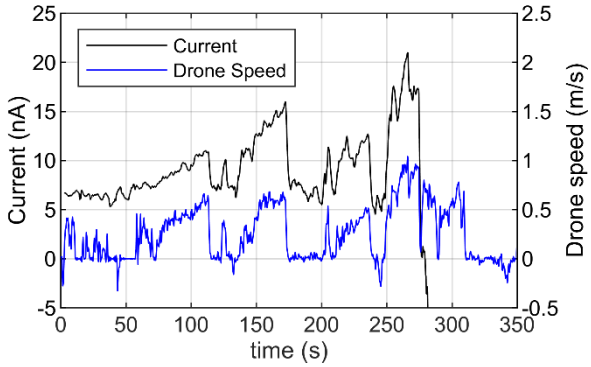


**Figure 11** – Measured current compared with drone speed.

The indications of current shown in Figure 11 suggest that the potential difference that the tip of the wire was subjected was enough for producing corona. However, if one takes into consideration the curve shown in Figure 5, in which the upper potential is positive, no inversion in the polarity of the current would be expected. In this case, with misty weather, we should not expect a uniform electric field with a positive potential gradient.

## 4 – Conclusions

This paper shows preliminary results of flights with a tethered drone and a sphere configured insulated from the ground or grounded. In the laboratory, we performed experiments that show how the effects of charge induction happen with the sphere and how corona discharges can charge the insulated system when it is subjected to a very high potential difference.

In the field, three flights were performed in different configurations for observing qualitatively how the potential rises and the charge separation. In the first flight, we observed that most of the charges were concentrated in the wire, and the sphere presented some positive charge after the rupture of the wire. In the second flight, the drone altitude was acquired simultaneously with the readings of the electric Field Mill, and we observed that the system gets charged after collecting the wire. In the third flight, in a different weather condition, we show some possible evidence of corona current, obtained when the drone altitude is higher than 80 meters.

We believe that the current probe was not able to measure corona pulses due to the large distance to the tip of the wire (in flights 2 and 3), and for solving this issue, we are currently developing a sensor that will be attached to the tip of the wire.

The data presented are useful for understanding some conditions that tall and elevated structures, such as wind turbine blades and towers are subjected to. In future works, we intend to conduct more flights and quantitatively assess the data, discussing, with the aid of models, electric field behavior and thresholds for corona occurrence, as well as improve the methods for measuring corona burst pulses.

## 5 – Acknowledgments

This work was funded by the European Union's Horizon 2020 research and innovation program under the Marie Sklodowska-Curie grant agreement No 722337. This work is supported by a research grant from the Spanish Ministry of Economy EXPLORA call with reference ENE2017-91636-EXP. This work is also supported by the MIT MISTI Global

Seed Funds MIT-Spain project “Smart Lightning Protection Systems for Wind Turbines and Aircraft” and “Small Unmanned Airborne Systems for Atmospheric Electricity Research”. Also, the Industrial Doctorate grant of the AGAUR with reference 2019 DI 039.

## 6 – References

[1] R. Davis and W. G. Standring, “Discharge Currents Associated with Kite Balloons,” Proc. R. Soc. Lond. A, 191, pp. 304-322,1947.

[2] B. Vonnegut, R. Markson, and C. B. Moore, “Direct measurement of vertical potential differences in the lower atmosphere,” J. Geophys. Res., 78(21), 4526–4528, doi: 10.1029/JC078i021p04526, 1973.

[3] R. H. Holzworth, “Hy-wire measurements of atmospheric potential,” J. Geophys. Res., 89(D1), 1395–1401, doi: 10.1029/JD089iD01p01395, 1984.

[4] J. Montanyà, O. van der Velde, and E. R. Williams, “Lightning discharges produced by wind turbines”, J. Geophys. Res. Atmos., 119, doi:10.1002/2013JD020225, 2014.

[5] Rachidi, F., M. Rubinstein, J. Montanyà, J. L. Bermudez, R. Rodriguez, G. Solà, and N. Korovkin, “Review of current issues in lightning protection of new generation wind turbine blades”, IEEE Trans. Ind. Electron.,55(6), 2489–2496, doi:10.1109/TIE.2007.896443, 2008.

[6] Wang, D., N. Takagi, T. Watanabe, N. Sakurano, and M. Hashimoto, “Observed characteristics of upward leaders that are initiated from a windmill and its lightning protection tower”, Geophys. Res. Lett., 35, L0280, doi:10.1029/2007GL032136, 2008.

[7] Wilson, N., J. Myers, K. Cummins, M. Hutchinson, and A. Nag, “Lightning attachment to wind turbines in central Kansas: Video observations, correlation with the NLDN and in-situ peak current measurements, presented in the EWEA (The European Wind Energy Association)”, Vienna, Austria, 2013.

[8] López, J., J. Montanyà, O. van der Velde, F. Fabró and D. Romero, “Fair Weather Induced Charges and Currents on Tall Wind Turbines and Experiments with Kites” in: Proc. of the 33rd Intl. Conference on Lightning Protection, ICLP, Estoril, Portugal, 25-30 Sept. 2016.

[9] Montanyà, J., J. López, P. Fontanes, M. Urbani, O. van der Velde and D. Romero, “Using tethered drones to investigate ESD in wind turbine blades during fair and thunderstorm weather” in: Proc. of the 34th Intl. Conference on Lightning Protection, ICLP, Rzeszow, Poland, 02-07 Sept. 2018.

[10] Hong, D., Rabat, H., Kirkpatrick, M., Odic, E., Merbahi, N., Giacomoni, J., Eichwald, O., “Evidence of a corona discharge induced by natural high voltage due to vertical potential gradient”. Plasma Research Express, 1(1), pp.015013. 10.1088/2516-1067/ab0563, 2019.

[11] Harrison, R.G. “The Carnegie Curve. Surv. Geophys. 34, 209. https://doi.org/10.1007/s10712-012-9210-2, 2013.

[12] Mazur, V., Lothar, H., “Model of electric charges in thunderstorms and associated lightning. https://doi.org/10.1029/98JD02120.

# B.2 Conference paper: Corona Discharges from Grounded Rods under High Ambient Electric Field and Lightning Activity

This section presents the results of corona discharges obtained in two setups contrasting with the setup where the results published in the first paper of this compendium were obtained. The post-print paper presented at the joint event of the 35th edition of the International Conference on Lightning Protection (ICLP) and the XVI edition of the Symposium on Lightning Protection (SIPDA) is depicted in the following pages.

## *B.2.1 Main results*

In the setups, it was measured currents along the grounded rod under high background electric field conditions or during its fast changes caused by lightning strikes. The current signals present the same features of laboratory experiments reported in literature, with polarity compatible with the background electric field. It was also observed that positive discharges required a lower electric field threshold than negative discharges. Their pulse frequency is also equivalent to one-tenth of the pulse frequency of negative discharges, for a similar electric field level. The rods were placed near the ground and on the roof of a conventional building. Pulses were registered on some occasions when there was lightning activity nearby, either before or after lightning events. This investigation is relevant for understanding the production of corona and space charges from high structures.

# Corona Discharges from Grounded Rods under High Ambient Electric Field and Lightning Activity

M. Arcanjo[1,2], J. Montanyà[1], M. Urbani[1], P. Fontanes[1,2], V. Lorenzo[2], E. Pons[2]

[1]Lightning Research Group (LRG), Polytechnic University of Catalonia, Terrassa, Barcelona, Spain.

[2]Dena Desarrollos S.L. (Ingesco), Terrassa (Barcelona), Spain.

Corresponding author: Marcelo Arcanjo (marcelo.augusto.sousa@upc.edu)

Post-print of paper presented at the 35th International Conference on Lightning Protection (ICLP) and the XVI International Symposium on Lightning Protection (SIPDA).

**Abstract:** We assess results of corona pulses detected under high background electric field in the laboratory and in the field in two different experimental sites. The first location is on the roof of a regular building, and the second is on a flat area. Due to the enhancement of the E-field caused by lightning strikes in the vicinity of a grounded rod with a sharp tip, we observed positive and negative pulses before or after the strikes. When lightning activity is far from the structure, but the electric field remains high, pulses are still observed.

**Keywords:** corona discharges, electric field associated with lightning.

## I. Introduction

Many studies were conducted on the effects of the electric field enhancement below thunderclouds [1-6]. Irregularities on the surfaces of grounded structures can provide conditions for corona discharges that generates ions and form a space charge layer that decreases the magnitude of the electric field at the ground level [1].

Measurements of the corona current through a grounded needle under thundery weather reported an average current of a few microamperes [2, 3]. An electric field threshold is required for corona inception and the average current increases with the increase of the background electric field. The geometry of the system and weather conditions such as humidity and wind can significantly affect these parameters. The role of wind was studied in [4, 5], which indicated that higher wind speeds accelerate the ion removal from the structures and increase the corona current.

The measurements performed by [6] revealed the features of pulsating discharges from a grounded sharp rod, 30 milliseconds prior to a return stroke nearby. The amplitude of these pulses and their duration are different than the induced currents caused by approaching downward leaders [7], as well as induced currents in vertical conductors during return stroke currents [8]. In the laboratory, the corona current has been extensively studied. The first studies performed [9, 10] reported the pulsating behavior of the current. As the applied electric field increases, the average current and pulse frequency also increases. However, amplitude and time durations seem to be constant for certain geometries [5, 11, 12].

The impacts of space charges on lightning strikes have been assessed by other works [13-16]. It was believed that the shielding of the electric field near grounded structures caused by the corona layer could delay the streamer inception from the structures [13]. However, the delay effect has been found not that severe since the shielding effect provided by glow corona discharges decreases rapidly in the lateral direction of the structures [14]. In upward lightning, [15] reported that self-initiated events were correlated with strong wind speeds that could remove space charges, creating conditions of high local electric field for the leader initiation. For wind turbines, observations reported in [16] indicate that moving structures are able to avoid the shielding effect caused by space charges and increase the probability of lightning strikes.

We performed in laboratory several experiments to characterize the corona current from a grounded sharp rod at atmospheric pressure. Although the phenomenon of corona discharges is well known, few studies have been conducted based on outdoor experiments. We measured corona pulses under stormy weather in two different experimental sites. In this work, we discuss the key features observed for the data obtained.

## II. Methodology and Instrumentation

In the laboratory, we measured the corona current using both a shunt resistor and a current transformer. Figure 1 shows the diagram of connections of the sensors in the setup.

A grounded conductive rod 30-cm high with a sharp tip is placed between two plates (with 1.4 meters and 2.0 meters of diameter) separated by 45 cm, leading to a

gap distance of 15 cm. The high voltage power supply provides up to 20 kV DC at positive or negative polarity, and it is connected to the upper plate. This setup reproduces the conditions of sharp grounded structures subject to high electric fields when charged clouds are in the vicinities.

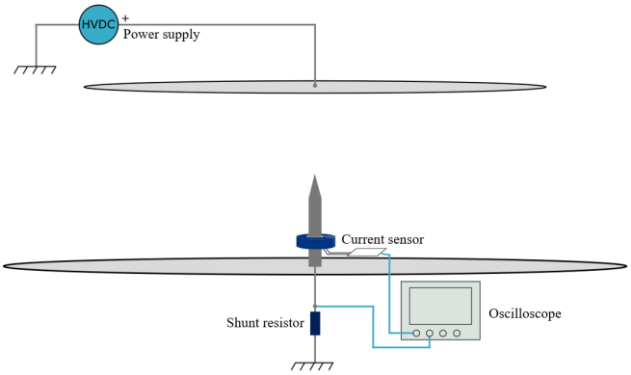


**Fig. 1.** Diagram of connections for the experiments in the laboratory.

We used a resistor in series with the grounding cable of the bottom plate with low inductance and low resistance to ensure that the shunt resistor would not affect the measurements. The current transformer is composed of a ferrite core with a secondary winding and a measuring circuit and does not affect the discharge circuit. For investigating one polarity of corona discharge, the opposite polarity was applied on the upper plate, in the setup described in Figure 1.

The shape of one single pulse is shown in Figures 2 (a) and (b), for respectively, -15 kV and +15 kV applied to the upper plate. The single pulse has a rising time of tens of nanoseconds and a duration of 200-300 nanoseconds. The current transformer presents a waveform representative of the measured discharges, and we applied a voltage ratio of 12 V/A for obtaining the equivalent current in amperes.

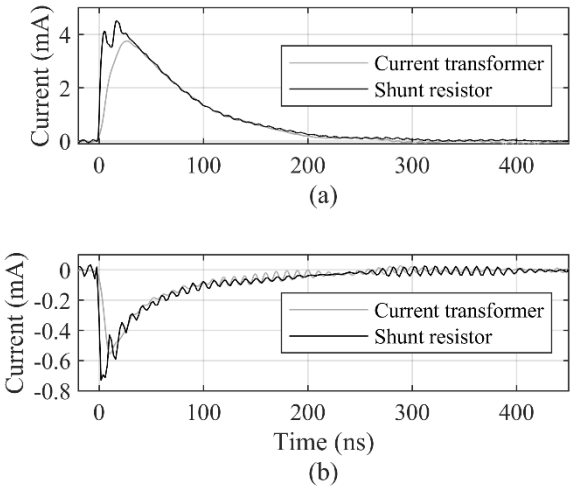


**Fig. 2.** Measurements obtained with the shunt resistor and the current transformer for (a) positive corona and (b) negative corona

The waveform of a single corona pulse reveals some differences: First, in the recording shown in Figure 2, it is considered the same voltage applied (different polarity). The amplitude is higher for positive corona, with an average of 4.2 mA, while for negative, the average was 0.75 mA.

Pulses of positive discharges last longer than negative discharges. In a steady-state mode, when a DC voltage is applied, the frequency (number of pulses per second) of negative pulses is almost one order of magnitude higher than positive.

## III. Experimental Investigation

For investigating the signatures of corona current from grounded rods, we used a conductive rod (about 1.5-meter-long) with a sharp tip placed over the ground surface. Fig. 3 shows the scheme of the installations. The current was measured using a shunt resistor and a current sensor. The resistor was placed in series with the grounding cable of the rod with low inductance and low resistance to ensure the quality of the measurements. The current sensor consisted of a ferrite core with a secondary winding and a measuring circuit and does not affect the discharge circuit.

The sensor provided detections that are correlated to the background electric field, measured by a 10-Hz electric field mill. The indications provided by the Field Mill consider the static component of the electric field. In this way, many lightning strikes happening within its sample rate cannot be perceived in the measurements individually. We also verified a lightning location network (Linet) to monitor the distances of lightning strikes to the sensor's site.

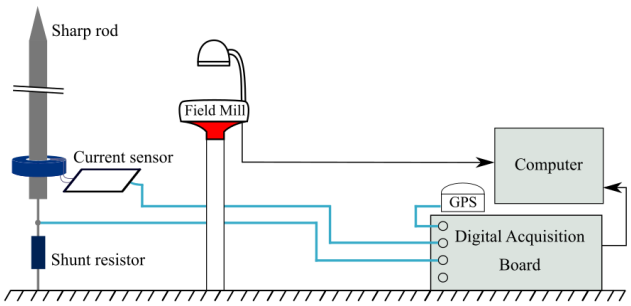


**Fig. 3.** Scheme of the setups for measuring corona discharges.

The first setup was installed over a typical roof of a building in Terrassa, Spain, and the second installation was performed in the Observatori de l'Ebre, in Roquetes, Spain. In this installation, the sensor's tip is 2 m above the ground level. Fig. 4 shows a picture of the installation of the sensor and the electric field mill, in both setups, separated by around 1 meter.

**Fig. 4.** Sharp grounded rod installed in the two setups: rooftop (left) and flat-ground (right).

At the beginning of the operation, both the shunt resistor and the current transformer were used for measuring currents through the rod. Fig. 5 shows the typical

pulse recorded from the experiment, using an 8-bits digitizer in the rooftop setup. The signals were matched with the volt ratio of the current sensor obtained for discharges produced in the laboratory (12 V/A). The shape of one positive pulse presents a fast rise time (in the order of tens of nanoseconds) and decay of hundreds of nanoseconds, similarly to what is reported for laboratory experiments [5-6, 11-12].

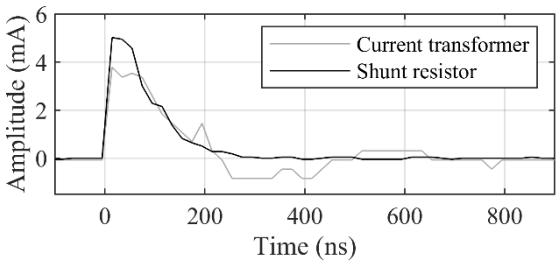


**Fig. 5.** Typical detection of pulse performed in the field comparing the current sensor and the shunt resistor.

The data obtained in the field allowed us to confirm several characteristics of the corona discharges. Pulses of positive discharges last longer than negative discharges. Their average amplitude is higher than negative pulses at the same E-field level (but opposite polarity). Conversely, their pulse frequency (number of pulses counted per second, over a nearly constant electric field) is lower.

For the following days of operation, the shunt resistor was removed from the sensor. Hence, only signals from the current sensor were recorded.

### *A. Rooftop experiment*

For this setup, due to the buffer constraints of the digitizer and the sampling rate (50 MS/s) needed for recording the pulses, it was not possible to perform long-time acquisitions. In this work, all electric field waveforms are presented according to the atmospheric electricity sign convention [17].

Fig. 6(a) depicts a recording of the Field mill for an interval of 3 hours, on May 21st, 2019, when a thunderstorm approached the region of Terrassa. Fig. 6(b) shows a detailed portion of 20 minutes of electric field intensification. The increase in the background electric field started at 13:20 (UTC) and, at 13:22, when the electric field reached about -7 kV/m, the system started to detect a large number of positive pulses, for around 2 minutes. The only lightning activity in the vicinities was registered at 13:30, as it can be seen from a small step in the FM. According to the lightning detection network (Linet), it corresponded to an intracloud discharge 11 km far from the sensor.

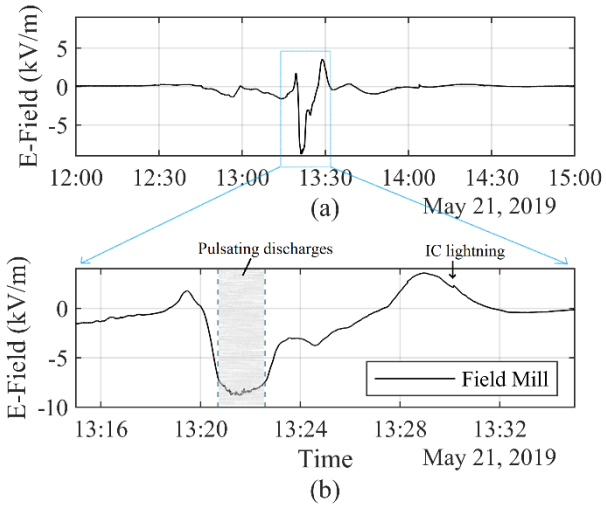


**Fig. 6.** Oscillation of the electric field over a 3-hour interval (a). Continuous detections of positive corona during a 2-minute depicted interval (b).

Fig. 7(a) depicts an interval of 10 minutes from the data of Aug 12th, 2019, in which several lightning strikes were observed. Since the field mill is a measurement of the quasi static electric field, the steps observed usually are related to all return strokes of a flash, or even different flashes that happened in a short time interval. Thus, the distances indicated by the arrows below the curve of the electric field are the distances to the nearest cloud-to-ground lightning strike detected by Linet.

Pulses were registered by the sensor at the instants shown by the dots. For the period shown in Fig. 7(a), they have negative polarity. One can note that all pulses exhibited were recorded after the step detected by the field mill, corresponding to periods of a few seconds of intense positive electric field.

A few hours later, on Aug 12th, 2019, more pulses were recorded, as seen in Fig. 7(b), in a time window of 20 minutes. One stepwise change in the electric field (labeled as 'ND') was not detected by Linet. Positive corona pulses were registered in high negative E-field, for several seconds before lightning strikes.

For the cases shown in Fig. 7(b), positive values of the E-field after the return strokes are probably not high enough for triggering negative pulses from the rod. However, in the event shown in Fig. 7(a), when the E-field is negative, one can see that it reaches similar values to the ones present in Fig. 7(b) (that led to positive corona detections), and positive corona was not detected in that specific interval. It is speculated that several other factors, such as humidity conditions, wind, and presence of water along the tip of the conductive rod can also affect the emergence of corona pulses from the rod, in such a way that establishing a E-field threshold for the discharges may not be consistent.

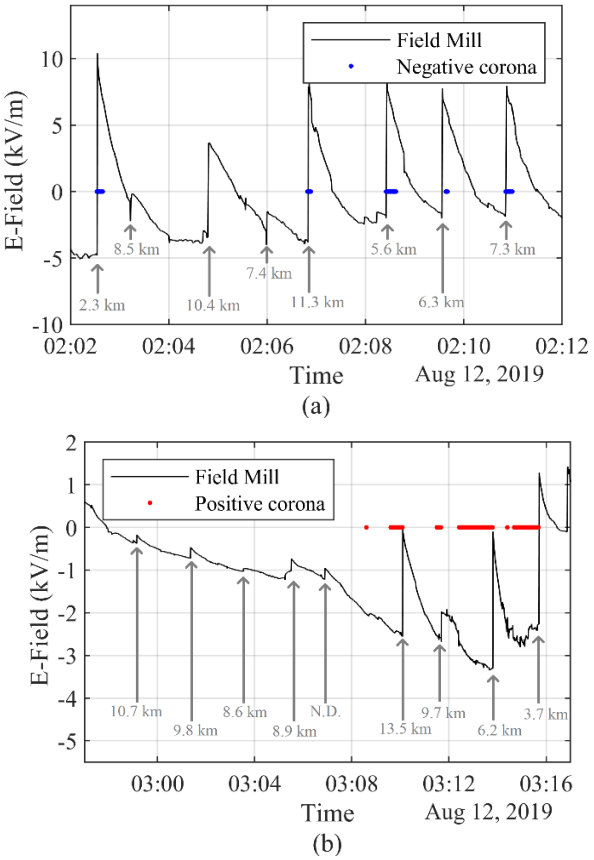


**Fig. 7.** E-field record leading to negative (a) and positive (b) discharges after and before nearby lightning strikes.

### *B. Flat-ground experiment*

The digitizer used in this setup allowed performing acquisitions at 33 MS/s in time intervals of 1 second. The grounded rod was placed 2 m above the ground level, in a flat area, with trees and shrubs, including some taller than the sensor. For this reason, during the campaign, we did not observe as many events as for the rooftop site.

Unlike the roof experiment, in which pulses were recorded continuously during periods of sufficiently high electric fields, the corona pulses obtained at this site were recorded only during fast variations in the electric field resulting from near lightning strikes. We also detected part of the atmospheric processes' signature in VHF due to the grounded rod behaving like an antenna. In this way, we considered only corona discharge pulses with similar features to those obtained in the laboratory, and higher amplitudes than the background noise.

Fig. 8(a) depicts a recording of the electric field for an interval of about 3 minutes, on Jan 21st, 2020, when lightning strikes were nearby the sensor's site. In Fig. 8(b) and (c), we show the current measurement obtained at the moment when the field mill reaches 7.1 kV/m. Due to the very different sampling rates of the two quantities, they are not displayed in the same figure. We indicate at time equals zero, a positive cloud-to-ground (CG) return stroke (RS) registered 4.2 km far from the sensor, with an estimated peak current of 12.5 kA. Negative current pulses start 70 milliseconds after the lightning strike and last for a short period (about 50 milliseconds). The pulse

amplitude reaches approximately 4 mA and decreases until the pulses are indistinguishable from the VHF background noise.

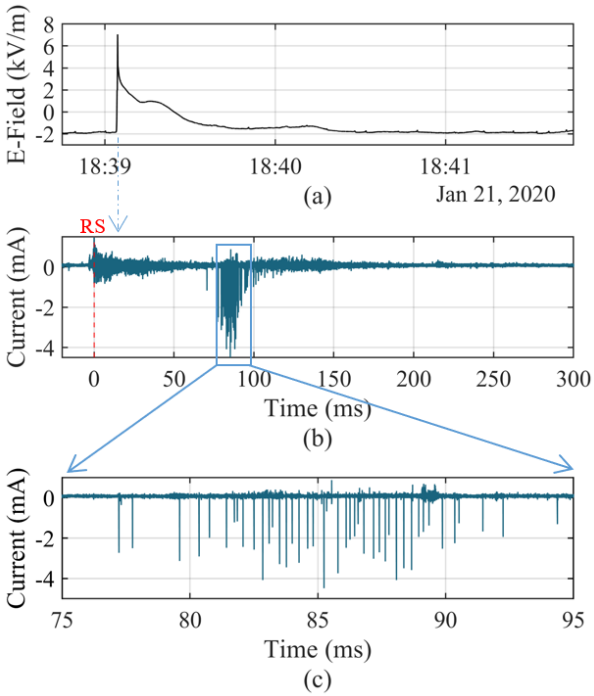


**Fig. 8.** E-field waveform of a positive CG lightning strike (a), that leads to negative corona pulses (b); enhanced view of negative pulses (c).

Fig. 9(a) shows a 3-minute field mill recording obtained on the same day. Three negative return strokes were detected in a wind farm at about 9.1 km away from the sensor. They exhibit a small VHF irradiated pulse measured by the current sensor, and together with our GPS allows for synchronization. The electric field reaches -5.2 kV/m and the return strokes have peak currents of -14.3, -9.1, and -4 kA, respectively. Several positive pulses with amplitudes greater than 10 mA start to be recorded 34 milliseconds after the first return stroke and cease after 150 milliseconds.

In Fig. 9(b), one can note that the highest concentration of pulses is observed after the third return stroke, and that decreases, as the interpulse interval increases and the electric field decreases. For the flat-ground setup, several events like the ones presented in Figures 8 and 9 were recorded.

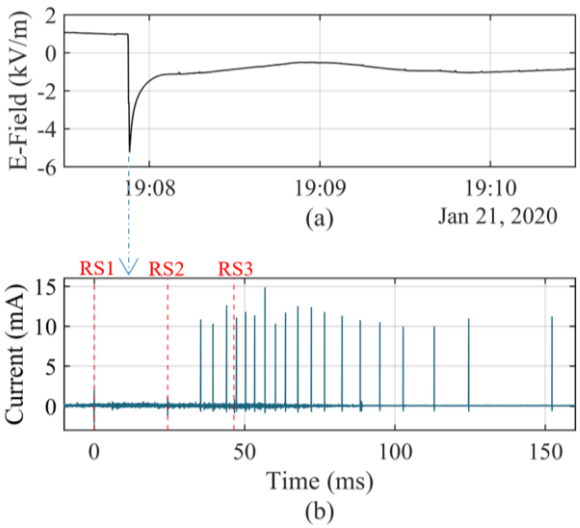


**Fig. 9.** E-field waveform of three negative CG lightning strikes (a) that lead to positive corona pulses from the grounded rod (b).

## IV. Discussion

From Fig. 8, the appreciable VHF content observed after the positive CG suggests that the movement of charges inside the cloud causes the emergence of negative corona pulses from the rod. The corona pulse polarity is not associated with the polarity lightning strike, depending only on the local electric field. We also observed positive pulses after positive strikes, which could be the precursors of negative upward leaders from grounded structures.

Table I shows the results of corona pulse parameters obtained in our setups, with their respective deviation. The rise time was determined as the time interval from 10% to 90% of the peak current. The charge per pulse was also calculated, but due to reflections on the decay of many measured waveforms, we do not present this data for the Rooftop setup.

TABLE I. CORONA PULSE PARAMETERS

| Site | Polarity | Rise time (ns) | Duration (ns) | Peak Current (mA) | Charge per pulse (nC) |
|---|---|---|---|---|---|
| *Rooftop* | + | 24 ± 2 | 364 ± 3 | 17.0 ± 3.6 | -- |
| | - | 16 ± 4 | 320 ± 3 | 4.2 ± 1.9 | -- |
| *Flat-ground* | + | 59 ± 9 | 516 ± 24 | 10.9 ± 1.6 | 2.3 ± 0.3 |
| | - | 44 ± 18 | 350 ± 49 | 2.7 ± 1.5 | 0.4 ± 0.2 |

The rise time observed for positive pulses (tens of nanoseconds) is significantly higher than for negative pulses in both setups, although their values are significantly different between the two setups. This is likely due to the different sampling rates and the actual bandwidth of the current sensors. The duration of the pulses is also higher (320 to 500 nanoseconds) for positive pulses.

The average peak currents obtained are about four times lower for negative pulses in both setups. The amplitude of negative pulses seems to be more variable than

positive pulses, as indicated by the deviation. The noticeable difference of negative pulses' amplitude can be exemplified in Fig. 8, whereas this is not remarkable for positive pulses (as seen in Fig. 9).

Since positive pulses are in average longer, and higher than negative pulses, their charge per pulse is much greater (2.3 nC per pulse versus 0.4 nC).

## V. Final Remarks

Corona pulses of negative and positive discharges from sharp grounded rods were measured with an optimized current sensor in two different installations. We present waveforms and pulse parameters obtained from measured data.

We observed that the rooftop setup was more susceptible to register corona discharges than the flat-ground setup, presenting steady detections over several seconds. For other grounded structures, such as high towers and wind turbines, the enhancement of the local electric field plays an important role. Consequently, corona discharges are expected to be more recurrent for lower levels of background electric field.

With the results obtained, we confirm that pulsating corona discharges, in addition to forming during the approach of descending leaders, as shown in [6], can also occur before and after lightning strikes nearby, or when atmospheric activity it is very far, but the electric field is high enough.

## References

[1] S. Chauzy, P. Raizonville, "Space Charge Layers Created by Coronae at Ground Level Below Thunderclouds: Measurements and Modeling," Journal of Geo. Res. vol. 87, C4, pp. 3143-3148, April 1982.

[2] F.J.W.Whipple, F.J. Scrase, "Point Discharge in the Electric Field of the Earth," Met. Off. of Geo physical Memoirs. 68(7), 20,1936.

[3] W.C.A. Hutchinson, "Point-discharge currents and the earth's electric field," Quar. J. of the Royal Met. Soc. vol. 77, pp. 627-632, 1951

[4] F. D'Alessandro, "Experimental study of the effect of wind on positive and negative corona from a sharp point in a thunderstorm," J. of Electrostatics, vol. 67, pp. 482-487, 2009.

[5] M. Arcanjo *et al.,* "Observations of corona point discharges from grounded rods under thunderstorms," *Atmos. Res.*, vol. 247, 2021.

[6] C. B. Moore, G. D. Aulich, and William Rison, "The case for using blunt-tipped lightning rods as strike receptors,"J. Appl. Meteorol., vol. 42,pp. 984–993, Jul. 2003

[7] A. Nag *et al.*, "Inferences on upward leader characteristics from measured currents," *Atmos. Res.*, vol. 251, 2021.

[8] J. Schoene *et al*., "Experimental Study of Lightning-Induced Currents in a Buried Loop Conductor and a Grounded Vertical Conductor," IEEE Trans. Electromagn. Compat., vol. 50, no. 1, pp. 110–117, 2008.

[9] G.W. Trichel, "The Mechanism of the Negative Point to Plane Corona Near Onset," Physical Review. 54, 1078. 1938.

[10] G.W. Trichel, "The Mechanism of the Positive Point-to-Plane Corona in Air at Atmospheric Pressure". Physical Review. 55(4), pp. 382–390, 1939.

[11] Y. Liu *et al*., "Detailed characteristics of intermittent current pulses due to positive corona," Phys. Plasmas, vol 21, 082108, August 2014.

[12] C. Wang *et al*., "Pulse Current of Multi-Needle Negative Corona Discharge and Its Electromagnetic Radiation Characteristics," Energies, 11, 3120, November 2018.

[13] E.M. Bazelyan, Yu P. Raizer, N.L. Aleksandrov, "Corona initiated from grounded objects under thunderstorm conditions and its influence on lightning attachment," *J. Phys. D: Appl. Phys., vol. 17,* 024015*, 2008.*

[14] M. Becerra, "Corona discharges and their effect on lightning attachment revisited: Upward leader initiation and downward leader interception," Atm. Res., vol. 149, pp. 316-323, 2014.

[15] N. Pineda *et al.*, "Meteorological aspects of self-initiated upward lightning at the Säntis tower (Switzerland)," *J. of Geophysical Res.: Atmospheres*; 124: 14162–14183, 2019.

[16] J. Montanyà, O. van der Velde, and E.R. Williams, "Lightning discharges produced by wind turbines", J. Geophys. Res. Atmos., 119, 2014.

[17] V. A. Rakov and M. A. Uman, Lightning: Physics and Effects. Cambridge University Press, 2003.